Field Evaluation of Near-Surface Mounted, Fiber-Reinforced Polymer Strips for Strengthening of a Continuous Reinforced Concrete Bridge

by

William Brown Childs

A thesis submitted to the Graduate Faculty of
Auburn University
in partial fulfillment of the
requirements for the Degree of
Master of Science

Auburn, Alabama
May 7, 2016

Keywords: in-place performance, load testing, retrofit, rehabilitation, structural strengthening, structural composites

Approved by

Robert W. Barnes, Chair, Associate Professor of Civil Engineering
Anton K. Schindler, Professor of Civil Engineering
Justin D. Marshall, Associate Professor of Civil Engineering

ABSTRACT

The Letohatchee bridge is a continuous, reinforced concrete, deck-girder bridge maintained by the Alabama Department of Transportation (ALDOT) along AL 97 over I-65 near Letohatchee, Alabama. The bridge is deficient in negative-moment capacity and was strengthened using near-surface mounted fiber-reinforced polymer (NSM FRP) strips.

The bridge was load tested before and after implementation of the NSM FRP strengthening program. A long-term test was also conducted one year after installation to evaluate behavior of the NSM FRP system after a year of exposure to the environment and service loads. Installation of the strengthening system is documented in this thesis.

The NSM FRP system exhibited an apparent 10% reduction in girder reinforcing steel stress, while stress in slab reinforcement may have increased due to a more even distribution of moment across the bridge cross section. The NSM FRP system did not show any signs bond degradation or strength loss one year after installation.

ACKNOWLEDGEMENTS

I would first like to thank Dr. Robert Barnes for his guidance and wisdom throughout my research and studies at Auburn University. I am also grateful to Dr. Anton Schindler and Dr. Justin Marshall for their time and direction as committee members and mentors throughout my collegiate career. I also must thank Mr. Billy Wilson for his invaluable support in preparation for load testing throughout this research. I am also very grateful for many undergraduate and graduate students at Auburn University that assisted throughout this research. Specifically, I appreciate the help of Dave Mante, Zach Skinner, Jonathon Campbell, Jamieson Matthews, Lester Lee, Rebecca Nylen, Oscar Yang, and Todd Christensen for the hours of work they contributed to the success of this research. I also am very appreciative of the Alabama Department of Transportation (ALDOT) and the Auburn University Highway Research Center (HRC) for their support of this research.

Finally, I am grateful to my parents, Sam and Leslie Childs, my brother Samuel, and the rest of my family for their continual support and encouragement.

TABLE OF CONTENTS

LIST OF TABLES

LIST OF FIGURES

CHAPTER 1:INTRODUCTION

1.1 General Background

The Alabama Department of Transportation (ALDOT) maintains many bridges with strength rating deficiencies for certain truck types. In 2004, ALDOT applied to the Federal Highway Administration (FHWA) to develop a strengthening program for a standard bridge type (Standard Drawing No. IC 2806) through the Transportation Equity Act for the 21st Century (TEA-21) Innovative Bridge Research and Construction Program (IBRC). The strengthening program addressed retrofit of the bridge along AL 97 over I-65 near Letohatchee, Alabama (Bridge Inventory Number 8847), shown in Figure 1.1 below, utilizing fiber-reinforced polymer (FRP) strips.

Figure 1.1 Letohatchee Bridge (Lowndes County, Alabama)

Fiber-reinforced polymer strips refer to polymer fibers that are bonded together within an epoxy matrix to form precured strips (Hughes Brothers, Inc. 2011). FRP laminates and fabrics are often externally bonded (EB) to girders, whereas FRP strips are typically installed using a near-surface mounted (NSM) technique. Figure 1.2 shows an example of externally bonded and near-surface mounted FRP applications.

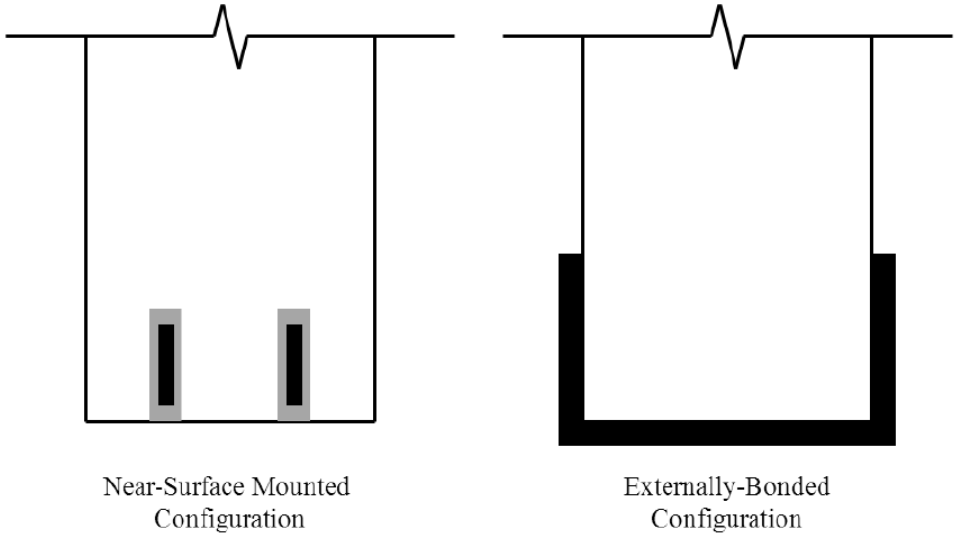

Figure 1.2 Typical NSM and EB FRP Applications (Bertolotti 2012)

NSM FRP provides greater protection from environmental conditions and improved bond quality when compared to EB FRP (Bertolotti 2012). External applications often apply to positive moment flexural strengthening of bridge girders due to unobstructed accessibility and ease of installation from beneath a bridge. EB FRP installations cover the member with FPR, resulting in a majority of the concrete no longer being exposed after a retrofit. However, for negative-moment flexural strengthening, a NSM FRP technique is often more appropriate. NSM FRP allows for embedment of FRP within the member while the concrete remains exposed. This is especially beneficial in a bridge deck retrofit for negative moment because it allows the deck surface to retain the traction of the concrete. Also, NSM FRP only involves work along the top

of the deck of a bridge, therefore road closures are limited to only the lane of the bridge being retrofitted.

While fiber-reinforced polymers have been a promising, innovative material in concrete retrofits for many years, there has been very little documented use of NSM FRP in applications similar to the standard ALDOT bridge design of interest. The bridge, near Letohatchee, Alabama, is a continuous, reinforced concrete, deck-girder bridge that was built with relatively low strength concrete and low reinforcement ratios in regions between supports and midspan. The bridge, constructed in 1965, is cracked due to years of exposure to service loads and is deficient in negative-moment flexural strength in the region where most of the negative-moment reinforcement terminates, as indicated in Figure 1.3 below. Therefore, in 2009 this project began with an exploratory review of models and codes to determine the optimum NSM FRP retrofit design for the Letohatchee bridge (Alexy 2009). Laboratory testing of cracked, NSM FRP repaired girders that closely resembled the conditions of the Letohatchee bridge followed (Bertolotti 2012).

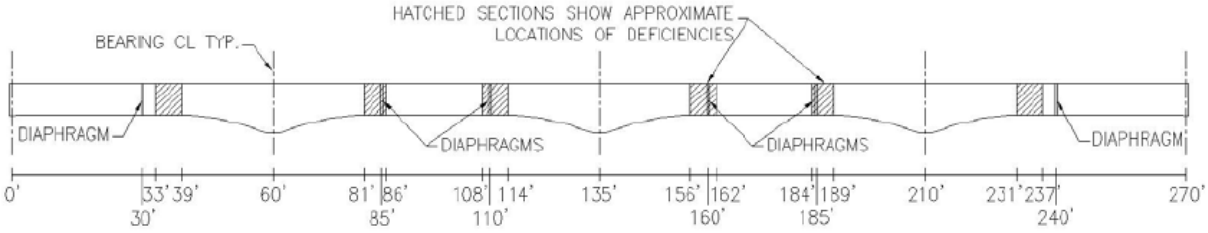

Figure 1.3 Approximate Locations of Flexural Deficiencies in the Letohatchee Bridge (Alexy 2009)

1.2 Research Objectives and Tasks

The primary goals of the research describe in this thesis are to determine the feasibility of NSM FRP reinforcement for negative-moment strengthening of continuous, reinforced concrete

girder bridges and to develop recommendations for the implementation of NSM FRP reinforcement for flexural strengthening of this bridge type. The construction method, as established by Bertolotti (2012), was implemented and documented during the retrofit. Details of the installation and performance improvements resulting from the retrofit are also provided. Recommendations are based on the NSM FRP construction method for further flexural strengthening of other ALDOT bridges of this standard bridge type.

Several tasks were required to achieve these objectives:

1. Pre-retrofit load test of the Letohatchee bridge in its existing condition,
2. Implementation of the NSM FRP retrofit,
3. Post-retrofit load test of the NSM FRP strengthened Letohatchee bridge, and
4. Long-term load test of the NSM FRP strengthened Letohatchee bridge eleven months after completion of the retrofit.

1.3 Organization of Thesis

An overview of NSM FRP research and reinforced concrete analysis is presented in Chapter 2. Previous research from Auburn University is presented, as it determined how the Letohatchee bridge retrofit was implemented. Typical concerns associated with NSM FRP as well as benefits of NSM FRP are also discussed and classical concrete analysis methods are described.

Chapter 3 documents the background of the Letohatchee bridge. The existing conditions and deficiencies of the Letohatchee bridge and other ALDOT standard bridges of this type are also covered in this chapter.

The bridge testing program is presented in Chapter 4. All three load tests are discussed, along with instrumentation details and an outline of each load test.

Installation of the bridge retrofit is presented in Chapter 5. Each step of the NSM FRP application method is documented and detailed. The effects of weather and external factors impacting construction are also discussed.

Results and analysis of data from the bridge testing program are presented in Chapter 6. Analytical investigations of the bridge before and after the retrofit are also presented. Bridge test results and analytical expectations are compared and the results discussed.

A summary of the retrofit is discussed in Chapter 7. This chapter also presents conclusions based on the research documented in this thesis and recommendations for the implementation of this retrofit process for similar ALDOT-maintained bridges.

CHAPTER 2:LITERATURE REVIEW

2.1 Introduction

Fiber-reinforced polymers have been used in many industries since the 1940s, and over the past two decades it has become a widely used material in structural retrofits (Bakis et al. 2003). FRP composites have been traditionally applied as externally bonded FRP on tension members and wraps on columns. Over the past decade near-surface mounted FRP has also been explored to increase efficiency of FRP retrofits. The Auburn University Highway Research Center (AU HRC) began investigating NSM FRP in 2009. This research and other published documentation of FRP is considered as it relates to the Letohatchee bridge retrofit.

2.2 Benefits of Fiber-Reinforced Polymers

Fiber-reinforced polymer composites are a valuable material for structural retrofits, especially when compared to traditional construction materials. FRP composites provide many advantages and are available in many different fiber types. Different fiber types and application methods provide different results, so it is important to implement the proper technique to achieve an adequate, durable structural retrofit.

2.2.1 Advantages Compared to Traditional Retrofit Materials

Reinforced concrete (RC) bridges, like all structures, reach a point in their lifespan where replacement or retrofit is required to withstand current operating conditions. In 2013, the American Society of Civil Engineers (ASCE) reported that one in nine bridges in the United States are structurally deficient, or require retrofit. Due to the high cost of removing and

rebuilding deficient structures, performing a less expensive structural retrofit is often the preferred choice.

Structural retrofits have been performed for several decades using traditional building materials; however, since the 1980s fiber-reinforced polymer composites have become widely used in the construction industry (Bakis et al. 2003). Prior to the introduction of FRP materials, structural repair primarily relied on the use of metals, shotcrete, or additional reinforced concrete. Steel plates have been one of the most popular retrofit materials for RC structures, and they are often attached with epoxy or bolts to areas of flexural deficiency. Reinforced concrete or shotcrete is often used in conjunction with steel jacketing of structural members.

While traditional reinforced concrete retrofit methods can benefit an aged structure, utilizing FRP composites can often result in a superior retrofit. Traditional retrofit methods using steel plates and concrete provide strength and stiffness to the member, but also can significantly increase cross-sectional dimensions and dead loads of the structure (Bakis et al. 2003). However, FRP materials are extremely lightweight in comparison to traditional construction materials. FRP composites are four to six times less dense than steel, with densities typically ranging from 75–130 pcf (1.2–2.1 g/cm^3). This can reduce material transportation costs as well as dead loads on the structure (ACI Committee 440 2008). Table 2.1 shows typical densities of steel and FRP materials.

Table 2.1 Typical Steel and FRP Densities, lb/ft^3 (g/cm^3) (ACI Committee 440 2008)

Steel	GFRP	CFRP	AFRP
490 (7.9)	75 to 130 (1.2 to 2.1)	90 to 100 (1.5 to 1.6)	75 to 90 (1.2 to 1.5)

Another advantageous property of FRP materials is their innate resistance to corrosion. Many applications leave retrofit materials exposed to environmental conditions, where corrosion

can greatly reduce the longevity and effectiveness of a retrofit. Therefore, FRP retrofits can also provide a long-lasting retrofit due to corrosion resistance.

2.2.2 Types of Fiber-Reinforced Polymers

There are three types of fibers used in concrete strengthening FRP applications: aramid (Kevlar™), glass, or carbon (graphite). Ultimate tensile strengths of fibers range from about 200 ksi (1380 MPa) to 900 ksi (6200 MPa), but fibers have very low strain at rupture. Table 2.2 shows typical tensile properties of fibers used in FRP systems.

Table 2.2 Typical Tensile Properties of FRP System Fibers (ACI Committee 440 2008)

Fiber type	Elastic modulus		Ultimate strength		Rupture strain, minimum, %
	10^3 ksi	GPa	ksi	MPa	
Carbon					
General purpose	32 to 34	220 to 240	300 to 550	2050 to 3790	1.2
High-strength	32 to 34	220 to 240	550 to 700	3790 to 4820	1.4
Ultra-high-strength	32 to 34	220 to 240	700 to 900	4820 to 6200	1.5
High-modulus	50 to 75	340 to 520	250 to 450	1720 to 3100	0.5
Ultra-high-modulus	75 to 100	520 to 690	200 to 350	1380 to 2400	0.2
Glass					
E-glass	10 to 10.5	69 to 72	270 to 390	1860 to 2680	4.5
S-glass	12.5 to 13	86 to 90	500 to 700	3440 to 4140	5.4
Aramid					
General purpose	10 to 12	69 to 83	500 to 600	3440 to 4140	2.5
High-performance	16 to 18	110 to 124	500 to 600	3440 to 4140	1.6

According to Table 2.2, glass FRP (GFRP) fibers have the least strength, but they exhibit the greatest strain at rupture. Carbon FRP (CFRP) fibers provide the highest strengths, but exhibit less strain at failure than glass or aramid fibers. Aramid fibers fall between glass and carbon fibers in both strength and rupture strain. Table 2.3 shows that typical tensile properties of FRP bars align with these observations regarding fiber properties from Table 2.2.

Table 2.3 Typical Tensile Properties of FRP Bars (ACI Committee 440 2008)

FRP system description	Young's modulus, 10^3 ksi (GPa)	Ultimate tensile strength, ksi (MPa)	Rupture strain, %
High-strength carbon/epoxy	17 to 24 (115 to 165)	180 to 400 (1240 to 2760)	1.2 to 1.8
E-glass/epoxy	4 to 7 (27 to 48)	70 to 230 (480 to 1580)	1.6 to 3.0
High-performance aramid	8 to 11 (55 to 76)	130 to 280 (900 to 11,930)	2.0 to 3.0

Fiber-reinforced polymer materials for structural applications are typically precured FRP pieces or FRP fabrics. Precured FRP materials are made of unidirectional fibers that are impregnated with epoxy, or a similar resin matrix, and are extruded into the desired shape. FRP fabrics consist of unidirectional or bidirectional FRP fibers that are woven together into thin, flexible sheets (Bakis et al. 2003).

Types of precured FRP materials include bars, laminates, and strips. Bars are created to mimic steel reinforcing bars and conform to the same bar size numbering system as mild steel reinforcement. Laminates are thin, wide pieces of FRP, about 0.055 inches (1.4 mm) thick and 2–4 inches (50–100 mm) wide. FRP strips are not as wide as laminates, typically about 0.079–0.177 inches (2–4.5 mm) thick and 0.63 inches (16 mm) wide (Aslan FRP 2015). Figure 2.1 shows samples of a FRP bar, laminate, and strip.

Figure 2.1 FRP Bar, Laminate, and Strip Samples

Fabrics are a unique type of FRP reinforcement because they allow the contractor to mold the reinforcement around members during installation rather than relying on standard dimensioned pieces. FRP fabrics are some of the most widely used composite materials for retrofits of existing structures. A sample of FRP fabric is shown in Figure 2.2, and FRP fabrics used to strengthen reinforced concrete beams and columns are shown in Figure 2.3

Figure 2.2 FRP Fabric Sample (Prior to Epoxy Saturation)

Figure 2.3 FRP Fabric Wraps of Beam (Left) and Column (Right) (Sheikh and Homam 2004)

2.2.3 FRP Application Methods

Externally bonded (EB) and near-surface mounted (NSM) are the two most common application methods for fiber-reinforced polymer retrofits. Externally bonded FRP is attached to the outside of members; near-surface mounted FRP is embedded in the concrete cover of a member. Both techniques utilize epoxy to bond FRP to the existing concrete.

Externally bonded FRP requires epoxy application prior to placement. First, epoxy is applied to the FRP and to the member being strengthened. After thoroughly coating both surfaces, FRP is placed in the desired position on the structural member. This method results in one FRP surface that is bonded to the structural member, while the other FRP surfaces are exposed to the environment. EB FRP is used for flexural strengthening of girders of varying materials, and it is the most commonly used technique of FRP retrofits (Bakis et al. 2003). A typical application of EB FRP in the War Memorial Bridge retrofit is shown in Figure 2.4.

Figure 2.4 EB FRP Laminate Retrofit of the War Memorial Bridge (Carmichael and Barnes 2005)

A newer method of FRP retrofit of structures is known as near-surface mounted FRP. NSM FRP refers to FRP strips or bars that are embedded below the surface of a structural member. Grooves are typically cut into a reinforced concrete member, and epoxy is placed into the groove, along with an FRP strip or bar. This method has not been documented as thoroughly as EB FRP, but it has steadily grown in use since the first NSM FRP retrofits in the 1990s (Parretti and Nanni 2004). Figure 2.5 shows a typical NSM FRP installation in a reinforced concrete bridge retrofit.

Figure 2.5 Typical NSM FRP Installation (Hughes Brothers, Inc. 2011)

2.2.4 Advantages of NSM FRP

There are many advantages to using an NSM FRP method to retrofit an existing bridge. NSM FRP exhibits improved bond strength, ductility, and environmental protection compared to

EB FRP. NSM FRP also allows for a more efficient use of FRP materials than EB FRP applications (Blaschko and Zilch 1999).

In NSM applications, FRP strips are embedded into the concrete. This allows for an epoxy bond between the FRP strip and three surfaces of concrete, while also covering the fourth surface of the strip with a layer of epoxy. Therefore, the bond strength in NSM applications is much stronger than EB installations, where epoxy is only between one side of the FRP and the adjacent concrete. Figure 2.6 shows test results of two identical specimens that were reinforced with the same amount of FRP. Specimen A1 was reinforced using EB FRP and specimen A2 was reinforced using NSM FRP (Blaschko and Zilch 1999). During flexural loading, both specimens exhibited very similar stiffness. However, the NSM FRP reinforced specimen (A2) exhibited over twice the ultimate strength of the EB FRP reinforced specimen (A1). The NSM FRP specimen failed due to tensile failure of the FRP strips, while the EB FRP specimen failed due to bond failure between the FRP strips and concrete surface.

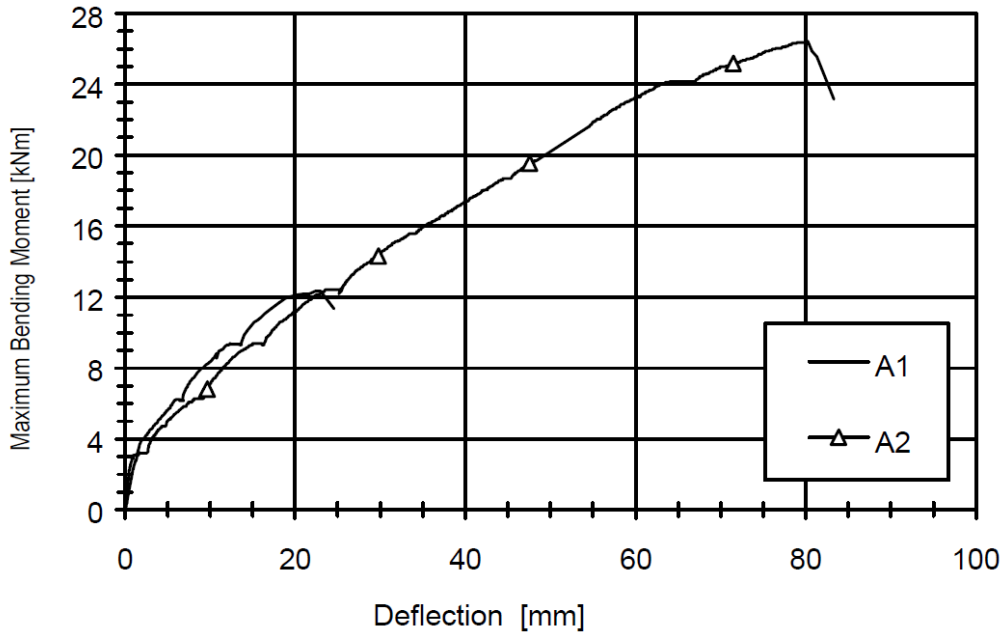

Figure 2.6 Moment-Deflection Behavior of EB (A1) and NSM (A2) FRP Beams (Blaschko and Zilch 1999)

NSM FRP also has additional protection from environmental effects due to the covering of epoxy on the fourth surface of the FRP strip. The epoxy covering provides FRP protection from exposure to degradation due to environmental conditions. There is also an increased resistance to fire damage because the FRP strip is embedded in the member (El-Hacha and Rizkalla 2004).

Bond strength is very important because in EB FRP applications, bond strength typically limits the performance of the FRP retrofit. EB FRP is susceptible to bond failure before the FRP is able to reach tensile failure, which reduces the design strength of EB FRP applications. However, in NSM FRP applications, tensile strength of the FRP material often controls failure of the repair. Therefore, NSM FRP retrofits more efficiently utilize the FRP reinforcement than EB FRP retrofits (Jung et al. 2005).

2.2.5 Disadvantages of NSM FRP

NSM FRP is a very useful strengthening method; however, there are disadvantages. Bridges that do not have adequate cover are not good candidates for a NSM FRP retrofit. There must be sufficient cover to allow for grooves to be cut in the bridge deck without damaging the reinforcement. Also, the existing concrete must be in good condition. NSM FRP would not perform well if installed in damaged concrete, where conditions such as spalling, corrosion, or other poor concrete conditions are present.

2.3 Tests of NSM FRP Strengthening Applications

There have been many laboratory tests on NSM FRP strengthened specimens. Some of these programs are discussed here, as they provide relevant information for the Letohatchee bridge retrofit. However, there are only a few published documents regarding testing of actual structures strengthened with NSM FRP. Therefore, all available information of actual structures strengthened with NSM FRP is reviewed for relevance to the Letohatchee bridge project.

2.3.1 Laboratory Testing of NSM FRP Strengthened Beams

Two laboratory studies involving NSM FRP strengthening are discussed as they pertain to the Letohatchee bridge retrofit. A more thorough exploratory review of laboratory testing of FRP was documented by Alexy (2009) and Bertolotti (2012) during prior phases of this research study. However, this chapter is focused on NSM FRP and applications that closely resemble the FRP strengthening application in the Letohatchee bridge.

2.3.1.1 Lab tests of NSM FRP strengthened T-Beams (El-Hacha and Rizkalla 2004)

In 2004, Raafat El-Hacha and Sami H. Rizkalla performed laboratory tests of NSM FRP strengthened T-beams. Eight specimens were constructed and tested as simply supported beams under a monotonically increasing load at midspan. The beams were constructed with Grade 60

reinforcing steel and exhibited a concrete compressive strength of 6500 psi (45 MPa). One beam was a control specimen and three beams were strengthened with NSM FRP using CFRP bars and strips. The other four specimens were strengthened using GFRP and EB FRP, but this review focuses only on the NSM FRP specimens. Embedment length and axial stiffness of the FRP strengthened beams were kept consistent in all specimens. Table 2.4 shows the specimens that were tested in this study.

Table 2.4 Laboratory Test Specimens (El-Hacha and Rizkalla 2004)

Beam no.	FRP strengthening system
B0	No strengthening
B1	One NSM CFRP reinforcing bar
B2	Two Type 1 NSM CFRP strips
B3	Two Type 2 NSM CFRP strips
B4	Five NSM GFRP thermoplastic strips
B2a	Two Type 1 externally bonded CFRP strips
B2b	Two Type 1 externally bonded CFRP strips
B4a	Five externally bonded GFRP thermoplastic strips

Table 2.5 shows a summary of test results. The NSM FRP strengthened beams exhibited increases in strength of 70–90% relative to the unstrengthened specimen.

Table 2.5 Summary of Test Results from Laboratory Testing (El-Hacha and Rizkalla 2004)

Strengthening systems	Beam no.	P_{cr}, kN (kips)	Δ_{cr}, mm (in.)	P_y, kN (kips)	Δ_y, mm (in.)	P_u, kN (kips)	Δ_u, mm (in.)	ε_u, %	Failure mode	Percent increase in P_u
—	B0	21.98 (4.94)	1.35 (0.053)	38.11 (8.57)	8.88 (0.35)	55.4 (12.5)	64.4 (2.54)	—	Crushing of concrete and steel yielding	—
Near-surface-mounted FRP reinforcement	B1	24.7 (5.55)	1.27 (0.05)	47.94 (10.78)	4.85 (0.191)	93.8 (21.0)	29.2 (1.15)	0.88	Debonding of NSM CFRP reinforcing bar (epoxy split failure)	69.3
	B2	22.24 (5.9)	1.08 (0.043)	48.62 (10.93)	5.61 (0.221)	99.3 (22.3)	30.5 (1.20)	1.34	Rupture of NSM CFRP strips	79.2
	B3	30.11 (6.77)	1.702 (0.067)	49.16 (11.05)	5.25 (0.207)	110.2 (24.7)	50.8 (2.00)	1.38	Rupture of NSM CFRP strips	98.9
	B4	24.46 (5.50)	1.6 (0.063)	48.17 (10.83)	5.67 (0.223)	102.7 (23.1)	44.3 (1.75)	1.35	Debonding of NSM GFRP strips (concrete split failure)	85.4
Externally bonded FRP reinforcement	B2a	22.46 (5.05)	1.22 (0.048)	44.88 (10.09)	4.42 (0.174)	64.6 (14.5)	43.7 (1.71)	0.48	Debonding of externally bonded CFRP strips	16.6
	B2b	—	—	—	—	64.3 (14.5)	21.7 (0.85)	0.44	Debonding of externally bonded CFRP strips	16.1
	B4a	29.13 (6.55)	0.95 (0.037)	48.16 (10.82)	4.39 (0.173)	71.1 (15.9)	22.2 (0.87)	0.62	Debonding of externally bonded GFRP strips	28.3

*Where P_{cr} = cracking load; Δ_{cr} = midspan deflection at cracking; P_y = yield load; Δ_y = midspan deflection at yielding; P_u = ultimate load failure; Δ_u = midspan deflection at failure; and ε_u = maximum tensile strain in FRP reinforcing bar or strip at failure.

Failure modes of the specimens were caused by epoxy split failure in beam B1 and FRP rupture in beams B2 and B3. Epoxy splitting failure is an uncommon failure mechanism in NSM FRP because it is caused by insufficient epoxy between the FRP and concrete, preventing adequate bond strength development. Epoxy splitting failure can be avoided by appropriately dimensioning grooves. Groove size dimensions and all FRP design standards are located in American Concrete Institute 440: Building Code Requirements for Structural Concrete Reinforced Internally with Fiber Reinforced Polymer (FRP) Bars (ACI 440). ACI 440 documents FRP reinforcement used in design, construction, and retrofit of reinforced concrete. However, this experiment was performed prior to NSM FRP inclusion in ACI 440 in 2008, therefore this failure mechanism is no longer a concern if properly designed (El-Hacha and Rizkalla 2004). Failure due to rupture of FRP is an undesirable failure mechanism, because it is followed by an immediate failure of the reinforcing steel in tension. This failure mechanism is also considered in ACI 440, therefore if a retrofit is properly designed according to ACI 440 then this mechanism is avoided (El-Hacha and Rizkalla 2004).

Load versus deflection results of the NSM FRP strengthened beams and the unstrengthened control beam are shown in Figure 2.7.

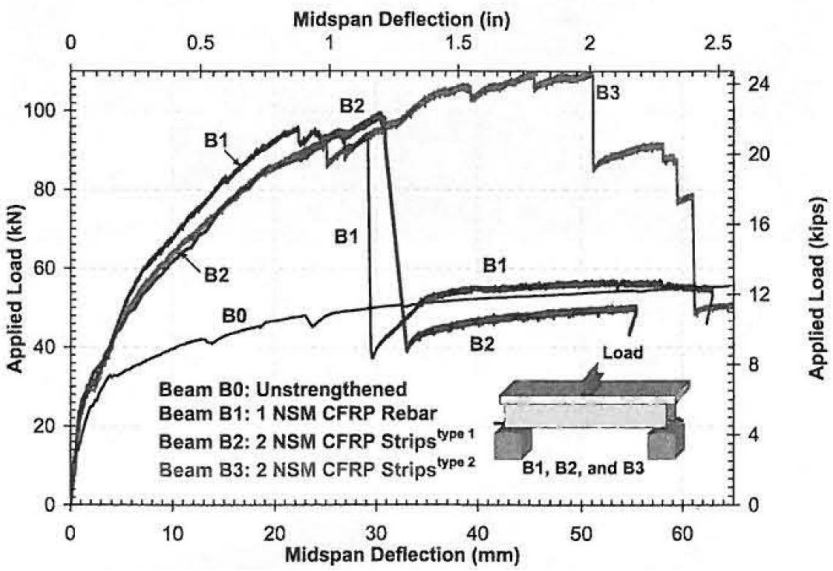

Figure 2.7 Load Deflection Results of Unstrengthened and NSM FRP Strengthened Beams (El-Hacha and Rizkalla 2004)

Retrofitted beams (B1, B2, and B3) exhibited a significantly larger ultimate load capacity, while also reducing deflection. However, it is evident that FRP failures due to epoxy splitting (B1) or FRP rupture (B2 and B3) result in brittle failure, rather than ductile failure exhibited by tensile steel yielding (B0), as in traditional reinforced concrete design.

Therefore, NSM FRP specimens exhibited increased ultimate strength and reduced deflection in these tests. However, in order to achieve better results, proper design methods should be utilized during design of the strengthening system (El-Hacha and Rizkalla 2004).

2.3.1.2 Lab tests of NSM FRP strengthened beams (Jung et al. 2005)

In 2005, additional laboratory testing was performed to examine behavior of NSM FRP strengthening of reinforced concrete beams. Eight beams were constructed and tested as simply

supported beams under an increasing four-point loading. The beams were constructed with Grade 60 reinforcing steel and exhibited a concrete compressive strength of 4500 psi (31.3 MPa). One beam was a control specimen and three beams were strengthened with NSM FRP using CFRP rods and strips. The other four specimens were strengthened using EB FRP and mechanically interlocking NSM, but this review will focuses on the NSM FRP specimens. Table 2.6 shows the test specimens that were tested in this study, and Figure 2.8 shows the layout of the loading apparatus and NSM FRP layout for the specimens of interest.

Table 2.6 Laboratory Test Specimens (Jung et al. 2005)

Specimen	CFRP area (mm^2)	CFRP type	ρ_{CFRP}(%)	Strengthening method
CONTROL	–	–	–	unstrengthened
SH-BOND	26.4	Sheet	0.0489	EBR[1)]
CPL-50-BOND	70	Strip	0.1296	EBR[1)]
CRD-NSM	63.6	Rod	0.1178	NSM[2)]
NSM-PL-25	35	Strip	0.0648	NSM[2)]
NSM-PL-15	21	Strip	0.0389	NSM[2)]
ROD-MI-20	63.6	Rod	0.1178	NSM[2)]+MI[3)]
PL-MI-20	35	Strip	0.0648	NSM[2)]+MI[3)]

1) EBR: Externally Bonded Reinforcement
2) NSM : Near Surfaced Mounted Reinforcement
3) MI : Mechanical Interlocking grooves; 12ea, width : 20㎜, space : 200㎜

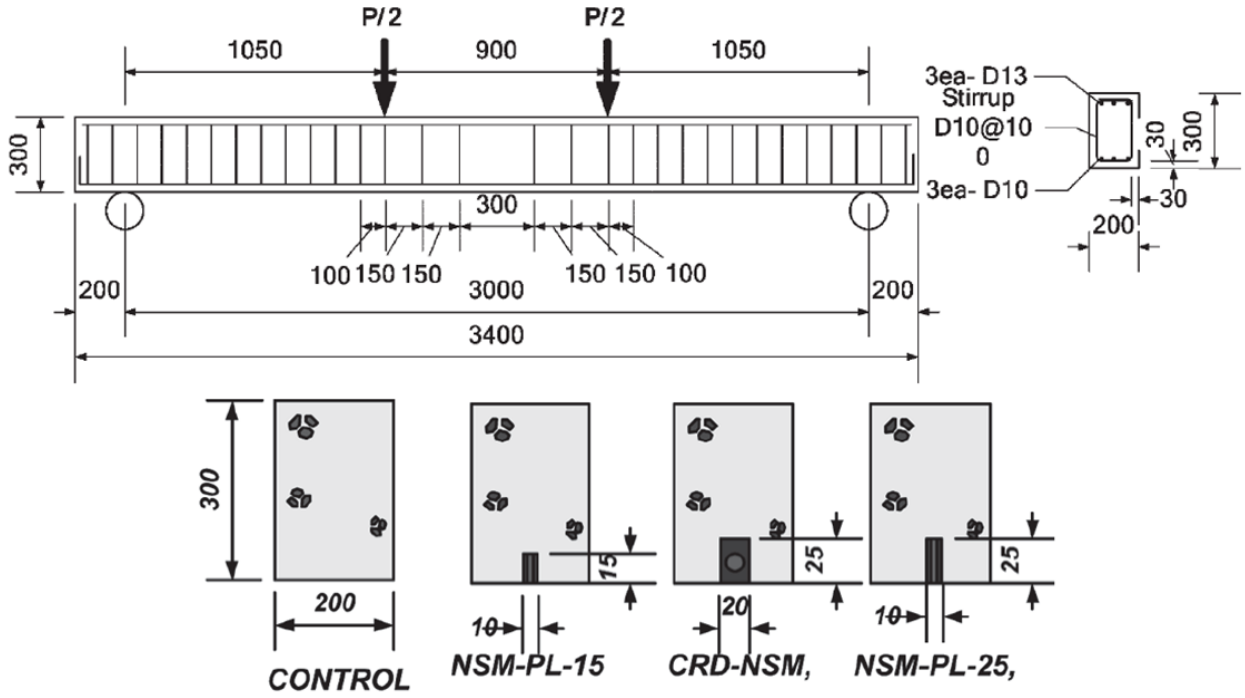

Figure 2.8 Load Test and NSM FRP Layouts (Jung et al. 2005)

Beams that were strengthened with NSM FRP exhibited an increased ultimate load of 35–65%, when compared to the unstrengthened specimen. Figure 2.9 shows load-deflection results from the NSM FRP strengthened specimens.

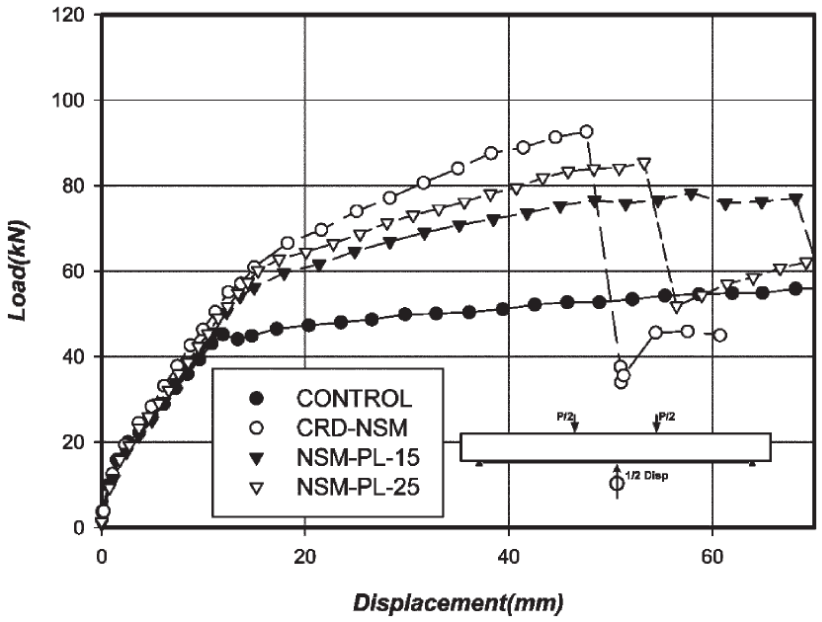

Figure 2.9 Load-Displacement Plot of NSM FRP Specimens (Jung et al. 2005)

The NSM FRP strengthened specimens behaved stiffer than the control beam, and exhibited an increased ultimate load capacity. FRP bars and strips used in these three specimens failed at 85–100% of the FRP ultimate strain, while externally bonded specimens in this expirement failed at 30–50% of the FRP ultimate strain. This verifies that using a NSM technique allows for more effective material strength utilization (Jung et al. 2005).

2.3.2 Testing of NSM FRP Strengthened Structures

There is very little published documentation of tests of NSM FRP retrofitted structures. Therefore, the following discussion will focus on relevant testing of four structures strengthened with NSM FRP.

2.3.2.1 Reinforced Concrete Interstate Bridge Girders Tested to Failure (Aidoo, Harries, and Petrou 2006)

The reinforced concrete bridge along I-85 northbound over Cherokee Creek near Gaffney, South Carolina was replaced in 2001 because it was not wide enough for current traffic

volume and did not satisfy safety requirements. The bridge, constructed in 1957, was disassembled and the girders were tested at the University of South Carolina to study NSM FRP strengthening of existing structures. Figure 2.10 shows a section view of the girders and the layout of the NSM FRP strengthening scheme.

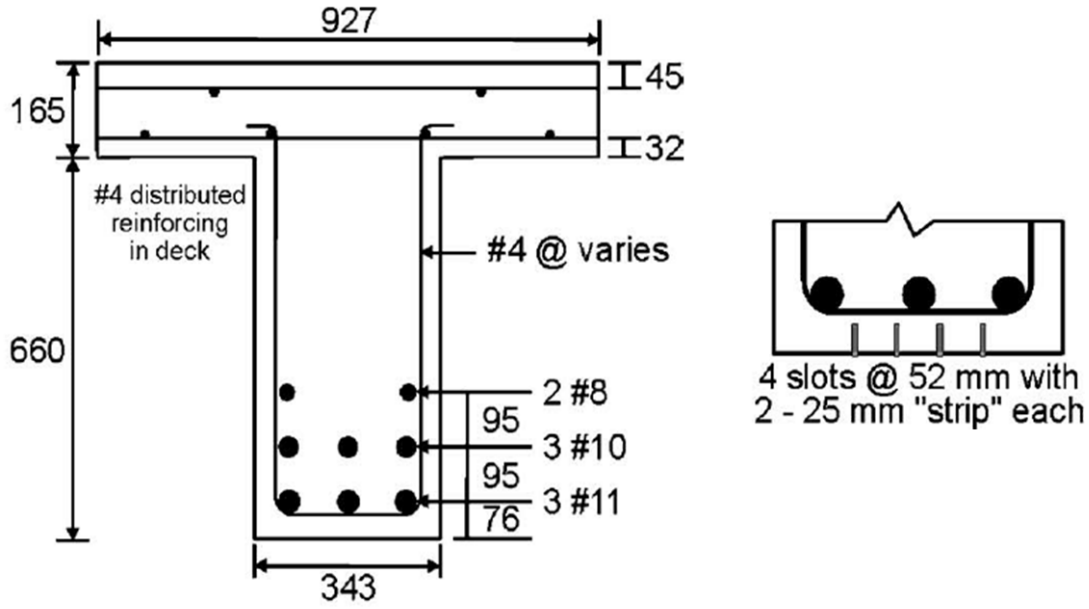

Figure 2.10 Cherokee Creek Bridge Girder Cross Section and NSM FRP Layout (Aidoo, Harries, and Petrou 2006)

Eight of the girders recovered from the bridge were tested in this study, but only the comparisons between the unstrengthened and NSM FRP tested specimens are of interest to this research.

The girders were constructed with Grade 40 reinforcing steel and cores were taken that indicated an average compressive strength of 6500 psi (45 MPa). Girders were split into two categories during testing—one group was loaded monotonically to failure, and the other was fatigue loaded for 2 million cycles before loading to failure. Table 2.7 shows results from girder testing. Girders are designated with two letters, where the girders of interest contain "U" for

unstrengthened or “N” for NSM retrofitted, followed by “S” for monotonically loaded or “F” for fatigue loaded.

Table 2.7 Summary of Test Results from Cherokee Creek Bridge Girders (Aidoo, Harries, and Petrou 2006)

Tests		US	CS	NS	PS	UF	CF	NF	PF
Fatigue conditioning	Minimum load (kN)		Not applicable			37.8	32.5	33.8	33.4
	Maximum load (kN)		Not applicable			352	359	359	359
	Calculated stress range on rebar (MPa)		Not applicable			115	99	139	115
	Offset following N=2,000,000 (mm)		Not applicable			3.9	1.5	4.1	2.5
Secant stiffness (kN/mm)	N=1	54.0	46.3	41.0	50.5	39.6	44.3	37.0	45.4
(determined from 0 and 359 kN)	N=2,000,000		Not applicable			28.6	33.0	23.6	31.4
General yield	Load (kN)	663	667	665	694	678	717	716	680
	Deflection (mm)[a]	18.0	18.5	22.0	20.0	20.8	23.6	24.6	18.0
Ultimate load	Load (kN)	787	823	831	921	766	809	864	909
	Deflection (mm)[a]	186	96	249	134	104	58	112	117
Displacement ductility		10.3	5.2	11.3	6.7	5.0	2.5	4.5	6.5
Ratio of maximum load relative to Specimen US		—	1.05	1.06	1.17	0.97	1.03	1.10	1.16

[a]Reported deflections do not include offset deflection.

In monotonic testing to failure, the NSM FRP retrofitted girder (NS) displayed the greatest displacement ductility—the ratio of midspan deflection at ultimate load to midspan deflection at yield. Yield of the NSM FRP strengthened girder occurred at a 6% larger load than the unstrengthened specimen (US). In fatigue loading, the strengthened girder (NF) also displayed increased strength of about 13% larger than the control specimen (UF). Failure in both NSM FRP strengthened specimens (NS and NF) was caused by a splitting failure in the horizontal plane between the NSM FRP and bottom layer of reinforcing steel. The weak plane was most likely due to the relatively thin width of the girder and the number of grooves cut in this section. Therefore, failure of the NSM FRP strengthened girders did not occur due to failure of the FRP. Therefore, the retrofitted girders exhibited increased strength, with no bond degradation at failure (Aidoo, Harries, and Petrou 2006).

2.3.2.2 Negative-Moment Strengthening of Two-Way Slabs (Tumialan, Vatovec, and Kelley 2007)

A two-way slab in a parking garage in Massachusetts was retrofitted with NSM FRP to provide negative-moment strengthening at columns. The garage was built in 1983, and was designed with 8 in. (0.2 m) thick two-way, reinforced concrete slabs with 10 ft x 10 ft x 4.25 in. (3.05 m x 3.05 m x 0.1 m) thick drop panels at interior columns. The parking garage layout is shown in Figure 2.11.

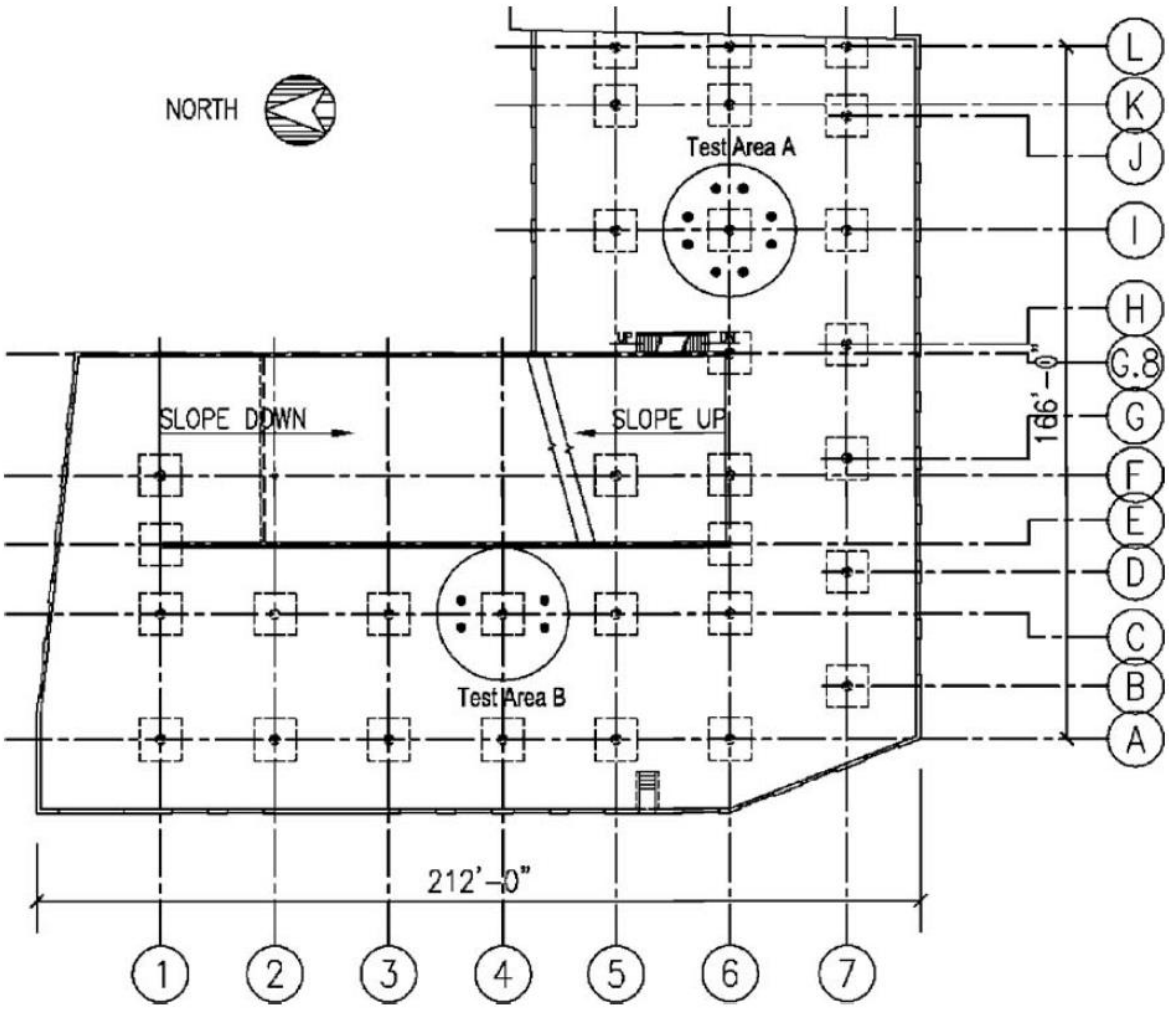

Figure 2.11 Parking Garage Layout and Test Locations (Tumialan, Vatovec, and Kelley 2007)

Deficiencies in the structure were caused by poor construction and resulted in large deflections at midspan of the two-way slab system. Ground-penetrating radar (GPR) indicated that concrete cover for negative-moment reinforcing steel varied from 1.5 in. (38 mm) to 4 in. (102 mm) throughout the garage. However, the original drawings called for 1.5 in. (38 mm) cover throughout. Structural analysis of the structure determined that excessive deflections at midspan locations were due to premature removal of formwork during construction. However, analysis verified that the midspan strength of the two-way slab system was adequate for current codes (at the time of the retrofit). Therefore, NSM FRP was used on top of the slab near column locations to increase the negative-moment capacity of the structure. The retrofit called for ten #3 CFRP bars that were embedded along the drop panel portion of the reinforced concrete slab. FRP bars were 14 ft (4.27 m) long, and spaced at 12 in. (30.48 cm) on each side of columns. The NSM FRP layout is shown in Figure 2.12.

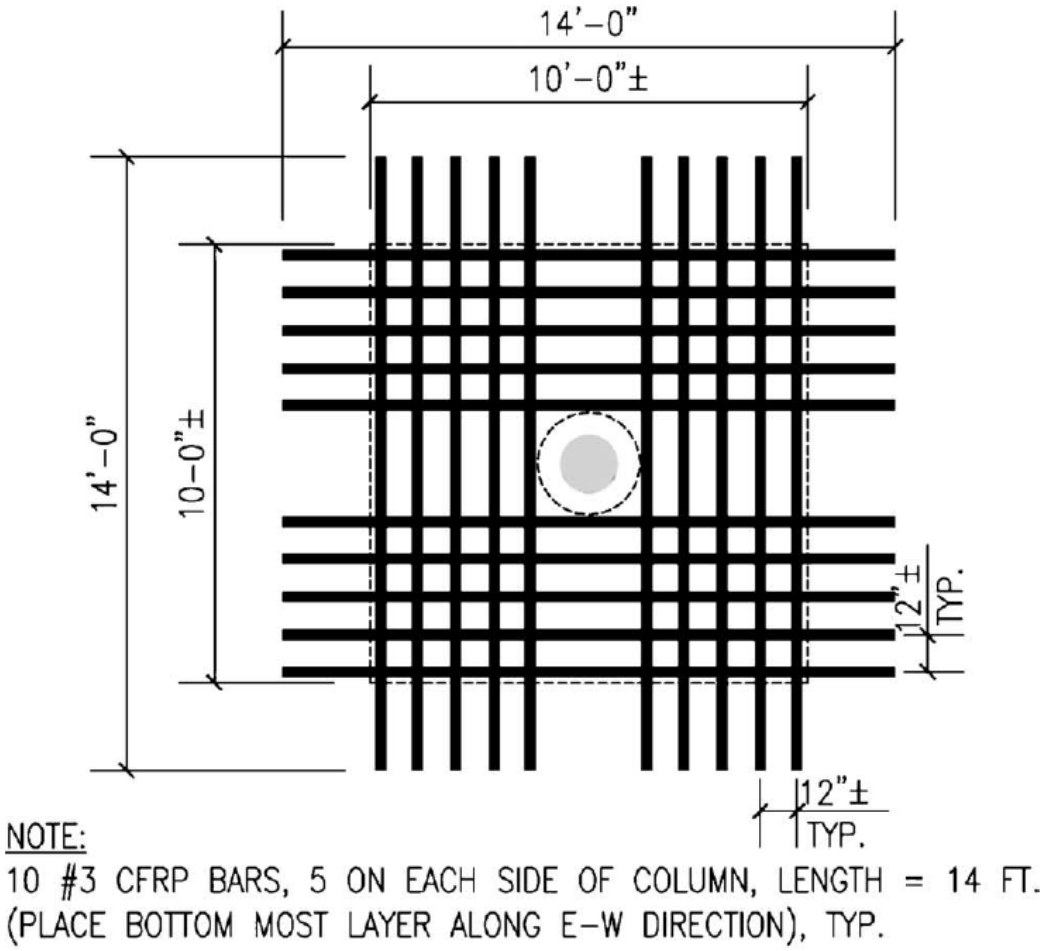

Figure 2.12 Two-Way NSM FRP Layout for Parking Garage Strengthening (Tumialan, Vatovec, and Kelley 2007)

The parking garage slab was tested before and after the retrofit to determine the initial and retrofitted strengths of the structure, respectively. Pre-retrofit tests limited loading to the maximum required load to allow for an FRP retrofit according to ACI 440 (1.2DL+0.85LL). For post-retrofit testing, loads were increased according to the American Concrete Institute 318: Building Code Requirements for Reinforced Concrete (ACI 318) and American Concrete Institute 437: Code Requirements for Load Testing of Existing Concrete Structures (ACI 437). These documents state that if the structure behaves linearly when loaded at 85% of the factored

design load (1.4DL+1.7LL) then it is considered adequate to support the full design load of the structure.

Cyclic load testing was performed by placing four point loads, two on each side of the column, to maximize negative-moment demand on the slab. On the bottom floor of the parking deck, hydraulic jacks reacted against mini-piles in the soil below the slab on grade. The loads were transferred through steel rods into a steel reaction beam on top of the tested slab. The loading apparatus below and above the tested slab is shown in Figure 2.13 and Figure 2.14, respectively.

Figure 2.13 Reaction Beams on Mini-Piles to Load Decks Above (Tumialan, Vatovec, and Kelley 2007).

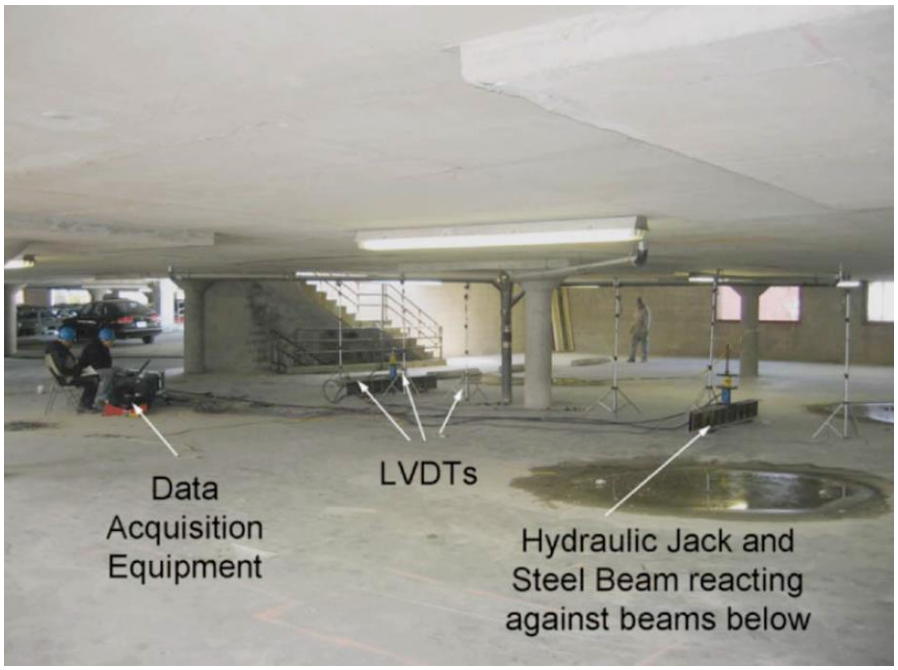

Figure 2.14 Hydraulic Jacks and Steel Beams Reacting against Beams Below the Loaded Deck (Tumialan, Vatovec, and Kelley 2007).

Results from the load tests for both the East-West and North-South directions in the most rigorously tested panel zone are shown in Figure 2.15 and Figure 2.16, respectively.

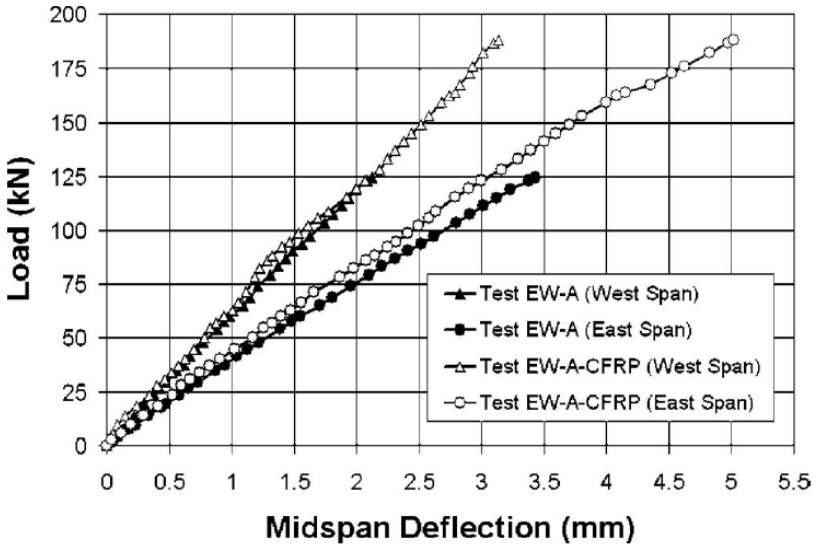

Figure 2.15 Load-Deflection Results in East-West Direction (Tumialan, Vatovec, and Kelley 2007)

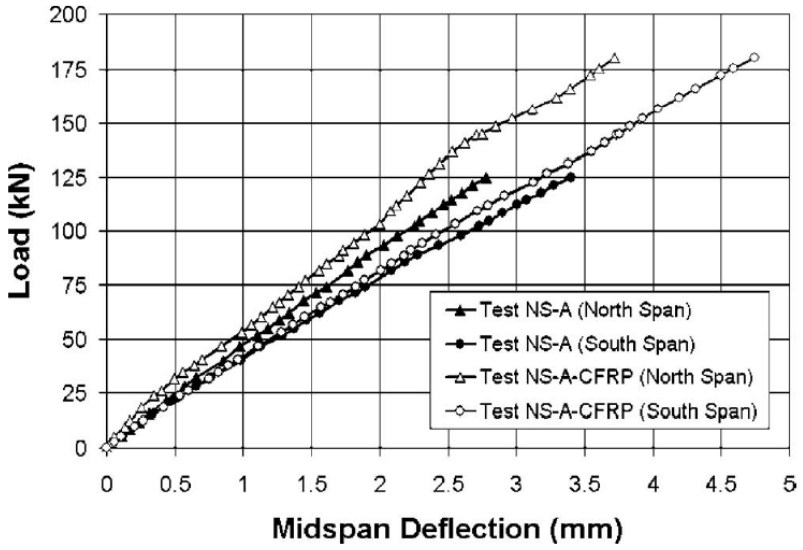

Figure 2.16 Load-Deflection Results in North-South Direction (Tumialan, Vatovec, and Kelley 2007)

Figure 2.15 and Figure 2.16 show that the retrofitted design provided increased strength and stiffness when compared to the pre-retrofit load test. These results also show that the retrofit behaved linearly during loading. Therefore, this study concluded that implementing the NSM FRP retrofit in this structure provided adequate reinforcement to strengthen the structure to carry loads according to current codes (Tumialan, Vatovec, and Kelley 2007).

2.3.2.3 Railway Bridge Strengthening (Bergström, Täljsten, and Carolin 2009)

The Örnsköldsvik Bridge, built in 1955, was a two-span railway bridge in Örnsköldsvik, Sweden that was strengthened with NSM FRP and then loaded to failure in 2006. The project included testing before and after strengthening in order to study the behavior of the NSM FRP retrofit. Samples of concrete and steel from the bridge were tested, and it was determined that the structure was composed of reinforced concrete with a compressive strength of 68.5 MPa (9940 psi) and reinforcing steel with a tensile yield strength of 404 MPa (58.6 ksi). The Örnsköldsvik

bridge and a section view of the NSM FRP strengthening scheme is shown in Figure 2.17 and Figure 2.18, respectively.

Figure 2.17 Örnsköldsvik Bridge (Bergström, Täljsten, and Carolin 2009)

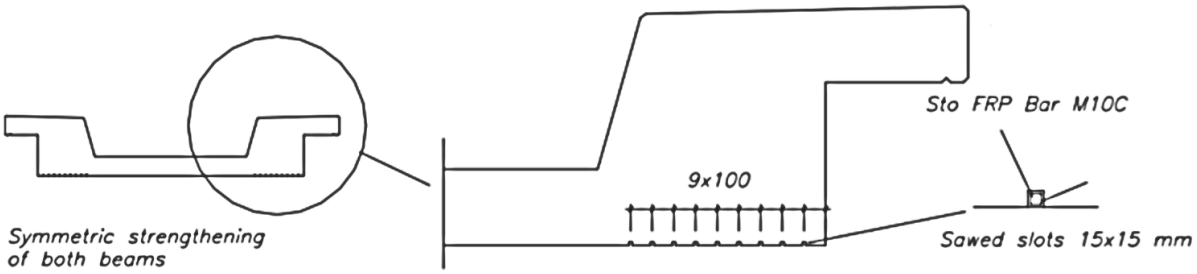

Figure 2.18 Section View of NSM FRP Layout (Bergström, Täljsten, and Carolin 2009)

The bridge was tested by applying a load at midspan, and strains in the concrete, steel, and FRP were recorded during load testing of the bridge. Figure 2.19 shows that tensile steel strains measured at midspan resulted in a strain reduction of about 20% in the post-retrofit test (T2) compared to pre-retrofit test (T1).

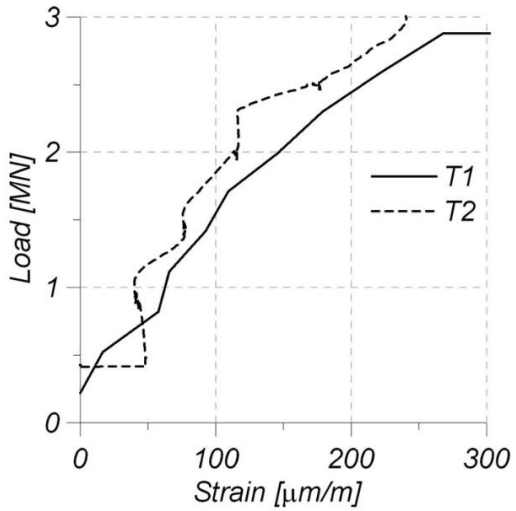

Figure 2.19 Load versus Strain in the Concrete for Pre-Retrofit (T1) and Post-Retrofit (T2) Load Tests of the Örnsköldsvik Bridge (Bergström, Täljsten, and Carolin 2009)

It was also observed that there was no failure in the FRP or in the epoxy bond between the concrete and FRP. The discrepancy in Figure 2.19 at low loads was attributed to development of shear deformation in the adhesive when the FRP strips begin to take some of the load. Figure 2.20 shows strains during the post-retrofit loading to failure.

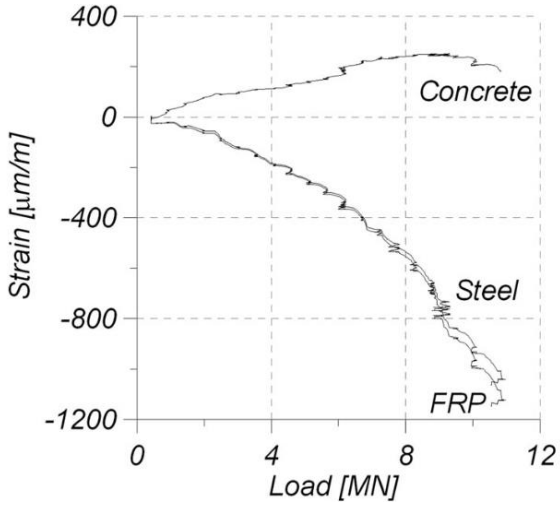

Figure 2.20 Strains During Post-Retrofit Failure Load Test of the Örnsköldsvik Bridge (Bergström, Täljsten, and Carolin 2009)

Concrete strains in Figure 2.20 begin to decline around 10 MN (2250 kips), indicating that the concrete is crushing and unable to carry additional load beyond that point. However, strains in the FRP and steel show no evidence of load-carrying capacity being reached.

The bridge was originally designed for a bending capacity of 4.6 MN (1035 kips), so the pre-repair load test stopped at a loading of 3.0 MN (675 kips). The capacity of the strengthened structure was found to be 11.7 MN (2630 kips), which exceeded analytical expectations of the retrofitted bridge capacity of 11.2 MN (2500 kips). Therefore, the NSM FRP retrofit application in the Örnsköldsvik Bridge doubled the load capacity of the structure, and did not exhibit any signs of FRP failure (Bergström, Täljsten, and Carolin 2009).

2.3.2.4 Strengthening of the Martin Spring Outer Road Bridge (Casadei et al. 2003)

The Martin Spring Outer Road Bridge is a three-span, reinforced concrete, slab bridge that was constructed along Route 66 in Phelps County, MO, in 1926. The bridge consists of concrete with an average compressive strength of 4100 psi (28 MPa) and reinforcing steel with a yield strength of 32 ksi (220 MPa). The bridge lacked transverse reinforcement, so there was an approximately 1.0-inch (2.5 cm) wide transverse crack along each slab at midspan. After repairing the crack, the bridge was strengthened using both EB and NSM FRP techniques. EB FRP was applied in Spans 1 and 3, while a combination of both EB and NSM FRP was used to strengthen Span 2. Figure 2.21 shows the Martin Spring Outer Road Bridge.

Figure 2.21 Martin Spring Outer Road Bridge in Phelps County, MO (Casadei et al. 2003)

This retrofit was performed by installing NSM FRP strips in the soffit of the bridge deck. Two strips of EB FRP laminates were also applied on the outer edges of the bridge soffit. Figure 2.22 shows the layout of FRP in Span 2.

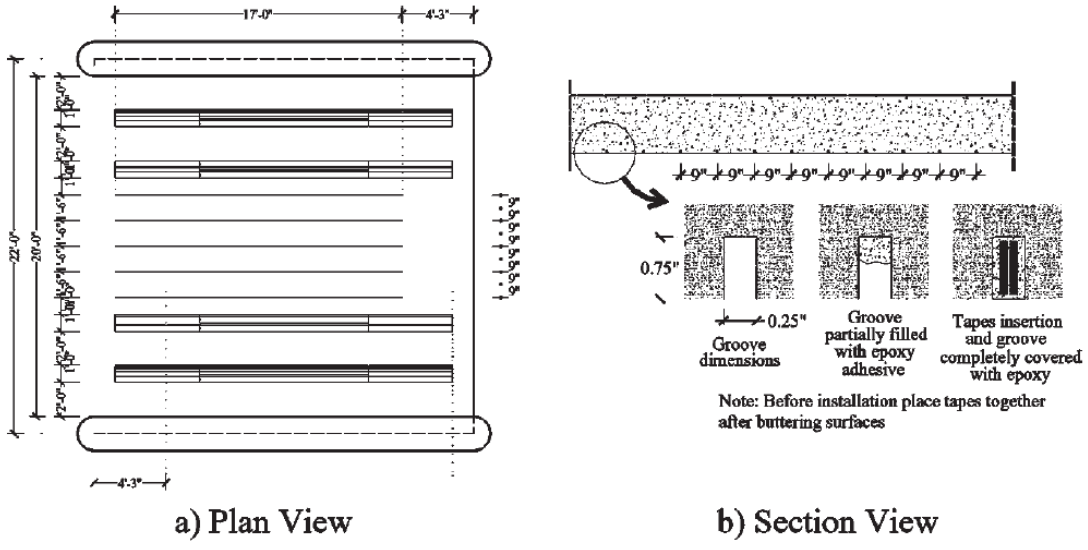

Figure 2.22 NSM FRP Strengthening Scheme on Span 2 of the Martin Spring Outer Road Bridge (Casadei et al. 2003)

Static load tests were performed on the bridge, before and after strengthening. Figure 2.23 shows the change in midspan deflection before and after strengthening.

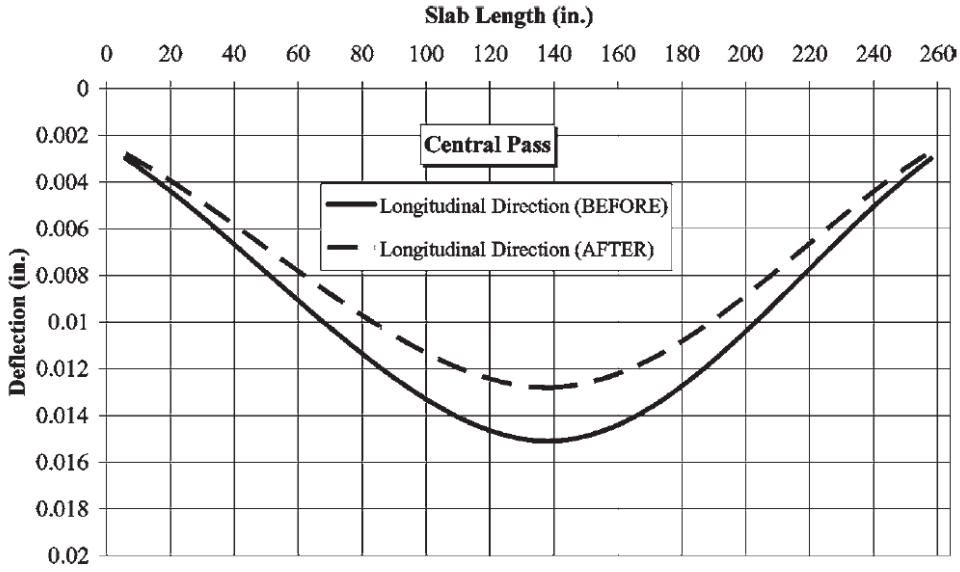

Figure 2.23 Center Line Deflection of the Martin Spring Outer Road Bridge (Casadei et al. 2003)

According to Figure 2.23, the strengthening system reduced midspan deflections by about 13%. This study also included finite-element modeling of the bridge, which very closely resembled the results of the load test. Therefore, this application concluded that NSM FRP is a feasible solution for strengthening reinforced concrete bridges and also that load testing of a retrofitted bridge, before and after strengthening, is a useful method for verifying increased strength (Casadei et al. 2003).

2.3.3 Summary of NSM FRP Research

After reviewing these published studies, it is evident that NSM FRP is a feasible, innovative solution to strengthen reinforced concrete structures. Documented specimens exhibited increased ultimate load carrying capacity in all cases. It is important to follow ACI 440 or other design methods to prevent premature bond failures (El-Hacha and Rizkalla 2004). When

following proper design methods, field testing of strengthened structures did not display any signs of epoxy bond or NSM FRP failure (Tumialan, Vatovec, and Kelley 2007; Bergström, Täljsten, and Carolin 2009; Casadei et al. 2003).

2.4 Previous NSM FRP Research of the Letohatchee Bridge

The Letohatchee bridge NSM FRP retrofit project began with an study of design methods and previously published FRP testing by Alexy (2009). After the design was determined by Alexy (2009), a laboratory testing program was conducted by Bertolotti (2012). Results from both of these phases of the Letohatchee bridge project led to the field application of NSM FRP.

2.4.1 Letohatchee Bridge NSM FRP Retrofit Design (Alexy 2009)

Alexy (2009) studied NSM FRP retrofit design methods for the Letohatchee bridge. Several design methods were used to compare design and experimental capacities of strengthened members that were previously tested. The design methods varied between two debonding failure mecahnisms: plate-end (PE) debonding and intermediate crack (IC) debonding. Plate-end debonding refers to failure caused by development of shear stresses at the edges of FRP that causes either the FRP strip or epoxy layer to peel off of the concrete member. Intermediate crack debonding refers to failure due to separation of the FRP from the concrete due to stresses formed at a flexural crack in the concrete. IC-debonding spreads from the crack to the edges of the FRP reinforcement (Vasquez Rayo 2008). Figure 2.24 and Figure 2.25 show illustrations of plate-end and intermediate crack debonding failures.

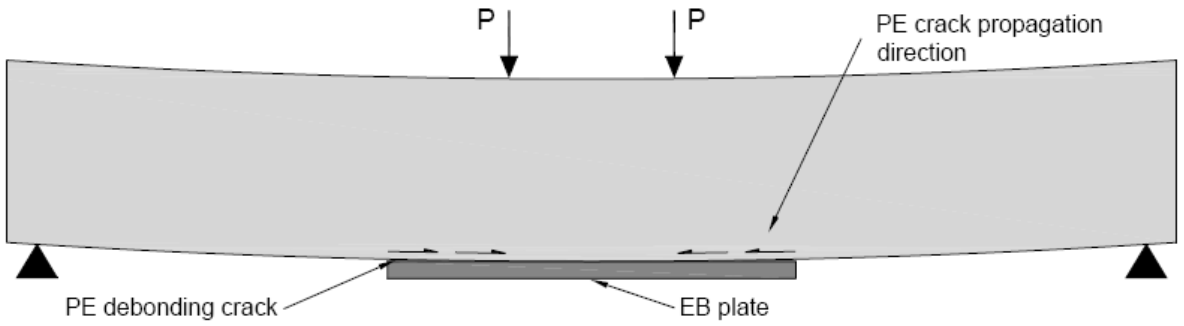

Figure 2.24 Illustration of Plate-End Debonding Failure (Vasquez Rayo 2008)

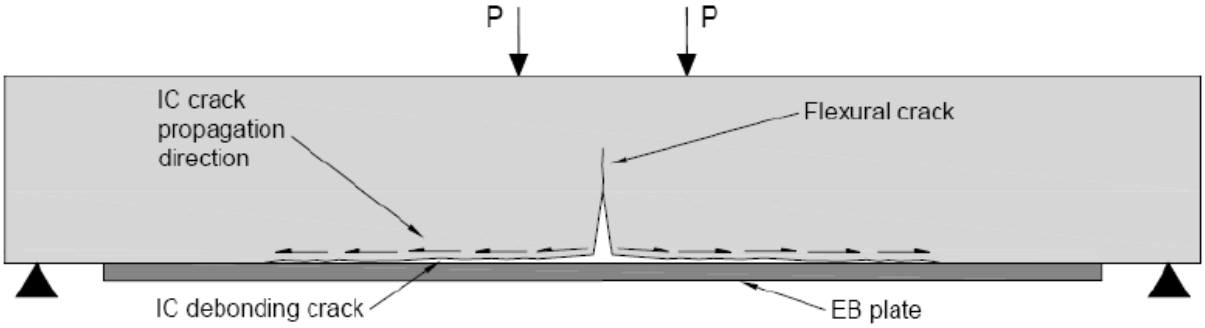

Figure 2.25 Illustration of Intermediate Crack Debonding Failure (Vasquez Rayo 2008)

Alexy (2009) determined that the three methods that provided the most accurate results were ACI 440 (2008), Standards Australia (2008), and Seracino et al. (2007). In all three of these methods, the design predicted intermediate crack debonding failure that closely corresponded with the previously tested specimens. Therefore, because these were the most accurate methods, Alexy (2009) used all three to determine the proposed strengthening design for the Letohatchee bridge.

Analysis of the existing structure and its deficiencies was required to propose an approriate NSM FRP retrofit of the Letohatchee bridge. Flexural demands on the bridge were evaluated using the Bridge Rating and Analysis of Structural Systems (BRASS™) program. Then the capacity of the bridge was calculated and deficient regions were located. Figure 2.26

shows an elevation view of the Lethotachee bridge with areas of deficiency indicated. Further detail on the Letohatchee bridge deficiencies are documented in Chapter 3.

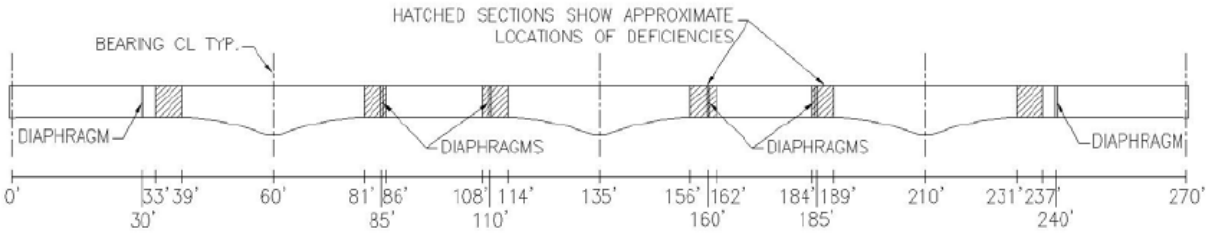

Figure 2.26 Approximate Locations of Deficiencies in the Letohatchee Bridge (Alexy 2009)

Layouts of the NSM FRP retrofit for the Letohatchee bridge were determined based on ACI 440, Standards Australia, and Seracino et al. (2007). However, Alexy (2009) found that there were two significant concerns with his comparisons between previously published experimental results and NSM FRP design methods. Reinforcement ratios and concrete compressive strengths for the Letohatchee bridge were less than most of the previous experimental specimens, and none of the previously tested specimens were cracked prior to NSM FRP strengthening. Therefore, Alexy (2009) proposed a laboratory testing program with four objectives:

- Develop a relationship between the proposed test specimens and the Letohatchee bridge to more effectively and more efficiently propose an NSM FRP-strengthening scheme for the bridge.
- Study intermediate cracking debonding to quantify if and when IC-debonding failure will occur.
- Study the effects of the concrete compressive strength, amount of steel reinforcement, amount of FRP reinforcement, and cross-sectional shape on the strengthened moment capacity.

- Evaluate the effectiveness of the FRP in a realistic strengthening application by cracking the unstrengthened specimens before applying the FRP (Alexy 2009).

2.4.2 NSM FRP Laboratory Testing Program (Bertolotti 2012)

Bertolotti (2012) conducted a portion the laboratory testing program outlined by Alexy (2009). The testing program involved eight specimens fabricated with Grade 40 reinforcement and 3000 psi (20 MPa) concrete. The specimens were split into two groups based on steel reinforcment ratio (ρ_s). In each group there was a control beam and the three remaining beams were strengthened with varying FRP reinforcement ratios (ρ_f). Figure 2.27 shows the reinforcment ratios that were used in the laboratory testing program.

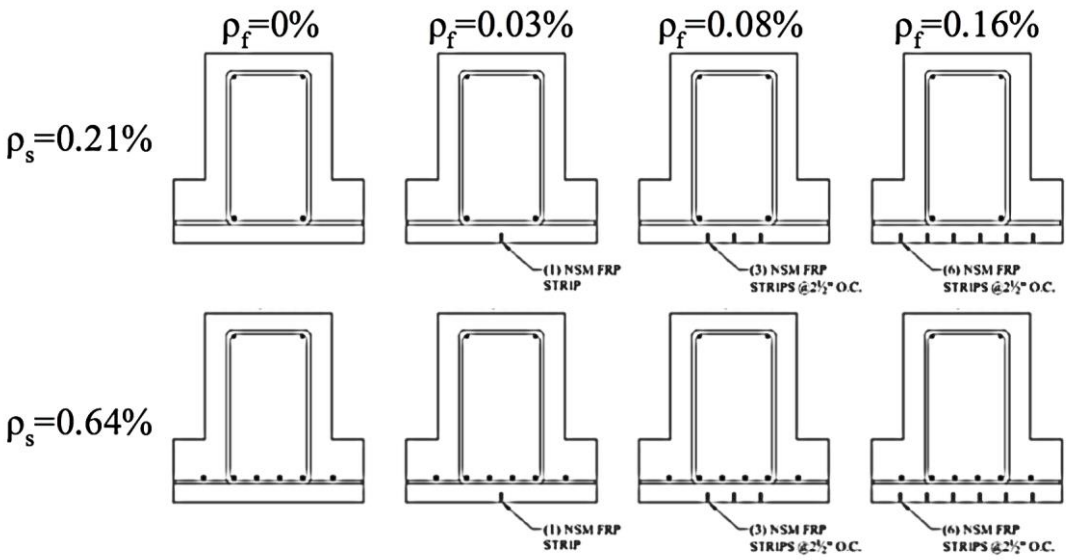

Figure 2.27 Laboratory Testing Program Specimens (Adapted From Bertolotti 2012)

The laboratory testing program specimens were cracked under service level loads prior to strengthening with NSM FRP strips. The beam that most closely resembled the proposed Letohatchee bridge strengthening scheme was the specimen with a steel reinforcement ratio of 0.21% and a FRP reinforcement ratio of 0.03%. The variety of steel and FRP reinforcement

ratios allowed Bertolotti (2012) to study the effects of NSM FRP retrofits on beams with different properties and the effect of different FRP reinfocement ratios on a retrofit.

Bertolotti (2012) found that the increase in flexural strength and bond strength both outperformed the design predictions according to ACI 440 and Standards Australia (SA). The strengthened beams performed according to standard reinforced concrete flexural analysis expectations if a perfect bond condition was achieved. In consideration of the perfect bond condition, it is assumed that there is no bond failure. The increase in flexural strength and strain at failure for the beams with a steel reinforcement ratio of 0.21% is shown in Figure 2.28 and Figure 2.29, respectively.

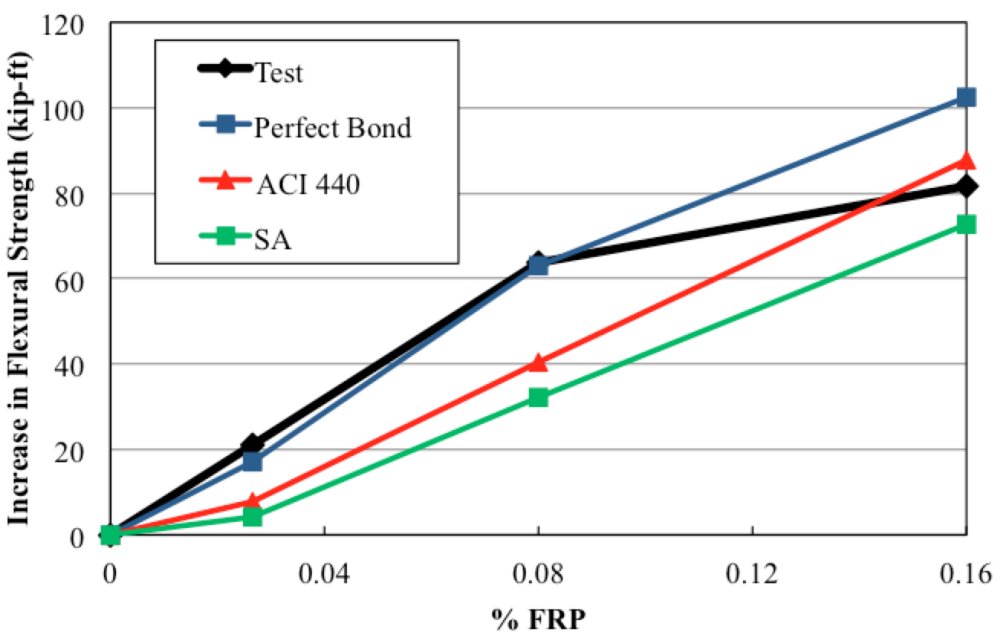

Figure 2.28 Increase in Flexural Strength at FRP Reinforcement Ratios for ρ_s=0.21% (Bertolotti 2012)

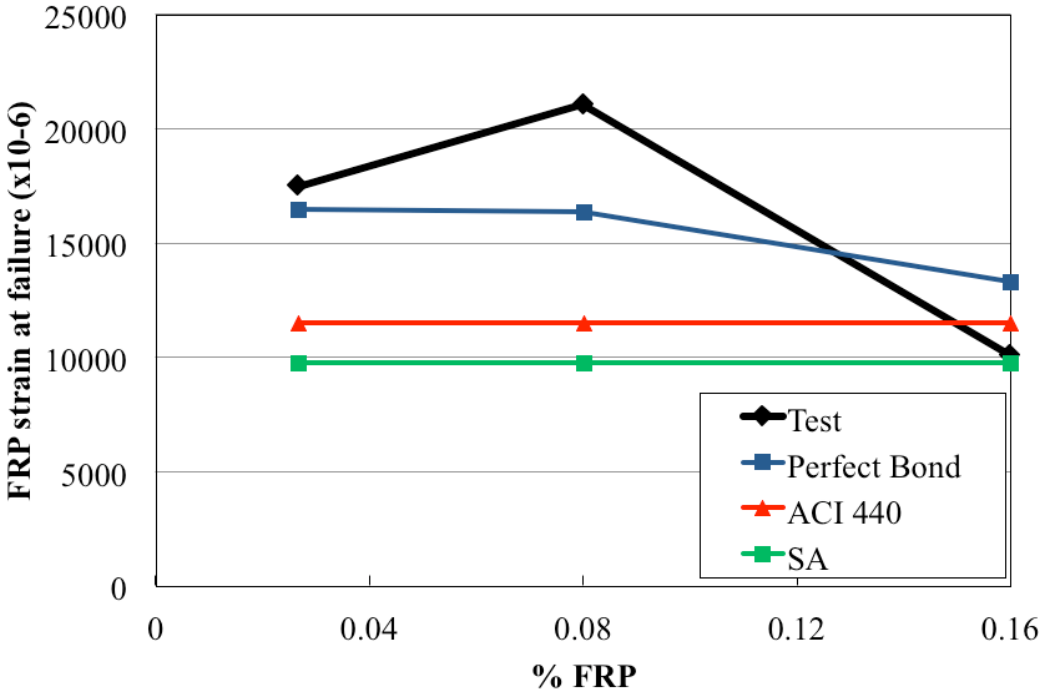

Figure 2.29 FRP Strain at Failure at FRP Reinfocement Ratios for ρ_s=0.21% (Bertolotti 2012)

The results indicated that there was no bond degradation during the laboratory testing program, as all FRP reinforcement performed close to expectations of the perfect bond condition. Therefore, there was no evidence of IC-debonding failure mechanisms. Failure occurred due to crushing of the concrete in the test specimens with 0.03% and 0.08% FRP reinforcement ratios. However, there was a discrepancy in the data at the FRP reinfocement ratio of 0.16%. This was due to a shear failure in the beam before a flexural failure could be achieved. Figure 2.30 shows this beam and the shear failure that occurred during laboratory testing.

Figure 2.30 Shear Failure of Beam with 0.21% Steel and 0.16% FRP Reinforcement Ratios (Bertolotti 2012)

Bertolotti's results indicate that NSM FRP retrofit is a very effective technique to increase flexural capacity of cracked beams. There was no evidence of bond degradation and NSM FRP strengthening outperformed design expectations. Therefore, Bertolotti's laboratory testing provided promising results for NSM FRP strengthening of cracked reinforced concrete beams and verified Alexy's proposed NSM FRP retrofit for the Letohatchee bridge (Bertolotti 2012).

2.5 NSM FRP Retrofit Analysis Technique

The Letohatchee bridge is an active bridge over I-65 in Lowndes County, Alabama. Therefore, it was desired to record data using nondestructive techniques without interfering with traffic below and over the bridge. This was achieved by implementing analysis techniques based on fundamental principles of reinforced concrete design.

2.5.1 Linear-Elastic Flexural Response of Cracked Reinforced Concrete

Reinforced concrete structures are expected to crack when exposed to service loads during normal use, and are designed based on this expectation. Flexural cracking occurs when tensile stresses in the member exceed the tensile capacity of the concrete. Therefore, a crack will develop at any point where the concrete tensile capacity is exceeded. Tensile stresses develop in the steel reinforcement to resist the tension no longer resisted by the concrete. Cracking will continue until a stable crack pattern has developed. This occurs when reinforcing steel reaches critical stress, typically around 20–30 ksi (140–205 MPa) (Broms 1965; Clark 1956; Frosch 1999). When critical stress is reached, reinforcing steel stress is below its yield stress. Until reaching the yield stress, steel reinforcement behaves elastically, or deforms with imposed stresses and returns to its original condition when the stress is removed. Therefore, steel reinforcement is within its elastic range of behavior when cracking occurs.

While there are no concrete stresses under service loads at cracks on the tension face, concrete develops compressive stresses on the opposite side of the neutral axis. Concrete compressive stresses under service loads exhibit linear behavior, from zero at the neutral axis to the maximum concrete compressive stress at the extreme compressive fiber. This phenomenon of reinforced concrete is known as linear-elastic behavior and is shown in Figure 2.31.

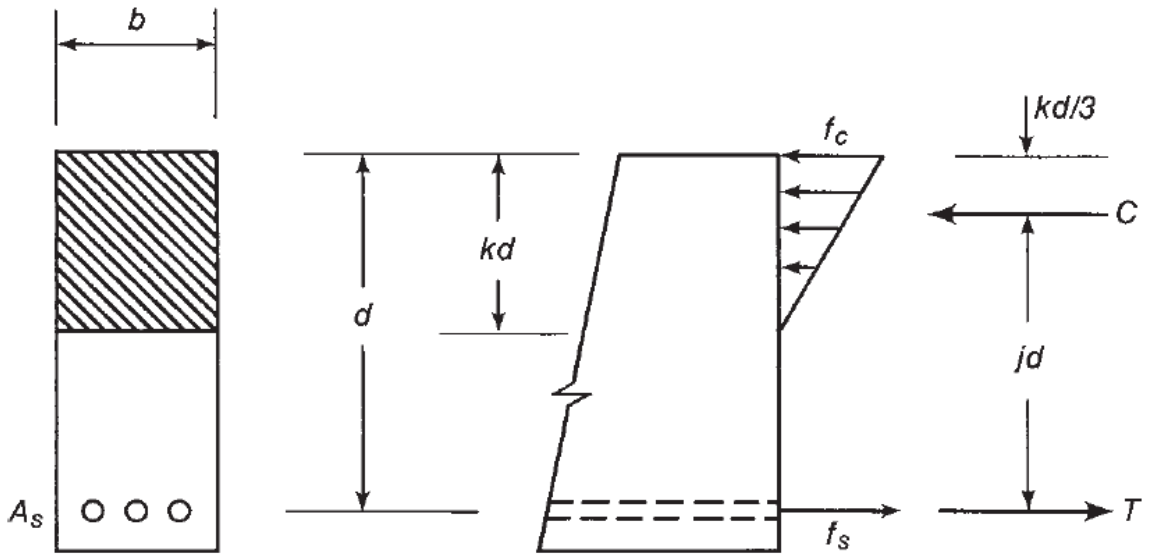

Figure 2.31 Post-Cracking Linear-Elastic Stress Profile (Wight and MacGregor 2012)

Linear-elastic behavior is valid for analysis of reinforced concrete members under service level loadings. Therefore, the Letohatchee bridge is analyzed according to principles of linear-elastic analysis. Linear-elastic analysis is based on the two assumptions of elastic bending—strains are linearly distributed through the member depth and stresses can be determined from strains according to Hooke's law (Wight and MacGregor 2012), or

$$\boldsymbol{\sigma = E\varepsilon} \qquad \textbf{\textit{Equation 2.1}}$$

where σ is stress; E is the modulus of elasticity; and ε is strain (Hibbeler 2011). Therefore, elastic bending stress can be calculated according to Equation 2.2,

$$\boldsymbol{\sigma = \frac{My}{I_{cr}}} \qquad \textbf{\textit{Equation 2.2}}$$

where M is the bending moment; y is the perpendicular distance from the neutral axis to the point where calculating stress; and I_{cr} is the cracked-section moment of inertia of the cross section about the neutral axis.

Therefore, tensile stresses in reinforced concrete cause cracking in the concrete. Typical flexural cracking of a reinforced concrete member is shown in Figure 2.32.

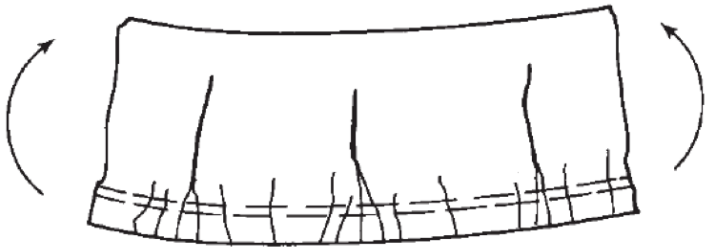

Figure 2.32 Cracking Due to Bending Stresses (Wight and MacGregor 2012)

At cracks, stress and strain in the concrete is zero, and reinforcing steel reaches its highest stress and strain. However, at midpoints between cracks, concrete reaches its maximum tensile stress and strain, because the bond results in shared tension between concrete and steel. Therefore, crack widths are described as the difference in steel and concrete elongation over a discrete length, expressed by Wight and MacGregor (2012) as,

$$w = \int_A^B (\varepsilon_s - \varepsilon_c) dx \qquad \textit{Equation 2.3}$$

where w is crack width; A and B are the start and end point of the beam length under consideration, respectively; and ε_s and ε_c are the strain in the concrete and steel, respectively. A crack opening displacement measured at a crack could be considered as representative of a change in strain in the steel. Further investigation into crack width theory verifies this assumption.

2.5.2 Crack Width and Crack Spacing Theory

Historically, there has been conflicting information regarding variables affecting crack widths. This is because many studies involve specimens of different characteristics and conditions (Gergely and Lutz 1968). However, in 1965, Bengt Broms began a study to obtain a fundamental method of calculating crack width and crack spacing. Gergely and Lutz (1968)

conducted further investigation of reinforced concrete cracking with statistical analysis, which built upon Broms's research and led to ACI 318 Building Code crack control requirements.

Broms (1965) tested reinforced concrete members in tension and flexure to study cracking patterns. He first states that cracking occurs when tensile stresses in concrete exceed the tensile capacity of the concrete. Broms also asserts that stress distribution of a cracked flexural member can be approximated according to linear-elastic theory. Cracking can be modeled by circular, high tensile stress areas, surrounded by areas of low compressive or tensile stresses, as show in Figure 2.33.

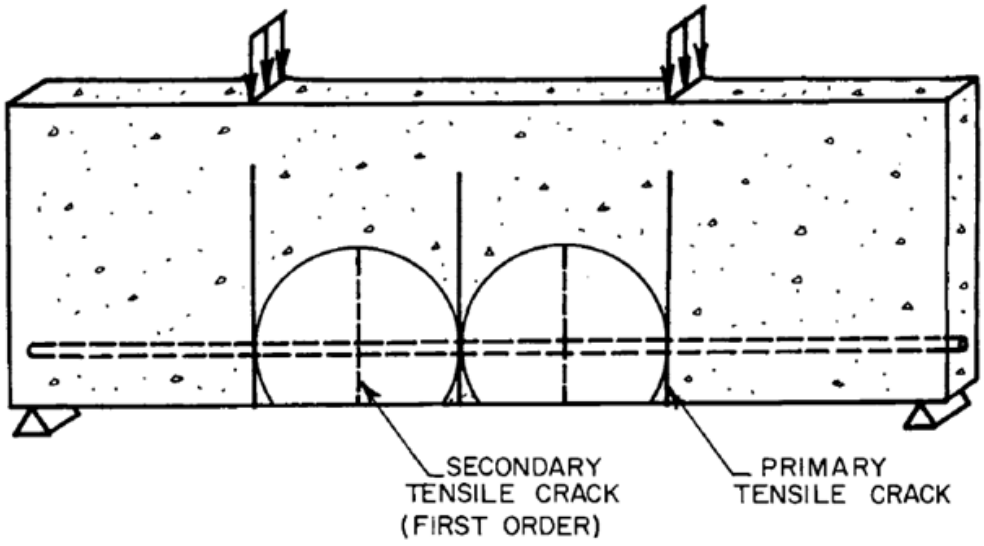

Figure 2.33 Tensile Circles Demonstrating Mechanics of Tension Cracking in Flexural Members (Broms 1965)

Further cracking will occur where the largest tensile stresses are located, or at midpoints between existing cracks. This phenomenon is further illustrated in Figure 2.34.

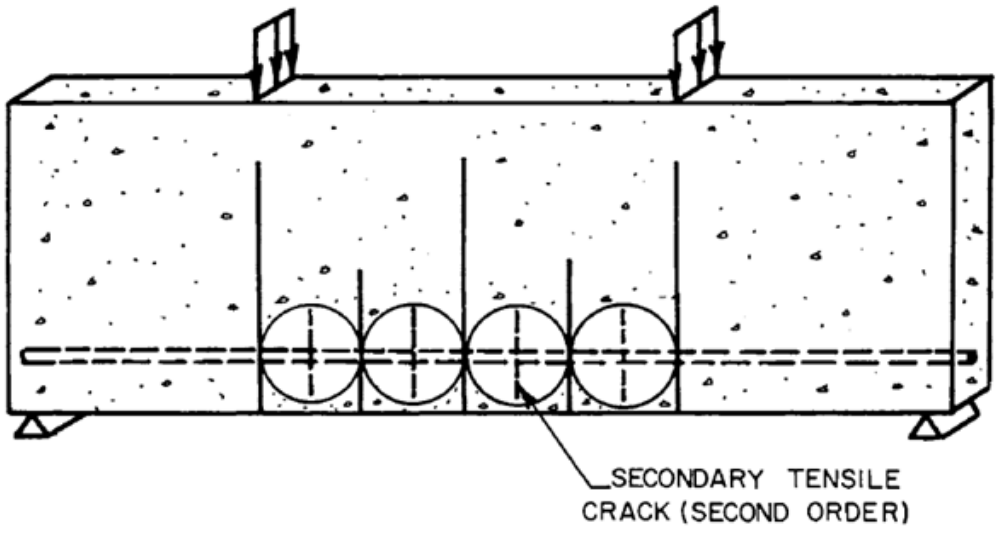

Figure 2.34 Tensile Circles Demonstrating Mechanics of Tension Cracking in Flexural Members (Broms 1965)

Broms also observed that crack width was larger at the level of the extreme tension fiber than at the level of the tension reinforcement. Crack widths of specimens observed in this test are shown in Figure 2.35.

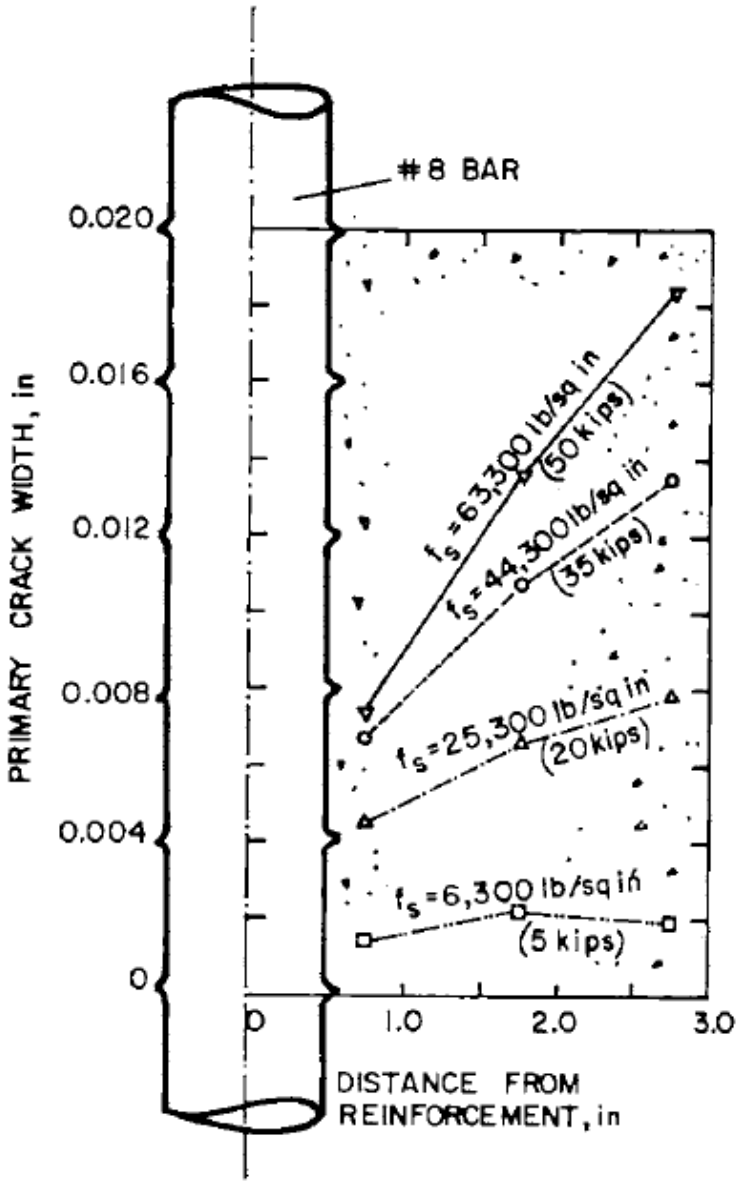

Figure 2.35 Primary Crack Width as Cracks Approach the Exterior Face (Broms 1965)

Therefore, Broms concluded that crack widths are based on distance from the tensile reinforcement. Based on these findings, Broms proposed a correction factor, *R*, for strain measurements taken at the tension face of the member. This resulted in Broms's equation for maximum crack width at the tensile face of a member as,

$$w_b = 4t_b R\varepsilon_s \qquad \textit{Equation 2.4}$$

where w_b is maximum tensile crack width at the tension face; t_b is the distance from the tensile face to the nearest reinforcing bar; and R is the correction factor for measurements taken at the tensile face of the member, calculated according to,

$$\boldsymbol{R = \frac{h_2}{h_1}} \qquad \textbf{\textit{Equation 2.5}}$$

where h_1 and h_2 are the distances from the neutral axis to the centroid of the tensile reinforcement and the extreme tension fiber, respectively. Therefore, if the strain measurement was recorded at the level of the reinforcing steel, the correction factor, R, would be 1.0 and Equation 2.4 would simplify to,

$$\boldsymbol{w = 4 t_b \varepsilon_s} \qquad \textbf{\textit{Equation 2.6}}$$

where w is the maximum tensile crack width at the centroid of the tensile reinforcement. The variables used in Broms's calculation of maximum crack widths are shown in Figure 2.36.

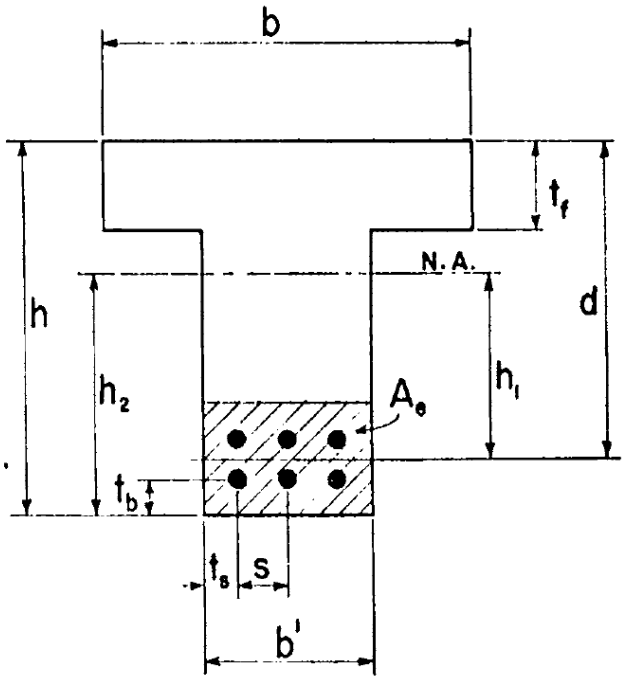

Figure 2.36 Broms's Strain Equation Dimensional Notation (Gergely and Lutz 1968)

After Broms's results were published, Gergely and Lutz (1968) conducted a statistical evaluation of six different crack width investigations to better understand reinforced concrete cracking. Through evaluation of 106 specimens and 632 cracks, they determined the most probable variables effecting crack widths and developed equations to describe the results. Steel stress was determined to be the most important variable, as established by Broms (1965). They also stated that other factors affecting cracking were the number of bars, cover, and effective area of concrete—or the area of concrete adjacent to reinforcement with the same centroid.

Gergely and Lutz also observed that crack widths increase along the strain gradient, and is largest at the level of the extreme tension fiber. Therefore, they adopted Broms's strain correction factor, *R*, into their proposed crack width equations to convert strain measurements at the tension face to the level of the tension reinforcement.

The research presented by Broms and Gergely and Lutz established the basis for determining and studying crack widths of reinforced concrete. Based on their observations, changes in crack opening displacements on the tension face of a member can be used to monitor changes in the tension reinforcement.

CHAPTER 3:LETOHATCHEE BRIDGE BACKGROUND

3.1 Bridge Description

The Letohatchee bridge on AL 97 over I-65 near Letohatchee, Alabama, was built in 1965 in Lowndes County. This bridge is a continuous, reinforced concrete, deck-girder bridge that was built according to Standard Drawing No. IC 2806 and is ALDOT BIN 8847. The location and Letohatchee bridge are shown in Figure 3.1 and Figure 3.2, respectively.

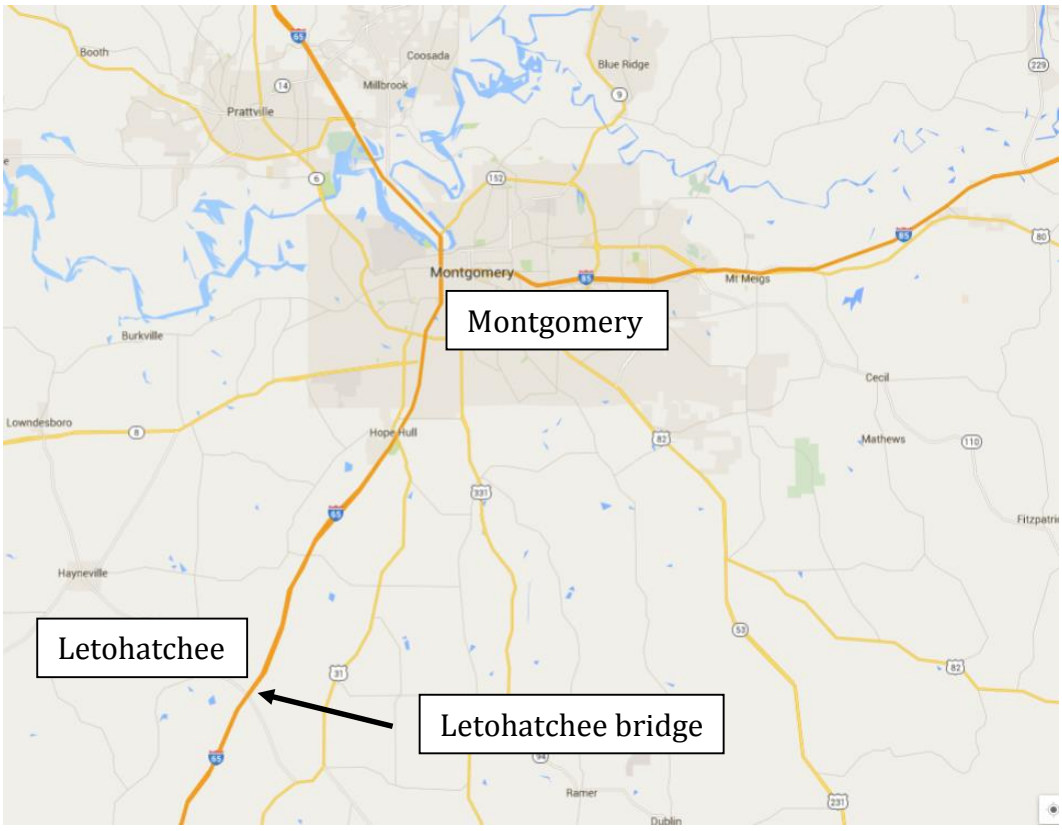

Figure 3.1 Location of Letohatchee Bridge (Google Maps 2015)

Figure 3.2 Letohatchee Bridge (Lowndes County, Alabama)

The Letohatchee bridge is 270 ft (82.3 m) long and consists of four spans constructed at a 12-degree skew angle. The exterior spans are 60 ft (18.3 m) and interior spans are 75 ft (22.9 m) in length. The bridge consists of four continuous, reinforced concrete girders with parabolic haunches at interior supports. The bridge deck is 6 ¼ in. (159 mm) thick with a roadway width of 28.0 ft (8.5 m). Girders are spaced at 8.0 ft (2.4 m) laterally, and the curb is located 2.0 ft (0.6 m) from the centerline of the exterior girder on each side of the bridge. A simplified plan and cross-sectional view of the bridge is shown in Figure 3.3 and Figure 3.4, respectively.

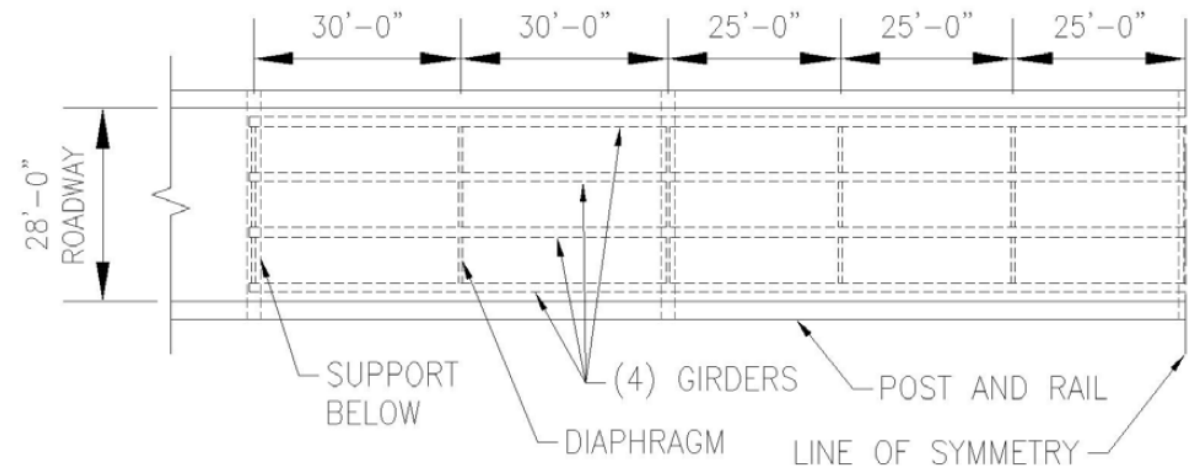

Figure 3.3 Simplified Plan View Showing Half of the Letohatchee Bridge (Alexy 2009)

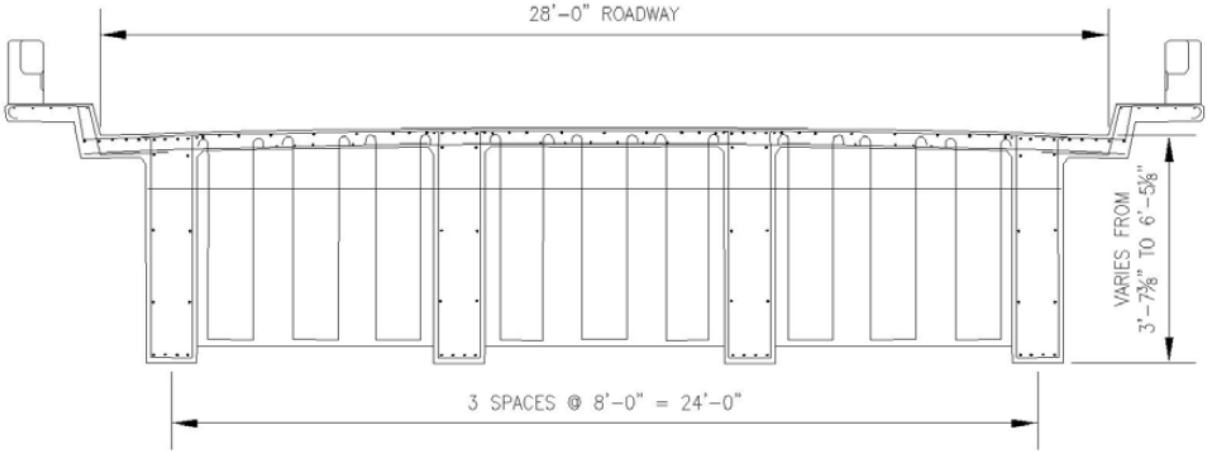

Figure 3.4 Cross Section at an Interior Support (Alexy 2009)

3.2 Bridge Deficiencies

In 2009, Alexy documented analysis of the Letohatchee bridge by ALDOT Bridge Rating and Load Testing engineers using the Bridge Rating and Analysis of Structural Systems (BRASS™) program (Wyoming Department of Transportation 2009). This analysis was completed in accordance with the *AASHTO Standard Specifications for Highway Bridges* (1996). Strength capacity of the Letohatchee bridge was determined by analysis of the bridge as

documented in the original plans, with an estimate of 3000 psi (20 MPa) concrete and 40,000 psi (280 MPa) reinforcing steel due to the age of the structure (Alexy 2009).

Alexy discovered that this bridge type has greater demand than the available factored resistance at some areas along the bridge. Moment envelopes for demand due to posting trucks are shown in Figure 3.5, along with resistance envelopes. Posting trucks are trucks that appear on ALDOT load-posting signs throughout Alabama, as shown in Figure 3.6.

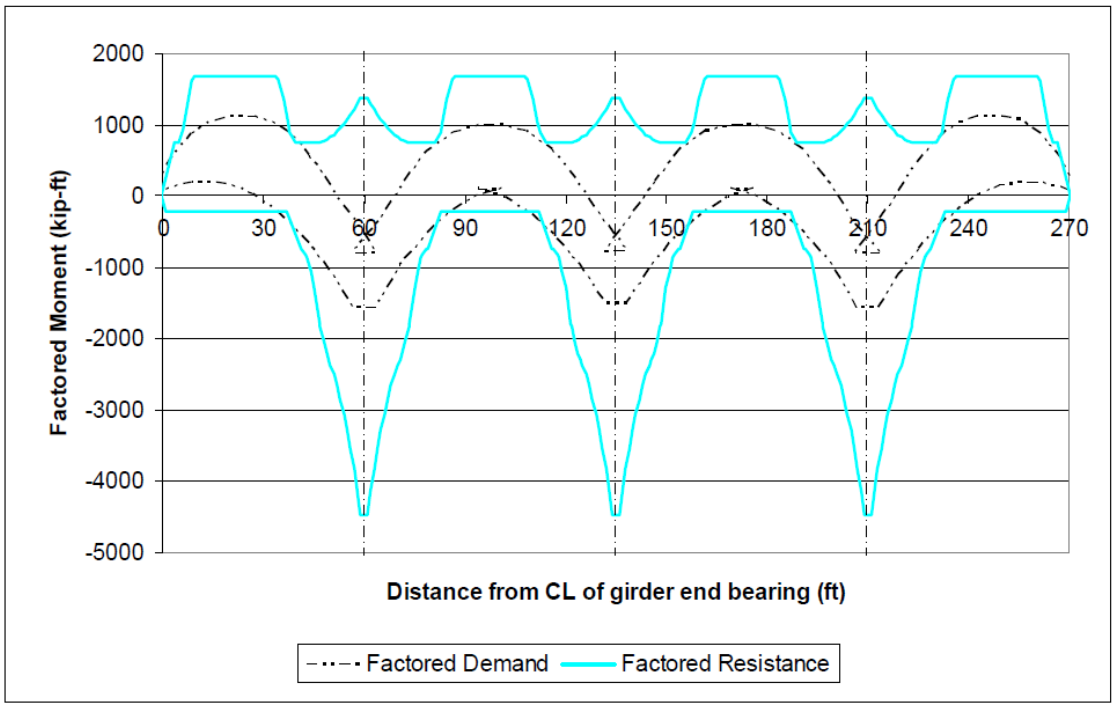

Figure 3.5 Factored Demand versus Factored Resistance for Posting Trucks (Alexy 2009)

Figure 3.6 Typical ALDOT Load-Posting Sign (Alexy 2009)

Positive- and negative-moment deficiencies were identified through this analysis at around 20 ft (6.1 m) from each bent, as evident in Figure 3.5. Alexy indicated that the positive moment deficiency was neglected for this project because it is less than 6% and occurs over such a small region (2009). However, negative-moment deficiencies were significant, especially in the exterior spans where the greatest deficiencies occur. Alexy determined a required increase of about 55% in these areas, or a need for an increase in flexural capacity from 226.0 kip-ft (306.4 kN-m) to 350.0 kip-ft (474.5 kN-m). Each zone of negative-moment deficiency occurred over a 7 ft (2.1 m) length, beginning 21 ft (6.4 m) from all interior supports, as shown in Figure 3.7.

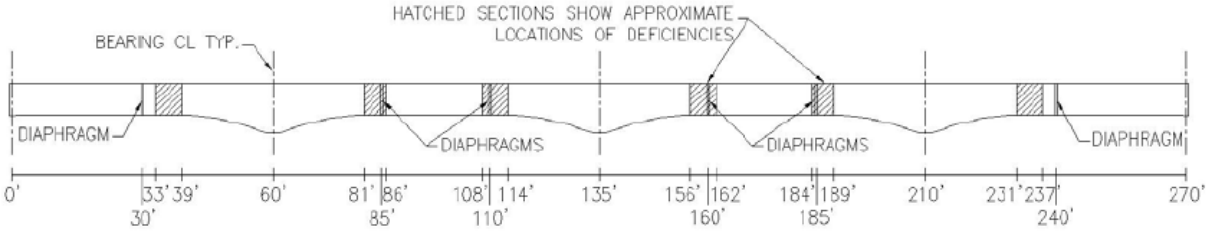

Figure 3.7 Approximate Locations of Flexural Deficiencies in the Letohatchee Bridge (Alexy 2009)

Examination of areas of negative-moment deficiency reveals an inadequate amount of negative-moment reinforcement in the areas between interior supports and midspan. Figure 3.8

shows a typical girder with distances from the centerline of the interior support indicating termination points of negative-moment reinforcement and the deficient region of the girders.

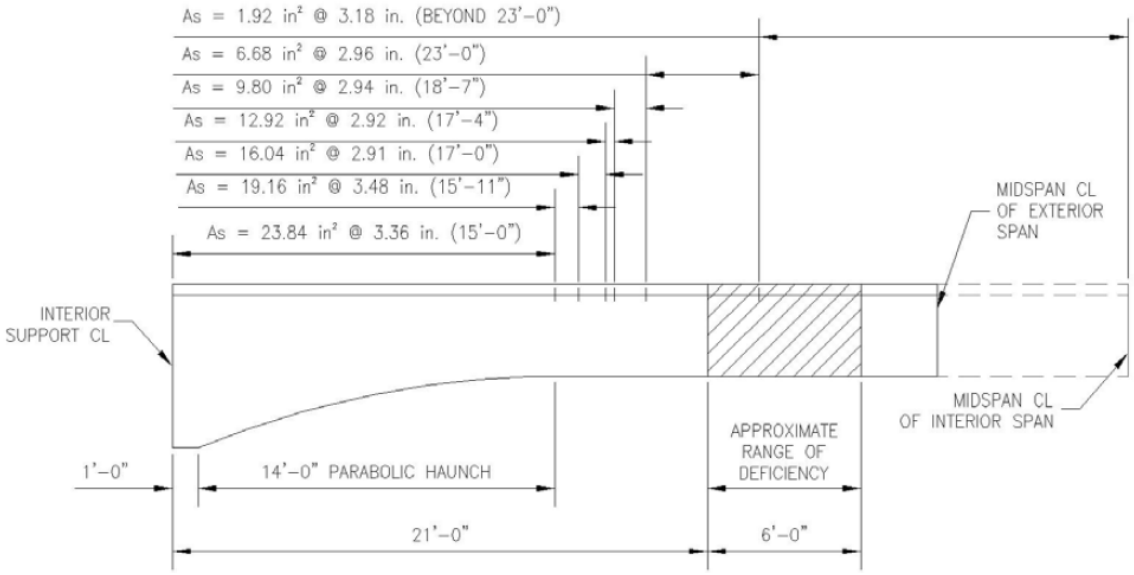

Figure 3.8 Bar Termination Points and Deficient Region Location from Interior Supports (Alexy 2009)

Figure 3.8 indicates that the deficiency in the Letohatchee bridge is due to premature termination of negative-moment reinforcement in areas about 21 ft (6.4 m) from interior supports. Therefore, this project was designed to address the lack of negative-moment reinforcement in this area of transition between positive- and negative-moment regions.

A NSM FRP strengthening technique, as proposed by Alexy (2009) and Bertolotti (2012) was implemented to alleviate the deficiencies in the Letohatchee bridge. The strengthening method is detailed in Chapter 4, followed by a discussion of the bridge testing program in Chapter 5.

CHAPTER 4:BRIDGE RETROFIT CONSTRUCTION

4.1 Bridge Retrofit Overview

Retrofit of the Letohatchee bridge began on Monday, December 8, 2014, and was completed on Wednesday, January 21, 2015. Construction required 19 working days, although the project stretched 44 days including weekends, holidays, and weather delays. Construction began by first marking the layout of all FRP strip locations on the bridge deck. After the complete layout was established and checked by the ALDOT inspector on site, construction began in the northbound lane. The construction documents required that one lane be open at all times and that the first lane must be completed before beginning the second lane. Therefore, the northbound lane was completely finished before beginning the southbound lane.

4.2 Construction Documents

The Letohatchee bridge retrofit required creation of the special provision specification and project notes specific to the NSM FRP bridge retrofit. The specification was developed through review of the California Department of Transportation (CALTRANS) NSM FRP specification and previous Auburn University FRP bridge-strengthening research findings (CALTRANS 2012; Bullock, Barnes, and Schindler 2011; Carmichael and Barnes 2005). Bertolotti's (2012) research was used to develop the project notes. The resulting special provision and project notes that were developed for the Letohatchee bridge NSM FRP retrofit are located in Appendices B and C, respectively.

4.3 Retrofit Materials

The Letohatchee bridge retrofit required the contractor to use a specific type of FRP and epoxy for the project. FRP strips and epoxy were selected according to recommendations from Alexy (2009), and they were detailed in the construction documents for the retrofit.

4.3.1 FRP Reinforcement

FRP strips were Aslan 500 series #2 (6mm) CFRP Tape, produced by Hughes Brothers, Inc. (Hughes Brothers, Inc. 2011). Material cost (from the supplier) for the Aslan CFRP tape was about $3 per linear foot, or about $14,000 for the complete Letohatchee bridge retrofit. The project specifications from ALDOT required tensile strength no less than 300 ksi (2068 MPa) and modulus of elasticity no less than 18,000,000 psi (124 GPa) (Alabama Department of Transportation 2014). Tensile testing of the CFRP batch used for the retrofit exhibited an average tensile strength of 466 psi (3220 MPa) and an average modulus of elasticity of 24,300,000 psi (168 GPa) (Aslan FRP 2014). The full test report from Hughes Brothers is included in Appendix A. Rolls of FRP on site during the retrofit are shown in Figure 4.1.

Figure 4.1 Rolls of FRP Strips Before Installation

4.3.2 Epoxy

Epoxy for the Letohatchee bridge retrofit was Hilti HIT-RE 500 produced by Hilti, Inc. (Hilti Inc. 2014). Material cost for the Hilti epoxy was about $6 per linear foot, based on groove void dimensions, or about $31,000 for the complete Letohatchee bridge retrofit. The project specifications required this type of epoxy due to its known compatibility with the Aslan FRP (Hughes Brothers, Inc. 2011) and its successful use in the laboratory test phase (Bertolotti 2012) of the research study. Hilti HIT-RE 500 epoxy and the Hilti electric epoxy dispenser are shown in Figure 4.2 and Figure 4.3, respectively.

Figure 4.2 Hilti HIT-RE 500 Epoxy

Figure 4.3 Hilti Electric Epoxy Dispenser

4.4 FRP Strip Layout

Marking of FRP strip locations occurred on Monday, December 8, 2014. The length of the bridge deck was first measured to locate the midpoint of the deck. The midpoint of the bridge deck was determined to be located directly over the center bent due to symmetry of the bridge. After locating the center bent, locations of the two other bents were marked along the bridge deck. The curb along the bridge deck and the marked locations of all the three bents were used as references to mark FRP strip locations. Figure 4.4 shows marking of strip locations along the bridge deck during the retrofit.

Figure 4.4 Layout of FPR Strip Locations

Special attention to the construction documents was required to properly determine FRP strip locations on the bridge deck. Plans indicated FRP strip lengths along the 12 degree skew of the bridge and transverse FRP strip locations at a 0 degree skew, or square to the curb of the bridge, as shown in Figure 4.5 and Figure 4.6, respectively. Transverse location of the FRP strips were marked according to the geometry presented in the plans, as shown in Figure 4.7.

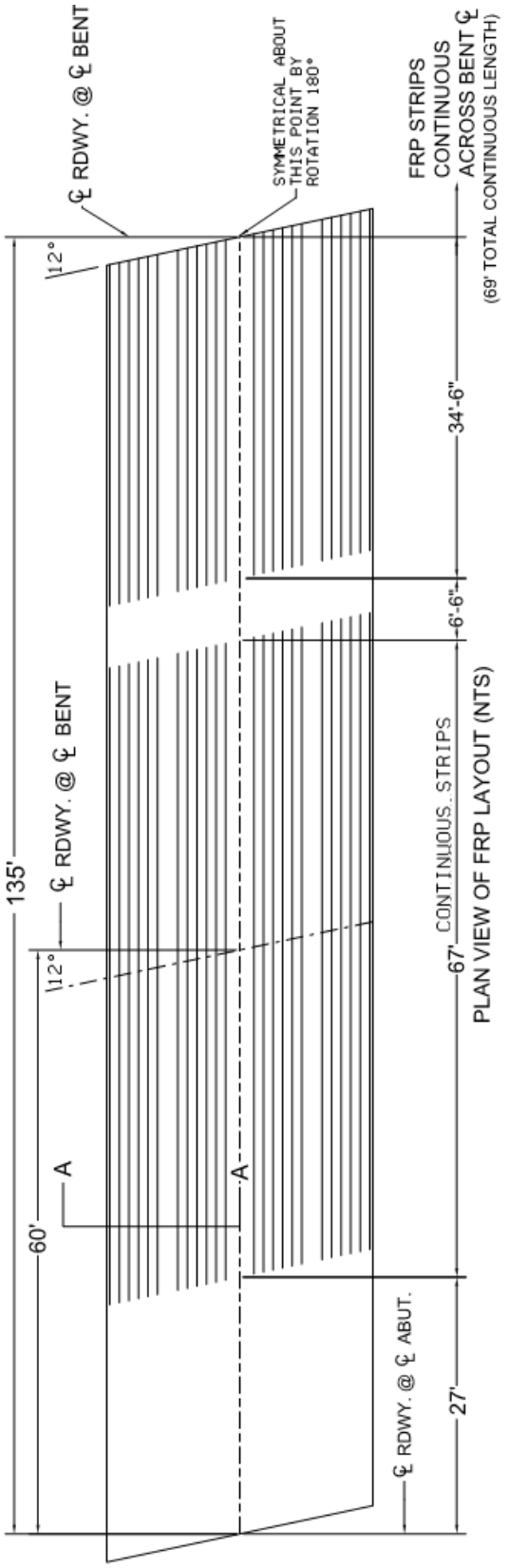

Figure 4.5 Plan View of FRP Layout (Alabama Department of Transportation 2014)

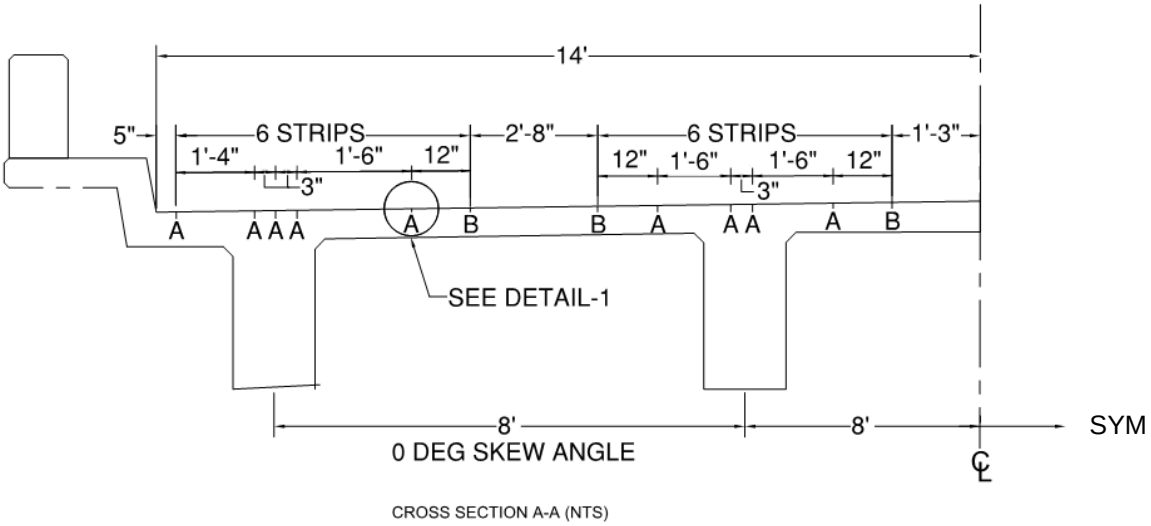

NOTE: REPEAT DESIGN FOR THE OTHER HALF OF THE CROSS-SECTION

A - Fixed location shall not be relocated without prior approval of the engineer

B - May be relocated laterally to avoid obstruction. The entire strip shall be shifted a uniform distance from the specified location, not to exceed 6 inches without prior approval of the engineer. Adjacent strips shall be spaced no less than 2 inches, center to center.

Figure 4.6 Cross Section View of FRP Strip Layout (Alabama Department of Transportation 2014)

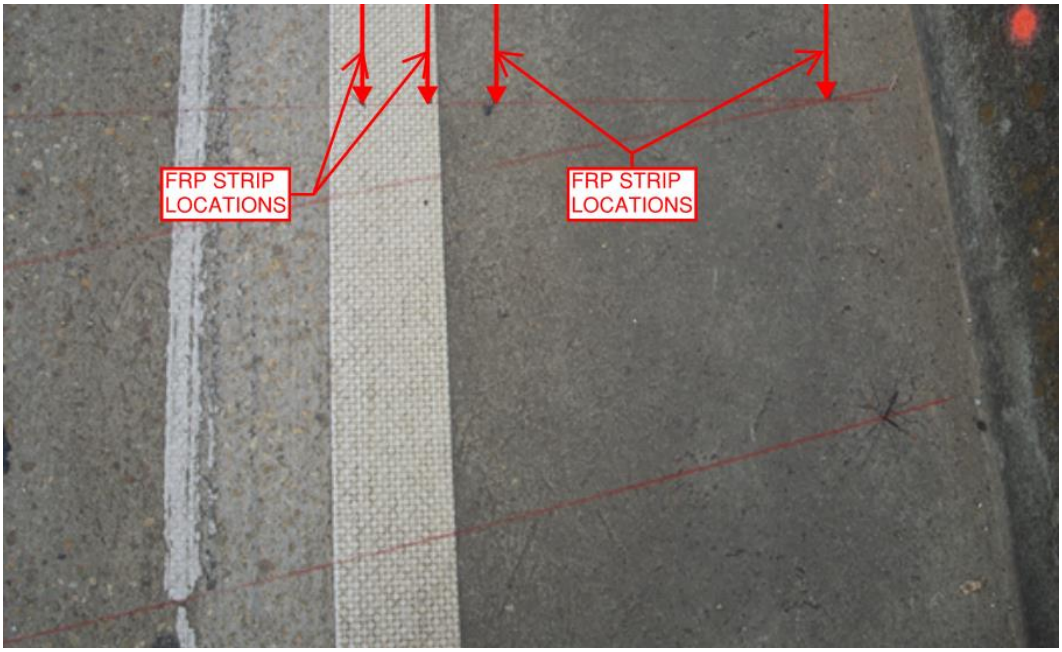

Figure 4.7 FRP Strip Locations and Endpoints

After marking all the strip locations, the contractor elected to mark the ends of each strip with a mag nail, as shown in Figure 4.8. This ensured that traffic and weather conditions would not cause loss of the FRP strip location endpoints once they were laid out.

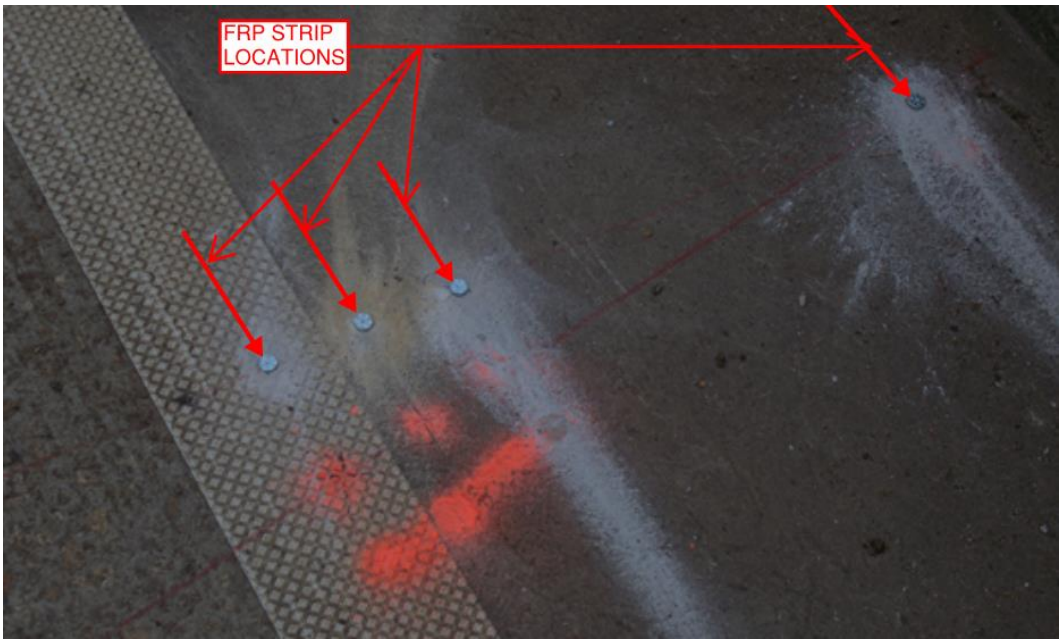

Figure 4.8 Mag Nails Marking FRP Strip Locations

Potential conflicts with strip locations were also addressed during the layout stage of the retrofit. Construction documents indicated that specific strips could be shifted up to 6 in. (15.3 cm) laterally from their designated position to avoid potential conflicts. Movable strips are located at the largest lateral distances from the face of the girders. Movable strips were limited to these specific strips to ensure that strips were not moved to the face of the girder, where inadvertent saw damage to the deck flexural reinforcement would have a significant detrimental effect on load carrying capacity of the deck slab. Movable strips are indicated as strip type “B” in the cross section shown in Figure 4.6.

For the Letohatchee bridge, there was a layout conflict with voids from cores that were previously cut in the southbound lane. Cores were cut during an exploratory investigation of the

bridge conducted by ALDOT and the AU HRC on Thursday, May 9, 2013, as shown in Figure 4.9.

Figure 4.9 Coring of the Letohatchee Bridge

Cores were used to check crack widths in the deck and calibrate ground penetrating radar (GPR) equipment. Crack widths were less than 0.01 in. prior to installation of the retrofit, and GPR was used to measure deck reinforcing steel cover and locate potential bar conflicts with FRP strips prior to installation of the retrofit. Figure 4.10 shows GPR data from the Letohatchee bridge with an overly of FRP strip locations. Areas of low concrete cover were identified from GPR data. This information was used to adjust the transverse position of several of the FRP strips during the final design phase. No conflicts with deck reinforcing steel were encountered during the groove cutting portion of the FRP installation.

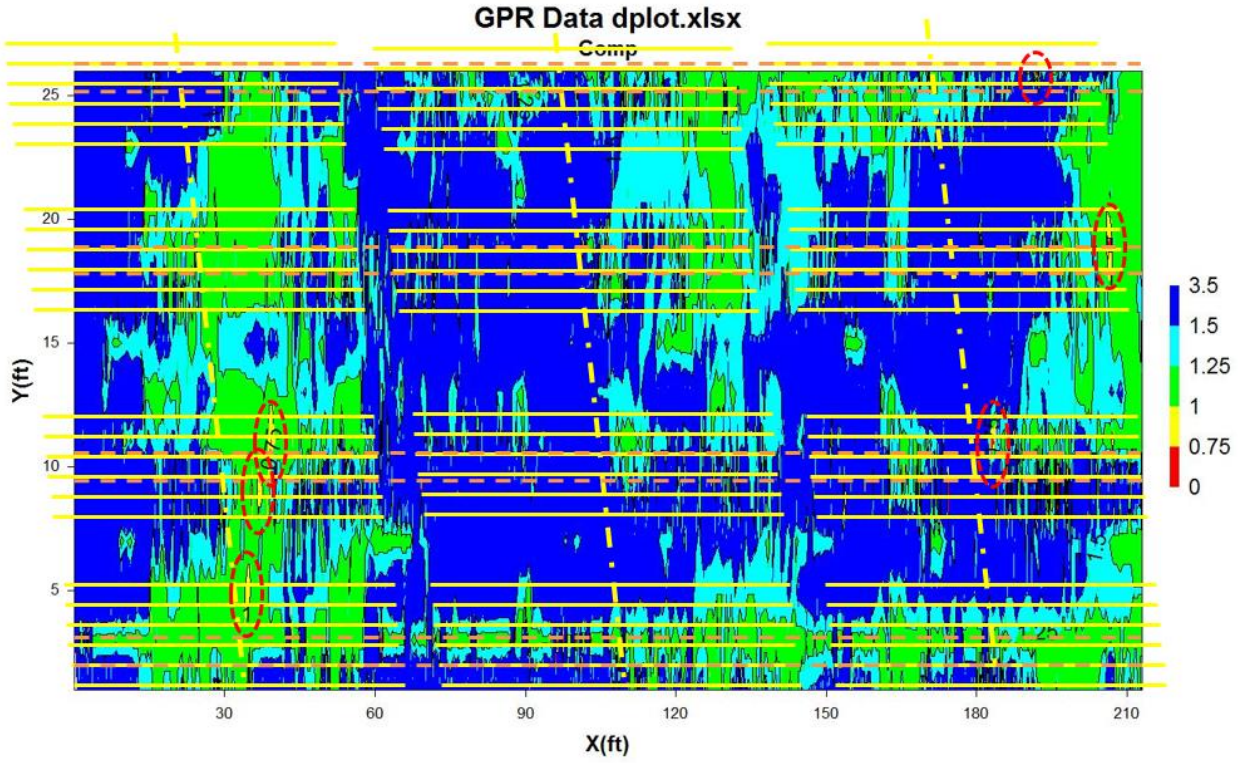

Figure 4.10 Ground Penetrating Radar of the Letohatchee Bridge

Core locations in the southbound lane were crossed by the outermost strip of the interior girder in both exterior spans of the bridge. Locations of core conflicts are shown in plan and cross sectional views in Figure 4.11 and Figure 4.12, respectively. A picture of the conflict during layout on the bridge is shown in Figure 4.13.

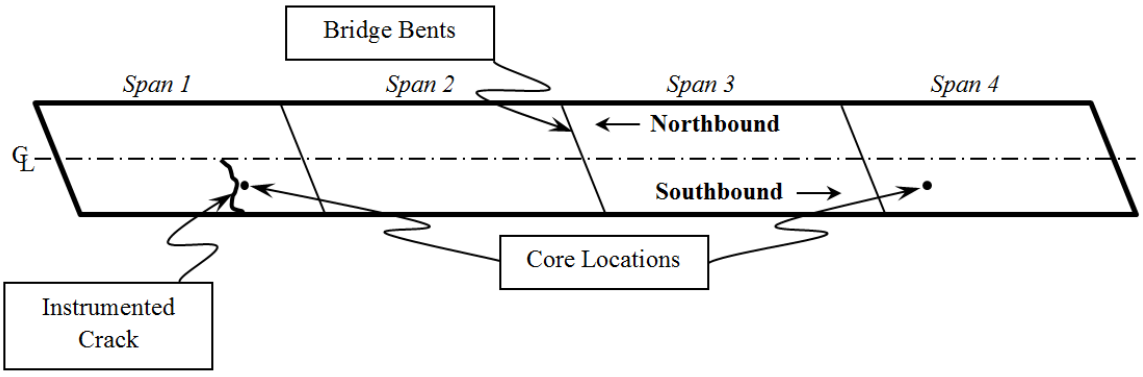

Figure 4.11 Plan View of Core Conflict Locations

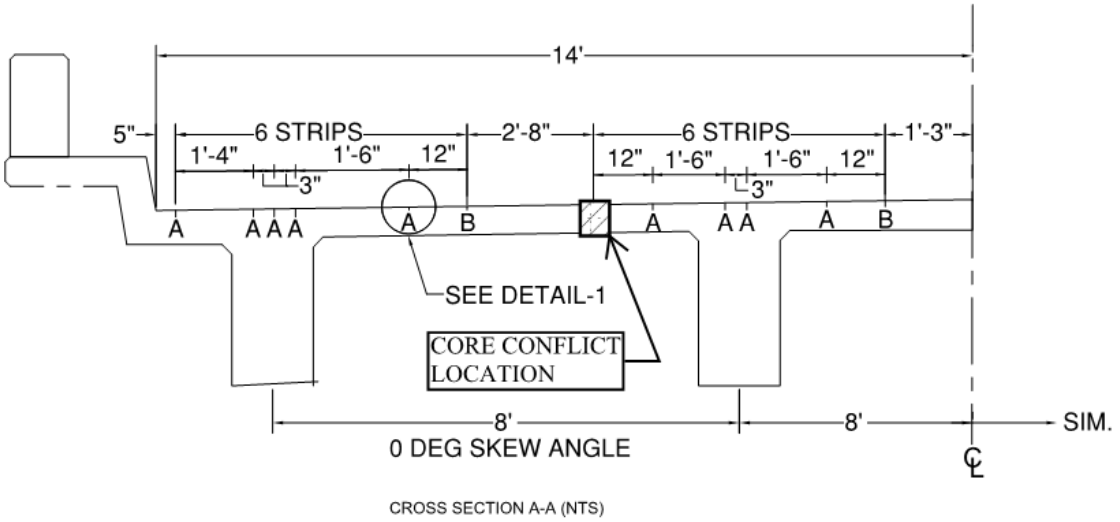

NOTE: REPEAT DESIGN FOR THE OTHER HALF OF THE CROSS-SECTION

A - Fixed location shall not be relocated without prior approval of the engineer

B - May be relocated laterally to avoid obstruction. The entire strip shall be shifted a uniform distance from the specified location, not to exceed 6 inches without prior approval of the engineer. Adjacent strips shall be spaced no less than 2 inches, center to center.

Figure 4.12 Cross Section Showing Core Conflict Location (Adapted From Alabama Department of Transportation 2014)

Figure 4.13 Core and FRP Strip Location Conflict

The FRP strip involved in this conflict was denoted as a movable strip in the construction documents. Therefore, the strip was shifted 2 inches (5.08 cm) laterally, toward the interior

girder. The corrected strip location is shown in a cross-section view of half of the bridge in Figure 4.14 and during layout of the retrofit in Figure 4.15.

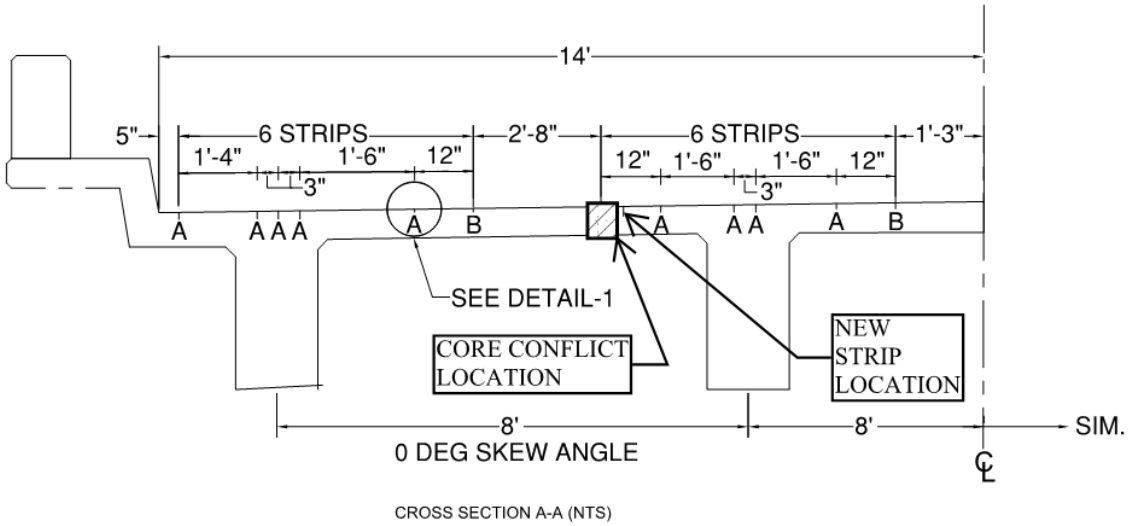

NOTE: REPEAT DESIGN FOR THE OTHER HALF OF THE CROSS-SECTION

A - Fixed location shall not be relocated without prior approval of the engineer

B - May be relocated laterally to avoid obstruction. The entire strip shall be shifted a uniform distance from the specified location, not to exceed 6 inches without prior approval of the engineer. Adjacent strips shall be spaced no less than 2 inches, center to center.

Figure 4.14 Shifted Strip Locations (Adapted From Alabama Department of Transportation 2014)

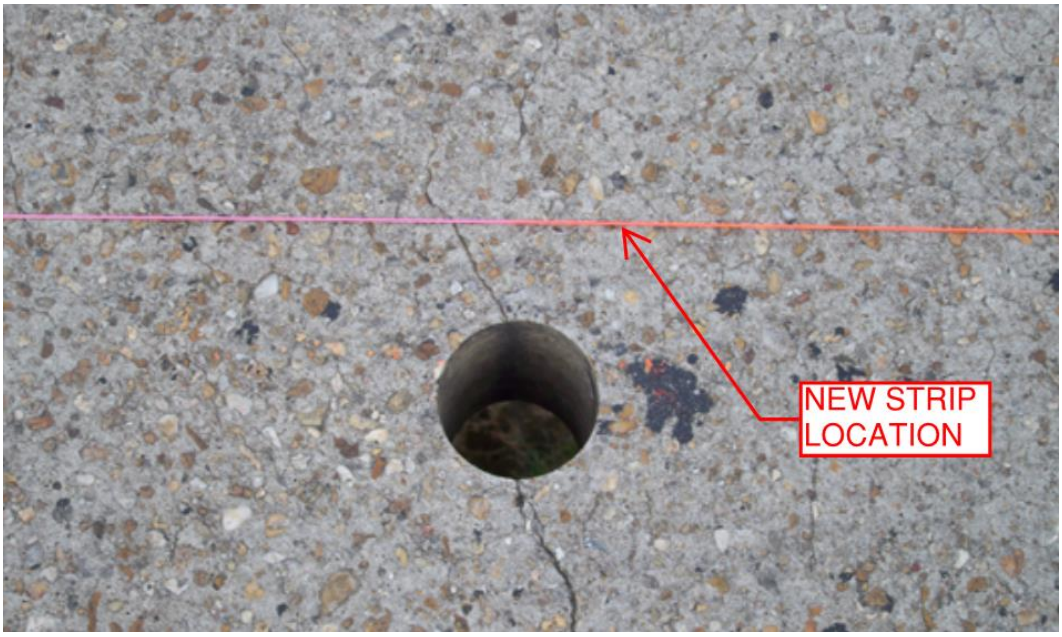

Figure 4.15 Location of FRP Strip Shifted 2 inches (5.08 cm) Laterally

4.5 Construction

Construction began first in the northbound lane and required 7 working days, stretching from Tuesday, December 9, 2014, through Wednesday, December 17, 2014. After the northbound lane was completed, further construction was delayed due to ALDOT holiday lane-closure policies. After the holiday travel period, construction began in the southbound lane. The second lane of construction required 11 working days, stretching from Tuesday, January 6, 2015, through Wednesday, January 21, 2015.

Weather during construction varied, with temperatures during working hours often between 40°F (4°C) and 68°F (20°C). Cooler temperatures did effect scheduling of epoxy use on the bridge and caused a few delays during the project. However, epoxy cure times are based on concrete temperatures, and direct sunlight did help warm the bridge deck and reduce initial cure times significantly. This is discussed in detail in Section 4.6. The only delay due to rain was on Thursday, January 15, 2015. Therefore, rain was not a large factor during the retrofit.

Implementation of the bridge retrofit consisted of two phases—saw cutting of grooves and FRP strip installation. Both lanes were completed using the same sequence, and each step is explained in detail in the following sections.

4.5.1 Groove Cutting

Groove cutting in the northbound lane began after the ALDOT inspector approved the FRP strip layout, and it began in the southbound lane after FRP strip installation in the northbound lane was completed. There were three groups of grooves in each lane—one group located over each bent—as previously shown in Figure 4.5. Each group consisted of twelve grooves—six over the exterior girder and six over the interior girder, as shown in Figure 4.6.

Grooves were specified to be cut to a depth of 1.0 inch (2.54 cm), with a tolerance of 3/32 inch (2.4 mm) less than specified, but no deeper. Groove width was specified as ¼ inch (6.4 mm), with a tolerance of 1/8 inch wider than specified, but no smaller. Figure 4.16 shows groove dimensions as specified in the construction documents. Actual groove depths and widths were measured during construction, and are shown in Figure 4.17 and Figure 4.18, respectively.

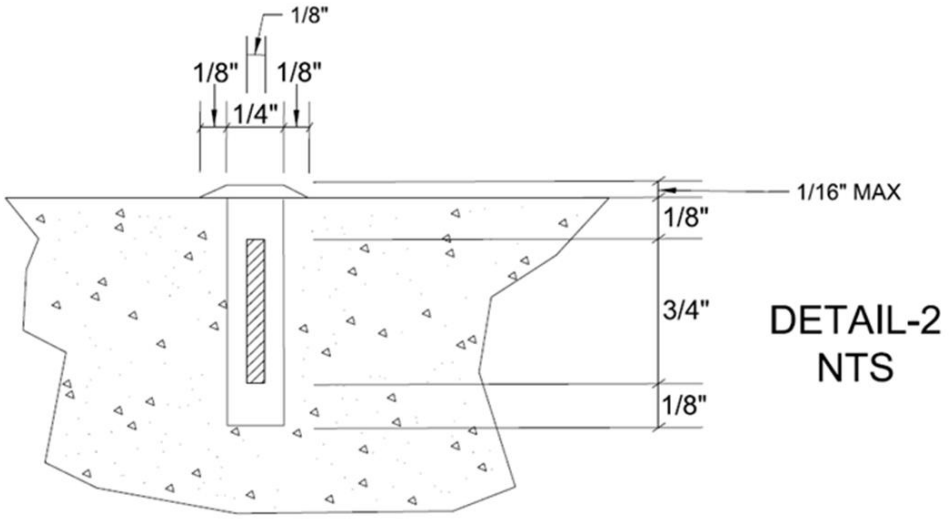

Figure 4.16 Groove Dimensions from Project Plans (Alabama Department of Transportation 2014)

Figure 4.17 Checking Groove Depth

Figure 4.18 Checking Groove Width

A track-mounted saw was used to cut grooves into the bridge deck, as shown in Figure 4.19. Track installation required concrete anchors to be driven into the bridge deck every 5 ft to support the track. The process to set up the track saw and cut a single groove required about 45

minutes. Therefore, the contractor could only saw cut about 11 grooves in a single day. Anchors driven into the bridge deck and track installation are shown in Figure 4.20. Holes from mounting anchors were filled with epoxy after groove cutting was completed.

Figure 4.19 Track-Mounted Saw during Northbound Lane Installation

Figure 4.20 Anchors in the Bridge Deck for Saw Track

Saw cutting created a large amount of slurry on the bridge deck. In an effort to minimize the amount of slurry built up in the newly cut grooves, the contractor used a vacuum to follow behind the saw as each groove was cut, as shown in Figure 4.21. At the end of each day, the contractor used pressurized water to clean the grooves and bridge deck of remaining slurry, as shown in Figure 4.22.

Figure 4.21 Vacuuming Slurry behind Saw Cutting

Figure 4.22 Groove Cleaning with Pressurized Water

Grooves were allowed to dry overnight, and compressed air was used to clear any remaining debris from the grooves the following morning, as shown in Figure 4.23. Once the

grooves were cut and completely cleaned, the ALDOT inspector checked the depth of the grooves, as shown in Figure 4.24.

Figure 4.23 Cleaning Dry Grooves with Compressed Air

Figure 4.24 ALDOT Inspector Checking Groove Depth

Groove depth varied slightly along the length of each cut because of deck undulations relative to track-saw mounts along the bridge. The inspector marked shallow areas of grooves,

and a handheld concrete saw was used to increase groove depth as necessary, as shown in Figure 4.25.

Figure 4.25 Shallow Locations Fixed by Handheld Concrete Saw

The contractor also cut one strip of FRP to the appropriate length and dry fit it into each groove to check groove depth, as shown in Figure 4.26. This allowed the contractor to verify there were no shallow areas along each groove that would prevent the strip from being fully seated below the bridge deck. Any areas of concern were brought to the attention of the ALDOT inspector and cut with a handheld concrete saw as necessary.

Figure 4.26 Contractor Checking Groove Depth along Length with FRP Strip

4.5.2 FRP Strip Installation

There were six steps followed to properly install FRP strips within the prepared grooves. Installation required about 20 minutes per strip—half the time required to cut a single groove. The process in the following outline and figures was used to install the FPR strips.

- FRP strips were cut to the proper length for each groove, as shown in Figure 4.27.
- Epoxy was injected into the bottom of the clean, dry groove, as shown in Figure 4.28.
- The FRP strip was placed into the groove and seated at the proper depth, as shown in Figure 4.29. The contractor used a custom-fabricated tool, as shown in Figure 4.30, to seat the FRP strip to ensure proper strip embedment depth.
- Epoxy was injected on top of the seated FRP strip, as shown in Figure 4.31.
- Epoxy was worked into the groove to fully surround the FRP strip and excess epoxy was scraped from the bridge deck, as shown in Figure 4.32.
- Sand was spread on top of the exposed epoxy to improve traction to the finished epoxy, as shown in Figure 4.33.

Figure 4.27 FRP Strips Cut and Ready for Placement

Figure 4.28 Epoxy Injected into Bottom of Prepared Groove

Figure 4.29 FRP Strip Placement within Epoxy Injected Groove

Figure 4.30 FRP Strip Seating Depth Tool

Figure 4.31 Epoxy Injection after Properly Seating FRP Strip

Figure 4.32 Working Epoxy into Groove and Excess Epoxy Removal

Figure 4.33 Sand Spread on Finished Epoxy to Provide Traction

4.6 Traffic Control

During installation of the FRP, the lane under construction was closed until the epoxy reached its initial cure. Table 4.1 shows initial cure times for Hilti HIT-RE 500 epoxy.

Table 4.1 Initial Cure Time for Hilti HIT-RE 500 Epoxy (Hilti Inc. 2014)

Base material temperature		Approximate initial cure time
°F	°C	
23	–5	36 h
32	0	25 h
50	10	12 h
68	20	6 h
86	30	4 h
104	40	2 h

The ALDOT inspector on site monitored deck temperatures with an infrared temperature gun. Initial cure times of 6 hours at temperatures around 68°F (20°C) caused the contractor to stop installation of FRP strips around 12:00 PM. This decision was made so that lane closures would not continue after dark for safety of traffic control personnel and road users.

4.7 Construction Complications and Issues

There were some issues that arose during implementation of the NSM FRP retrofit. There were some ideas for expediting construction that caused problems, some methods that were learned during construction to increase productivity, and some issues due to weather conditions.

Most notably, the track-mounted saw required a significant amount of time to cut a single groove. If the contractor had been able to cut a group of 12 or more grooves in a single day, then FRP installation could have begun one day after groove cutting and worked behind the groove cutting for the next three days to complete the installation. However, because the contractor could not cut all of the grooves in one lane over a single bent in one day, there were two full days required to saw cut a group of grooves and allow for drying overnight. This caused the FRP installation to be delayed until the 5^{th} day of construction, and then the FRP installation was completed on the 7^{th} day. If grooves could be cut quicker, then the project could reduce construction days to 1 day of only groove cutting, 2 days of simultaneously cutting grooves and installing FRP into previously cut grooves, and 1 day of only FRP installation into the last group of grooves. This would reduce time of installation for a single lane from 7 to 4 working days, or a 43% reduction in construction time and lane closure.

The contractor originally planned to mount the track saw to an H-pile, as shown in Figure 4.34. During the first day of saw cutting this method was attempted, and problems were immediately discovered. Due to the length and weight of a 70-foot H-pile, two small excavators were required to move it along the bridge deck. Flexibility of the pile, in combination with the weight of the H-pile, made it impossible to efficiently align the full length of the pile a consistent distance from the required cut location. After attempting approximately 10 ft of a cut using this

method, it was determined that the track saw needed to be attached directly to the bridge deck to ensure a straight cut.

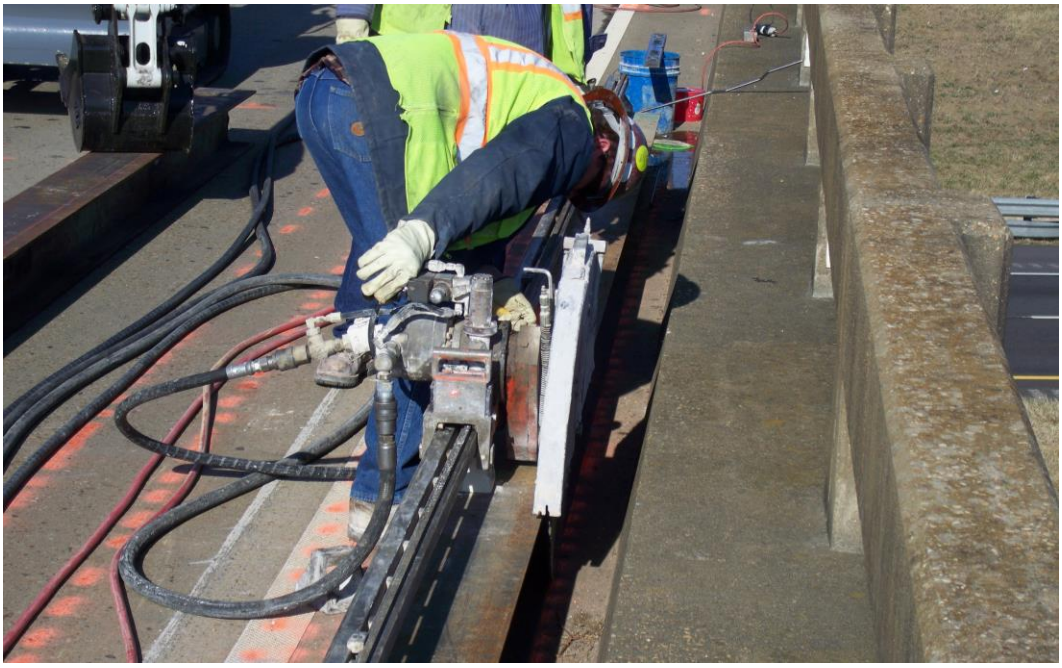

Figure 4.34 Attempted H-Pile Mounted Track Saw Setup

The contractor also did not adequately anticipate the amount of slurry produced by the track-mounted saw and its effect on subsequent steps of construction. The large amount of slurry on the deck after cutting the first few grooves can be seen in Figure 4.35. After the first few days of cutting, the contractor decided to expedite the cleaning process by vacuuming behind the saw to quickly remove as much of the slurry from the bridge deck as possible. This reduced the amount of slurry that was present on the bridge deck and helped prevent buildup of slurry in grooves that had already been cut. This also reduced the amount of slurry that was pressure washed from the bridge deck and exposed to the environment through the deck drains.

Figure 4.35 Slurry on Deck after One Day of Cutting

Weather also created some issues during construction. The Hilti epoxy used for this project is only allowed for use in concrete with temperatures ranging from 23°F (-5°C) to 104°F (40°C) with no bond strength degradation (Hilti Inc. 2014). It is also noteworthy that initial cure and gel times reduce greatly with higher temperatures, as shown in Figure 4.36 and Figure 4.37, respectively.

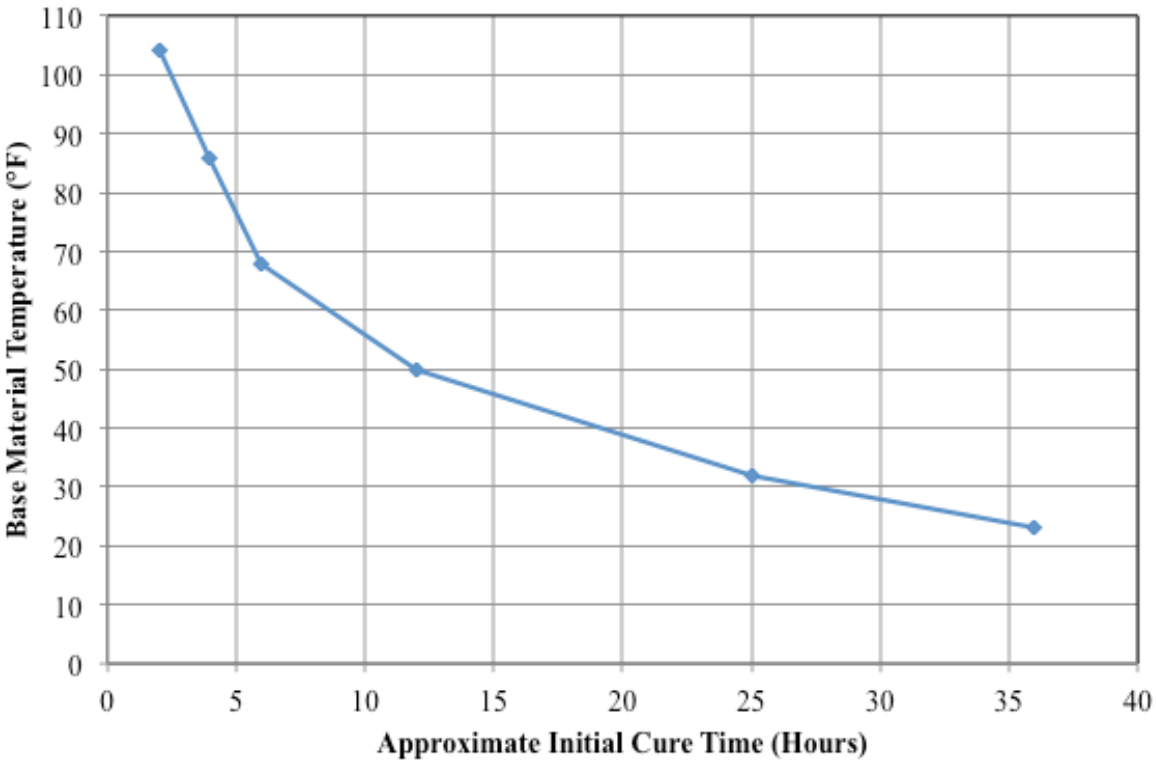

Figure 4.36 Hilti HIT-RE 500 Initial Cure Time (Adapted from Hilti Inc. 2014)

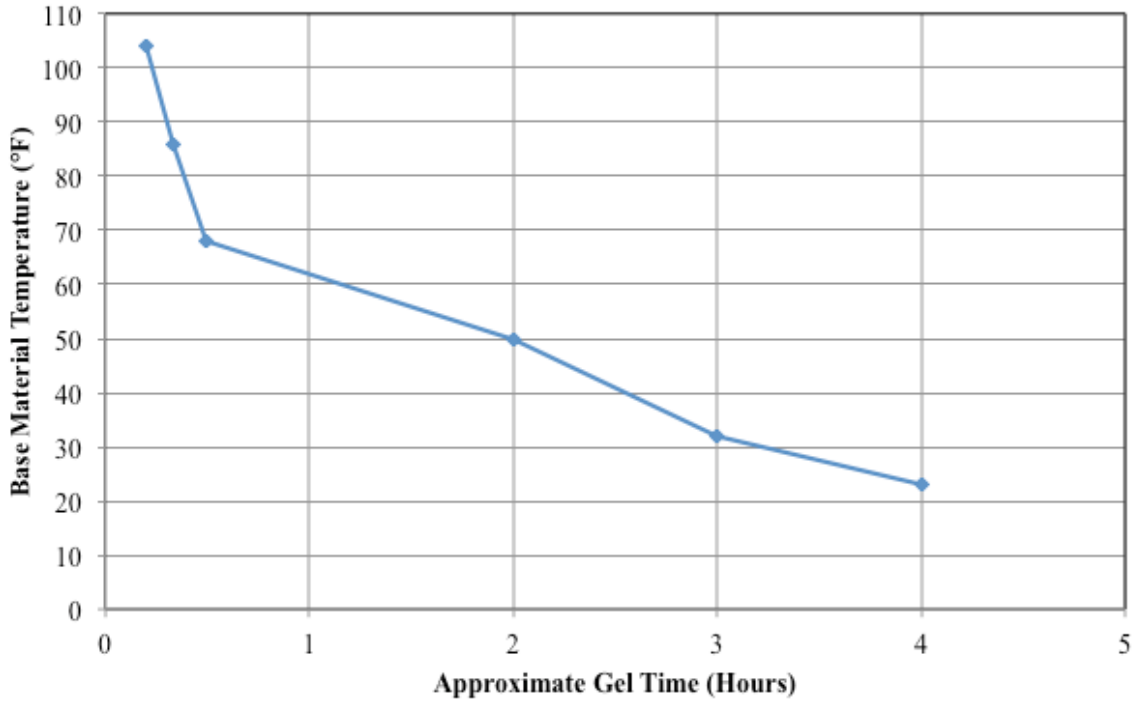

Figure 4.37 Hilti HIT-RE 500 Gel Time (Adapted from Hilti Inc. 2014)

Exposure to sunlight warmed the deck by about 10°F (5.6°C) during the Letohatchee bridge retrofit. This helped shorten initial cure times from 7 hours at 65°F (18.3°C), to less than 5 hours at 75°F (23.9°C). However, it should be noted that during warmer months this could have a negative effect, possibly elevating deck temperatures above 104°F (40°C) when exposed to direct sunlight. Warmer weather could also create issues related to gel time of the epoxy. During the Letohatchee bridge retrofit, temperatures of 65°F (18.3°C) allowed for over 30 minutes of workable time. But if the temperature is around 90°F (32.2°C), then workable time would be reduced to less than 20 minutes, making installation of FRP strips more difficult.

Rain also caused a minor delay during construction because the project required dry grooves during epoxy placement (Alabama Department of Transportation. 2014). This ensured proper bond between the bridge deck and injected epoxy. During the retrofit of the Letohatchee bridge, rain only delayed installation of FRP strips on Thursday, January 15, 2015. There were no other rain delays during this retrofit, but rain could cause significant delays during future installations.

CHAPTER 5:BRIDGE TESTING PROGRAM

5.1 Bridge Test Overview

The testing program for the Letohatchee bridge consisted of three load tests: 1) pre-retrofit, 2) post-retrofit, and 3) long-term load tests. First, the preliminary site investigation conducted to determine proper setup for load testing the bridge is discussed. Load truck configurations, load truck placements on the bridge, traffic control, and weather conditions for each test are detailed in this chapter.

5.1.1 Preliminary Site Investigation

A preliminary site investigation was conducted on Tuesday, October 14, 2014, to determine the load test setup. Areas of negative-moment deficiency, as outlined by Alexy (2009) and shown in Figure 5.1, were first located on the bridge deck. Once deficient regions were marked on the deck, a significant transverse crack within these regions was selected to be instrumented during testing. A crack in the southbound lane in the first span of the bridge was selected because it was one of the most distinct, continuous cracks in a deficient region and likely to respond to negative flexure. Figure 5.2 shows an overview of the bridge and the selected crack location.

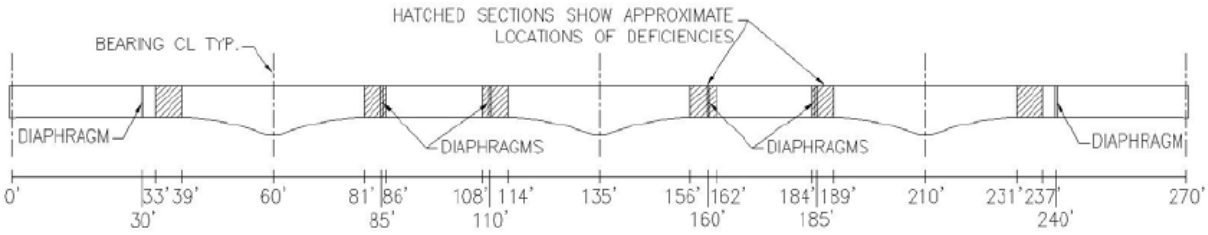

Figure 5.1 Approximate Locations of Flexural Deficiencies in the Letohatchee Bridge (Alexy 2009)

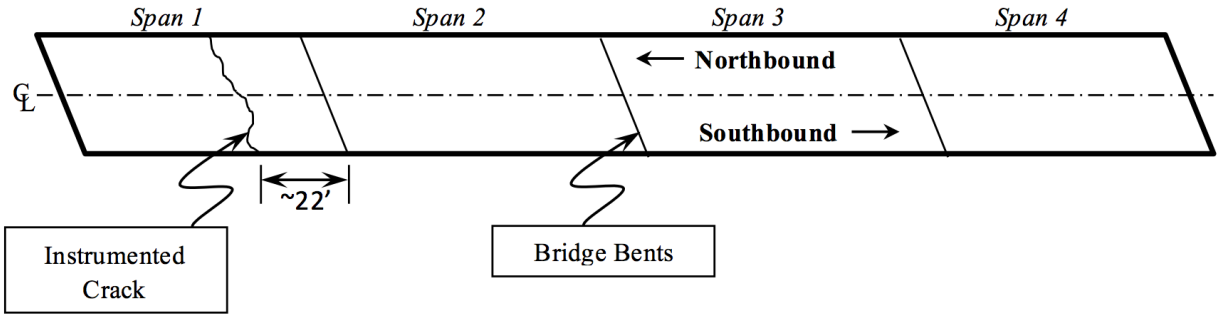

Figure 5.2 Location of Instrumented Crack

Crack opening displacement (COD) transducer positions were determined by considering the location of negative-moment reinforcement. Placing COD transducers directly over reinforcing steel provided the closest representation of the behavior of the existing negative-moment reinforcement. Transducer locations were marked with paint during the preliminary site investigation, as shown in Figure 5.3. The location of each transducer with respect to the bent between Spans 1 and 2 and the curb of the bridge is shown in Figure 5.4.

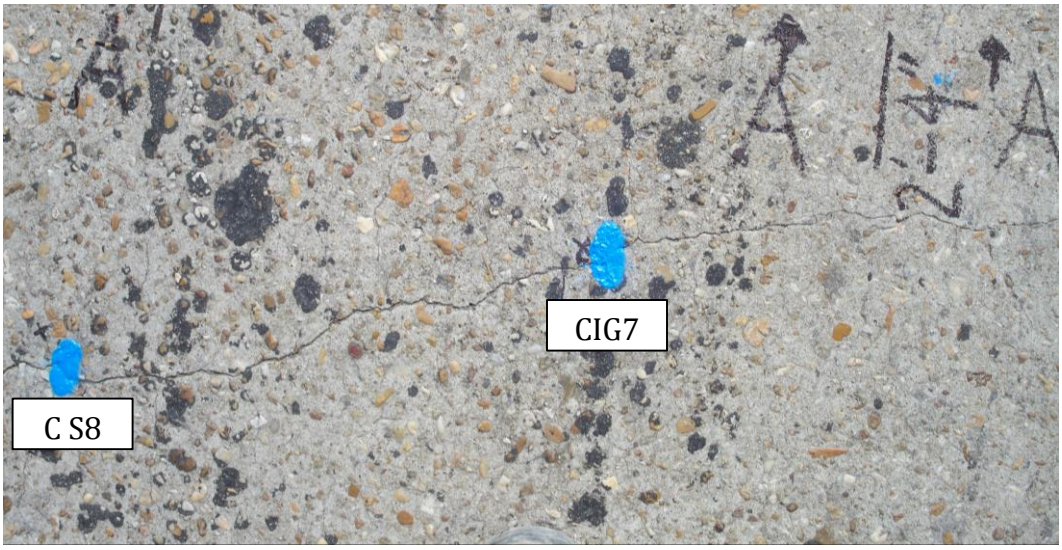

Figure 5.3 Two Transducer Locations Marked by Paint During Preliminary Site Investigation

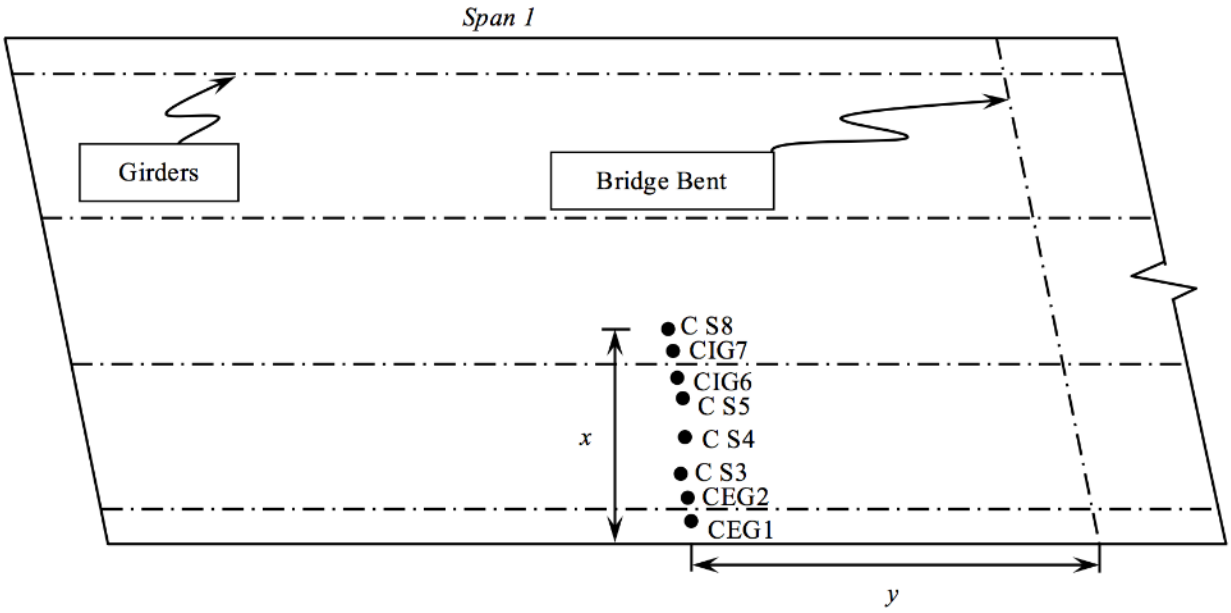

Gage	x	y		Gage	x	y
CEG1	15.6”	271.0”		C S5	97.8”	256.5”
CEG2	32.4”	272.5”		CIG6	111.6”	258.5”
C S3	48.3”	269.5”		CIG7	128.3”	258.5”
C S4	72.0”	262.5”		C S8	144.0”	259.5

Figure 5.4 Crack Opening Transducer Layout

Figure 5.4 also displays labeling convention for crack opening displacement transducers. Transducers were labeled with a code, according to placement over a girder or slab region of the bridge and numbered from exterior to interior of the bridge. The first character, *C*, indicates the sensor is a crack opening displacement transducer. The second character indicates lateral location of the instrumented girder as interior (*I*) or exterior (*E*), or is blank if the transducer is not located over a girder. The third character indicates that the transducer is located within a girder (*G*) or slab (*S*) region, and the fourth character is sequential numbering from 1–8 from the exterior of the bridge deck to the interior of the bridge deck.

After all instrumentation was laid out, decisions were made regarding placement of load trucks and the Auburn University Highway Research Center (AU HRC) van, which contained all recording equipment for the tests. Load trucks were determined to be placed in the second span,

adjacent to the instrumented span. Placing load trucks in the adjacent span allowed for the maximum negative bending influence in the instrumented region from the applied load. It was also decided that the AU HRC van be parked off of the North end of the bridge, about 60 ft (18.3 m) from transducer locations. This allowed for reasonable cable lengths during testing while removing the van weight from the bridge. Figure 5.5 shows an overview of the layout of the bridge testing equipment as determined during the preliminary site visit.

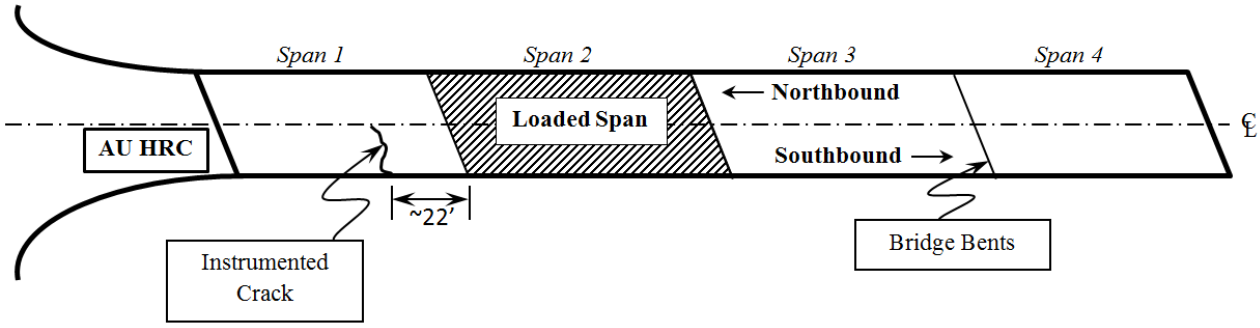

Figure 5.5 Location of AU HRC Van, Instrumented Crack, and Loaded Span

5.1.2 Load Test Preparation

Bridge preparation, including painting of load truck stopping positions on the bridge deck and installation of transducer mounts, was completed on Thursday, October 16, 2014, and Tuesday, March 31, 2015, for the pre-retrofit and post-retrofit load tests, respectively. For the long-term load test, preparation for testing was completed on Tuesday, September 22, 2015. Layout for tests with one load truck and two load trucks are shown in Figure 5.6 and Figure 5.7, respectively. Load truck placement is discussed in further detail in Section 5.1.4.

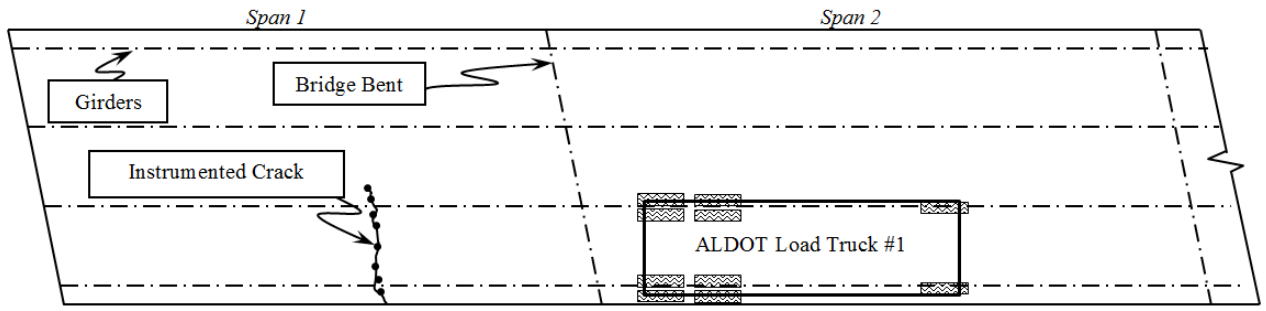

Figure 5.6 Load Test Layout with One Load Truck

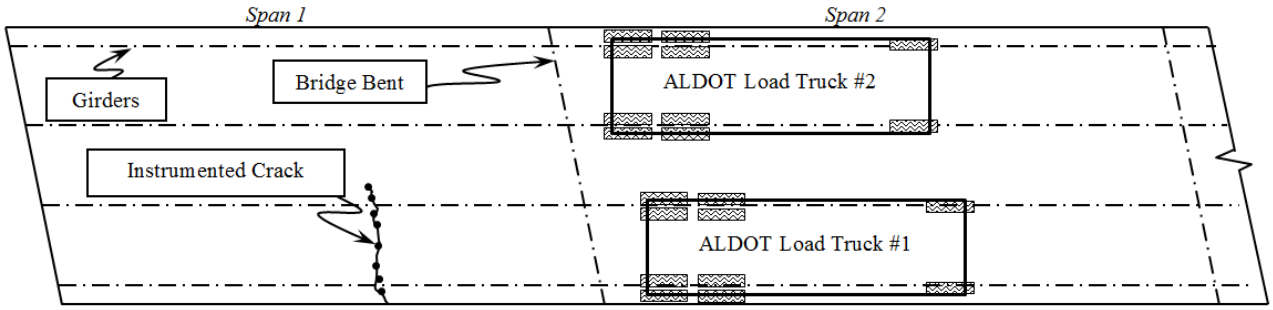

Figure 5.7 Load Test Layout with Two Load Trucks

In order to allow transducer installation flush with the bridge deck, mounting hardware was placed into the bridge deck. At each transducer location two holes approximately ⅜" deep were prepared with hammer drill using a ½" concrete drill bit as shown in Figure 5.8.

Figure 5.8 Drilled Holes for Transducer Mount Installation

Hex nuts were attached to installation brackets provided by the transducer manufacturer (Tokyo Sokki Kenkyujo Co.) to ensure proper distance between the mounting nuts, as shown in Figure 5.9.

Figure 5.9 Installation Bracket with Hex Nuts Attached

After clearing all dust and debris from the drilled indentions, the two holes for each transducer were filled with epoxy. While still in the epoxy's workable time, hex nuts attached to

the installation brackets were pushed into the epoxy until flush with the bridge deck, as shown in Figure 5.10.

Figure 5.10 Hex Nut Placement in Epoxy

Hex nuts remained attached to the installation bracket for 15 minutes, and were monitored to ensure all mounts remained oriented upright until the epoxy cured, as shown in Figure 5.11.

Figure 5.11 Installation Brackets during Epoxy Curing

Once the epoxy cured, installation brackets were unscrewed from the hex nuts, leaving the hex nuts installed below the deck surface. Installed hex nuts were capped with washers and short screws to prevent dust and debris from filling the mounts before transducers were installed on the day of testing. Figure 5.12 shows one exposed mounting nut after removing the installation bracket and one capped mounting nut after a completed mount installation.

Figure 5.12 One Hex Nut Mount After Installation Bracket Removal (Left) and One Completed Mount Installation Capped with Washer and Screw (Right)

5.1.3 Load Truck Configuration

Load trucks used for testing the Letohatchee bridge were standard ALDOT load trucks, as shown in Figure 5.13. The pre-retrofit load test involved only one truck and began with ALDOT load configuration LC-4, as shown in Figure 5.14. After running some initial tests, it was determined that the heavier LC-5 load configuration would provide more meaningful results. Therefore, the load was switched to the LC-5 load configuration, also shown in Figure 5.14. The LC-5 load configuration was used to complete the pre-retrofit load test, and it is the only load truck configuration used for the post-retrofit and long-term load tests.

Figure 5.13 ALDOT Load Truck with LC-5 Configuration

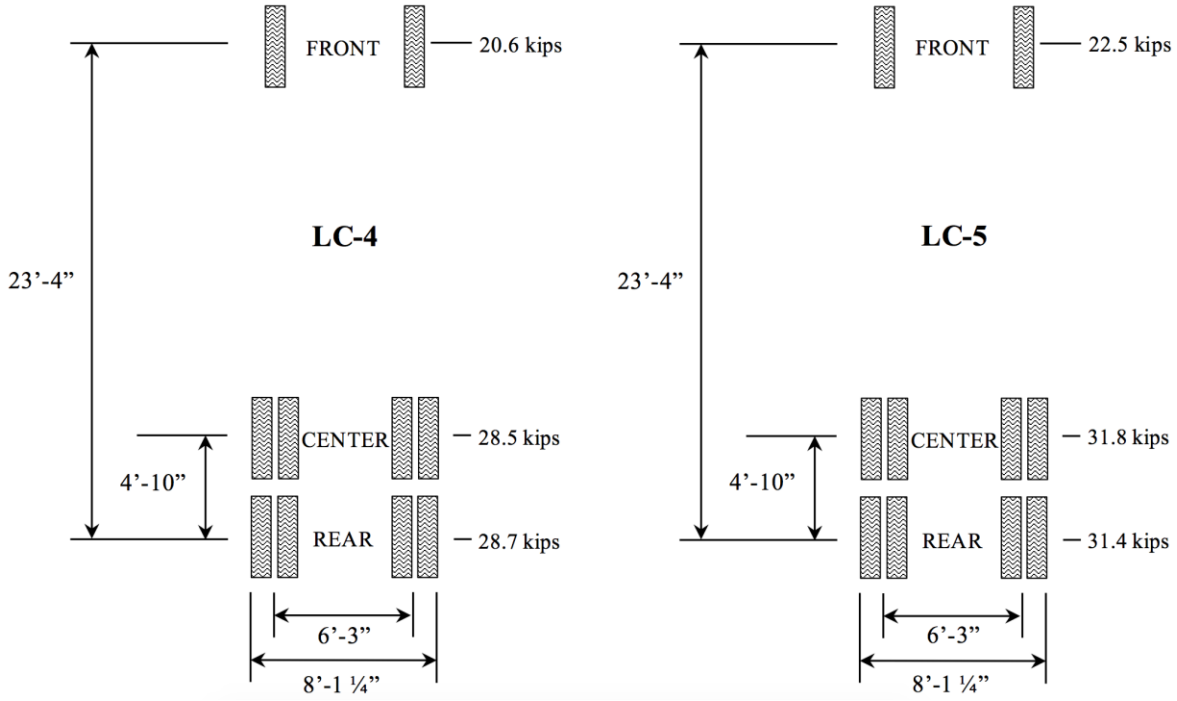

Figure 5.14 ALDOT LC-4 & LC-5 Load Truck Configurations

For the post-retrofit and long-term load tests the single load truck test regimen from the pre-retrofit load test was repeated according to the same process as the pre-retrofit load test. However, the post-retrofit load test also included a test series with two LC-5 load trucks. Each load test is discussed in detail in Sections 5.3–5.5.

5.1.4 Load Truck Placement

Load truck placement was determined according to basic structural mechanics and based on locations causing maximum negative-moment influence for the instrumented location. Therefore, load trucks were positioned in the span adjacent to the instrumented span of interest. Also, load trucks were backed into position during load testing in order to maximize influence on the span of interest.

For testing with one load truck, the truck was stopped at 10-foot increments from the bent in the span adjacent to instrumentation. Load truck stopping points were numbered 1 through 6, as shown in Figure 5.15.

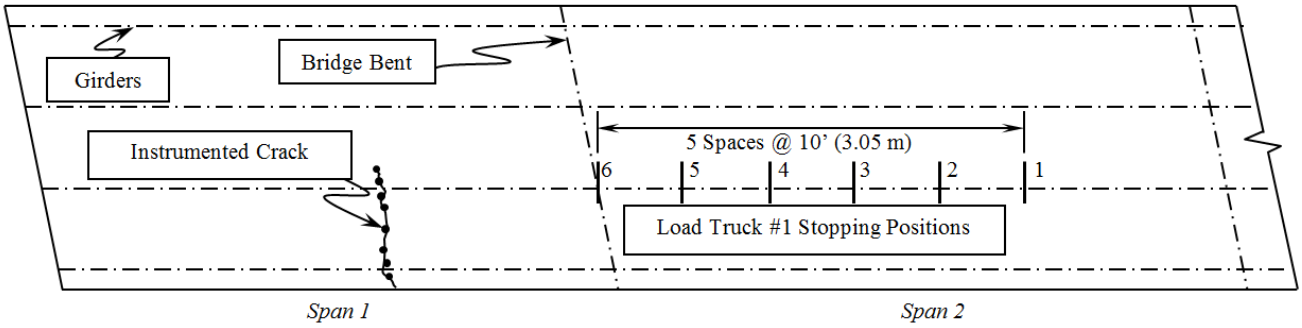

Figure 5.15 Load Test Stopping Positions for Single Load Truck Test

Lateral placement of the load truck was configured to center the back driver-side tire group over the interior girder of the desired lane. In order to achieve proper load truck stopping positions, a longitudinal guide line was painted onto the bridge deck to indicate the left side of the left wheel group while moving along the length of the bridge. Stopping points were also marked on the bridge deck with painted crossing marks on the bridge deck. The truck placement marks are shown in Figure 5.16.

Figure 5.16 Load Truck Guideline Striping on Bridge Deck

For the Letohatchee bridge load tests, the stopping points indicated the center of the back driver-side tire of the load truck, as shown in Figure 5.17. This method of load truck placement was used throughout all three load tests that were conducted.

Figure 5.17 Load Truck Placement with Back Left Tire along Guideline Positions

Also, there were a series of tests with two load trucks for the post-retrofit load tests. Guide marks for the second load truck were laid out similar to the first load truck. However, the

second load truck was positioned laterally to center the back passenger-side wheel group over the interior girder in the northbound lane, as previously shown in Figure 5.7. The truck was also positioned so that it was aligned with the original load truck along the bridge skew. The layout of the second load truck is shown in Figure 5.18.

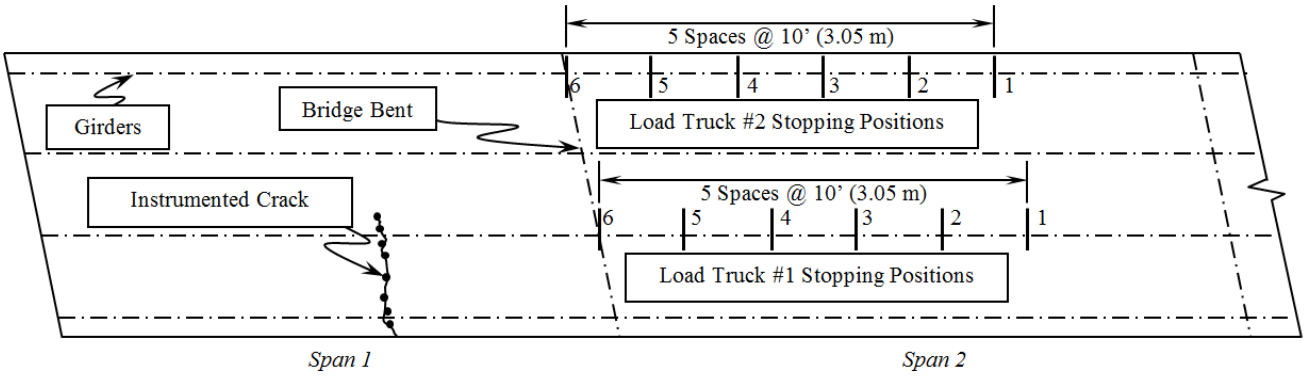

Figure 5.18 Stopping Positions for Tests with Two Load Trucks

5.1.5 Instrumentation and Data Acquisition

Crack opening displacements on the bridge were measured via crack opening displacement transducers installed on the bridge deck. Crack opening displacement transducers for this project were of type PI-2-50 manufactured by Tokyo Sokki Kenkyujo Co. A typical crack opening displacement transducer is shown in Figure 5.19. These are full-bridge sensors that measure displacement over a 50 mm span between attachment points.

Figure 5.19 Crack Opening Displacement Transducer

Eight transducers were used for testing. Two were placed over each girder, and the remaining four transducers were placed in areas between girders. A cross section of one lane of the bridge showing the layout of all eight transducers is shown in Figure 5.20. Transducers were all located in one lane of the bridge in order to allow traffic flow in the other lane between truck load placements.

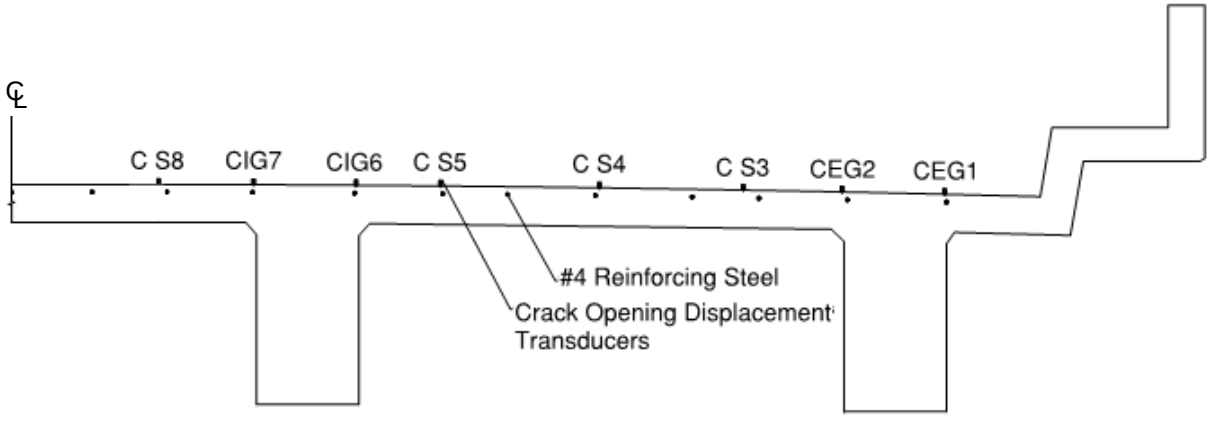

Figure 5.20 Cross Section of Instrumented Lane with Transducers and Reinforcing Steel

Crack opening displacements were recorded using an Optim Megadac® data acquisition system and data were stored and analyzed during testing using TCS for Windows. The data acquisition setup during testing is shown in Figure 5.21.

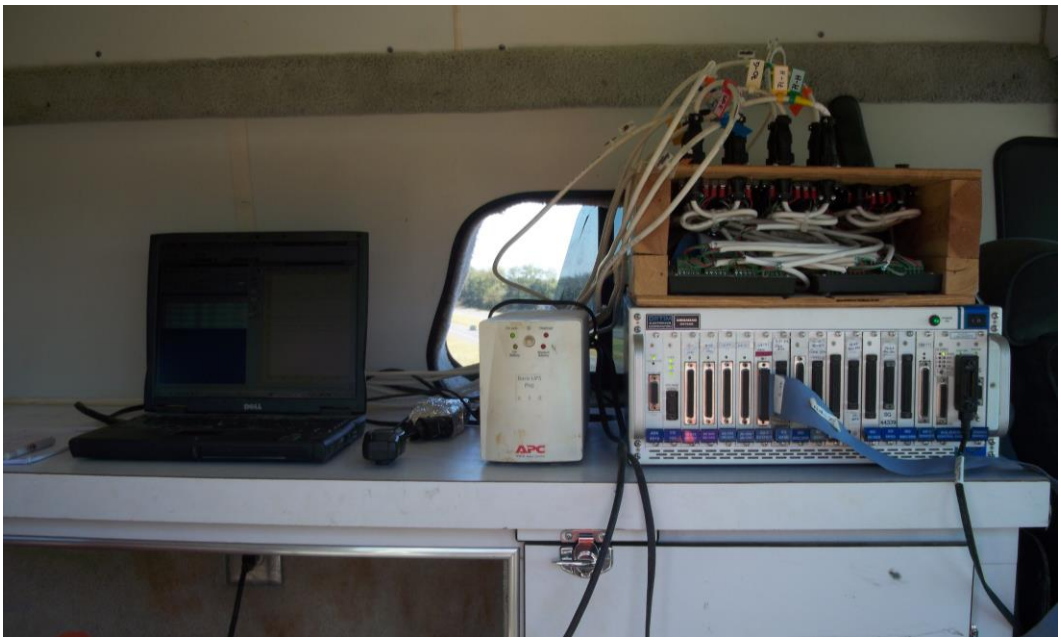

Figure 5.21 Optim Megadac® setup with TCS for Windows

5.2 Crack Opening Transducer Installation

Crack opening displacement transducers were installed onto the bridge deck at the beginning of each day of testing. Mounts installed prior to each load test were first examined to determine the quality of the mount after exposure to traffic between installation and testing.

Any mounts needing replacement, such as the one shown in Figure 5.22, were repaired and reinstalled prior to testing. Damaged epoxy was removed, and all dust and debris was cleared from the depression in the bridge deck. Epoxy was prepared and placed into the holes and hex nuts attached to the installation brackets were inserted into the epoxy. After the epoxy had hardened, the installation brackets were unscrewed from the hex nuts. These steps were

followed prior to every load test to ensure proper mounts were available on the bridge deck for load testing.

Figure 5.22 Transducer Mount Damaged by Traffic

After checking all mounts, two screws were used to attach crack opening displacement transducers to the prepared mounting hardware. A typical installed crack opening displacement transducer and installed transducers prior to a load test are shown in Figure 5.23 and Figure 5.24, respectively.

Figure 5.23 Installed Crack Opening Displacement Transducer

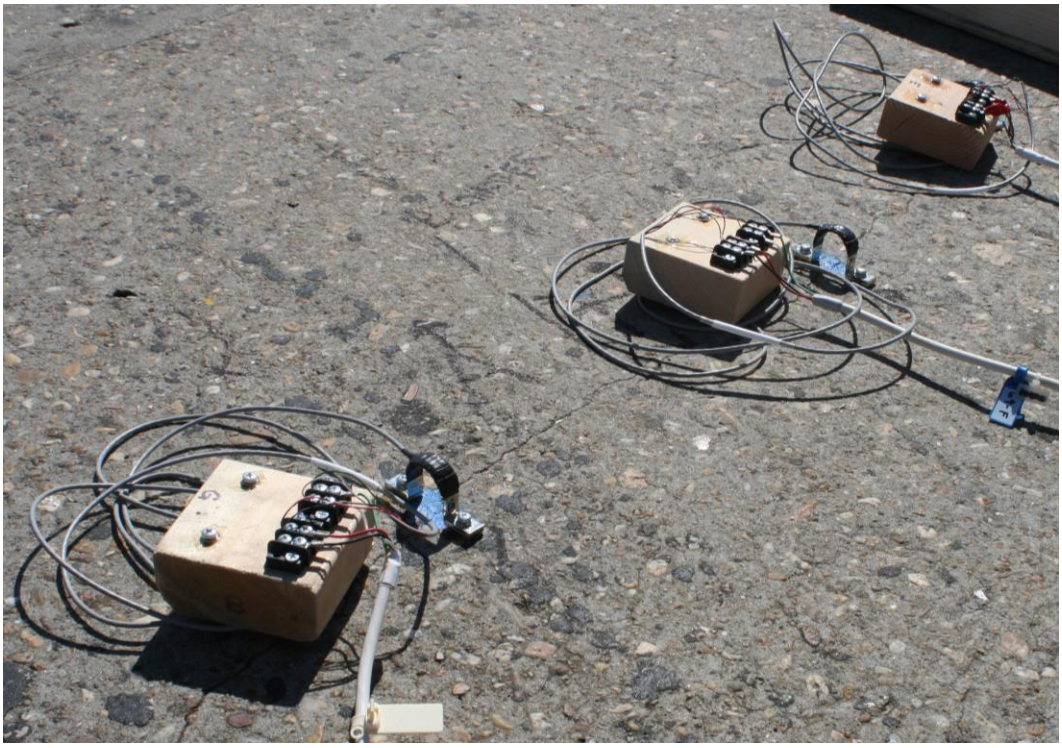

Figure 5.24 Installed Crack Opening Displacement Transducers Prior to Load Testing

After installing all crack opening displacement transducers, they were covered with 5-gallon buckets to provide protection from rapid thermal changes due to exposure to direct sunlight, as shown in Figure 5.25.

Figure 5.25 Instrumented Zone Ready for Load Test

5.3 Pre-Retrofit Load Test

The pre-retrofit load test took place on Tuesday, October 21, 2014. The AU HRC team arrived at the Letohatchee bridge around 7:30 AM to begin preparation for the load test. After examining and replacing damaged transducer mounts, instrumentation was set up and tested. The ALDOT load truck arrived at the bridge around 9:00 AM. Weather during testing was clear and sunny, with ambient temperatures ranging from 70°F (21°C) at 9:55 AM, when testing began, to 78°F (26°C) at 12:55 PM, when testing ended. Winds varied between 5 and 10 miles per hour throughout testing.

Testing began at 9:55 AM with the LC-4 load truck configuration. For the first testing sequence, the load truck was moved in reverse onto the bridge into Position 1 and stopped for about 20 seconds before moving from Position 1. The load truck was then moved into Position 2

and stopped for about 20 seconds before moving from Position 2. This pattern of stopping at each position for about 20 seconds continued in sequence until Position 6. The same sequence was continued while removing the load truck from the bridge, in reverse numerical order from Positions 5–1. For reference, load truck positions are again shown in Figure 5.26. The LC-4 load truck is shown being directed on the bridge in Figure 5.27.

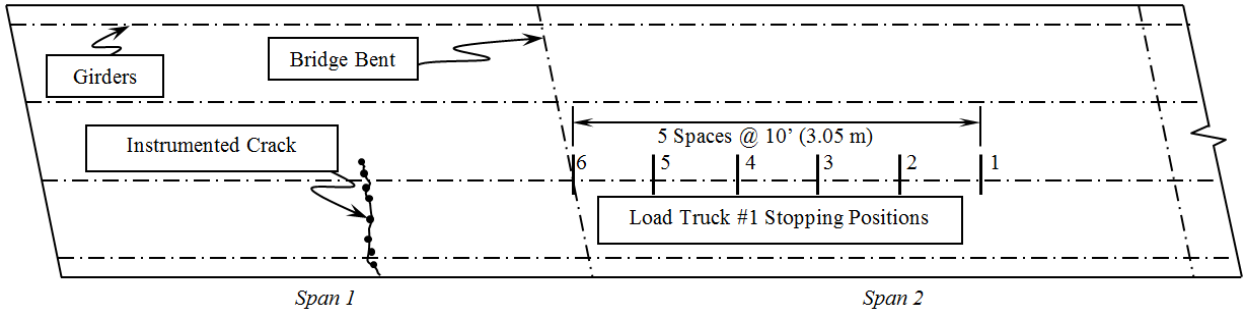

Figure 5.26 Stopping Positions for Tests with Two Load Trucks

Figure 5.27 LC-4 Load Truck Backed into Position during Testing

This testing sequence with the LC-4 load truck configuration was repeated once and then the data was examined. After a brief analysis of the results, it was decided that the LC-5 load

truck configuration would yield more appropriate results from the instrumented crack. Therefore, the load truck returned to the ALDOT facility in Montgomery, Alabama to be reconfigured.

The LC-5 load truck arrived on site at 12:00 PM. Load truck positioning was repeated according to the same sequence with the load truck stopping at each position in ascending order while moving onto the bridge, then descending order while moving off of the bridge. Figure 5.28 shows the LC-5 load truck during the pre-retrofit load test.

Figure 5.28 LC-5 Load Truck during Pre-Retrofit Load Test

After running through a test sequence stopping at every position, the data from the LC-5 load test was examined. Figure 5.29 shows the data from this test.

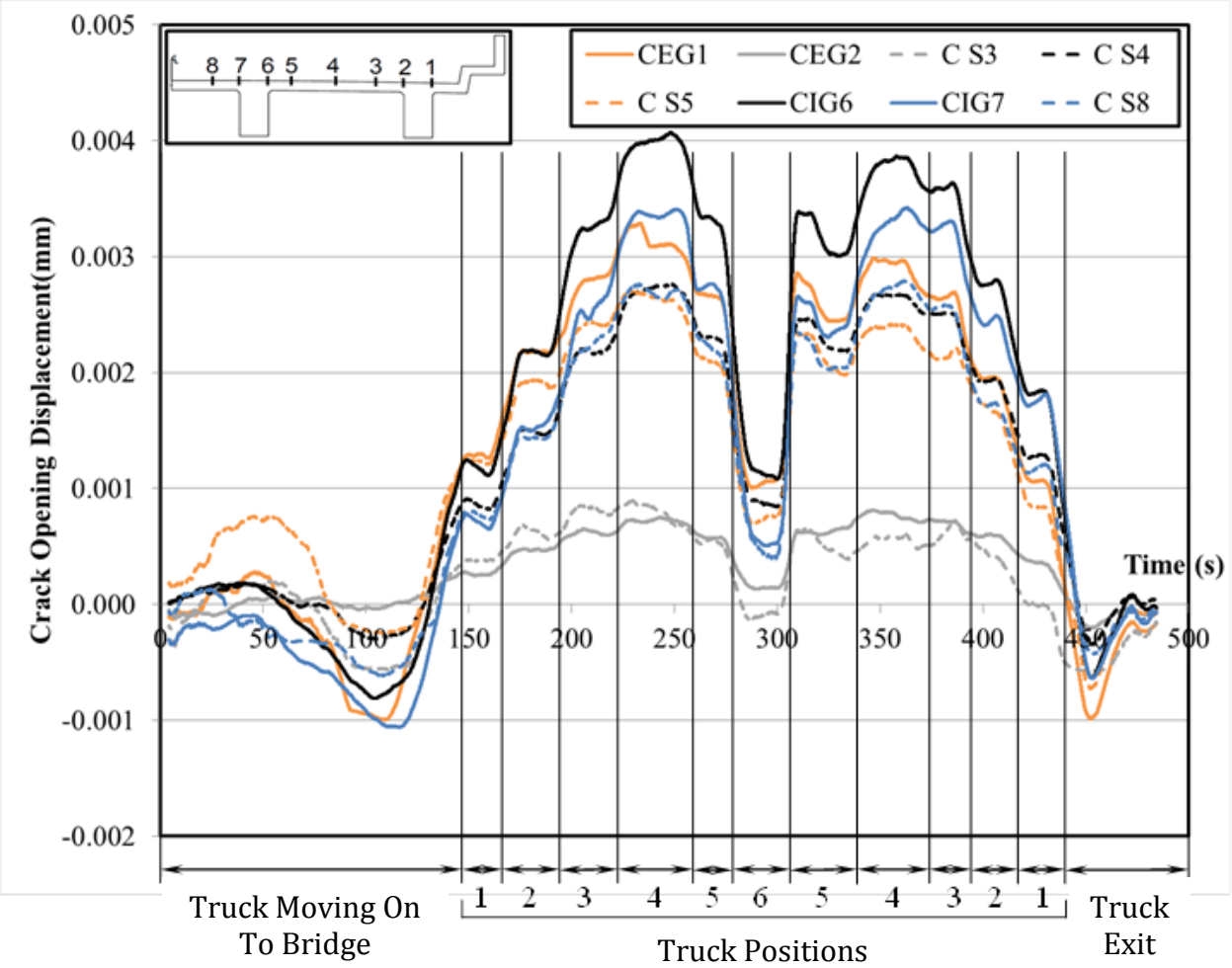

Figure 5.29 Data from the First Test Sequence with LC-5 Load Truck Configuration

Position 4 was determined to be the critical loading position because it created the largest crack opening displacement, as shown in Figure 5.29. Therefore, a second test sequence was conducted where the load truck stopped only at Position 4, then returned to a position off the bridge. This sequence was repeated for a total of four data sets.

The two loading sequences with the LC-5 load truck were vital to the pre-retrofit load test of the bridge, and those sequences were repeated in every load test for comparison to the pre-retrofit bridge behavior.

5.4 Post-Retrofit Load Test

The post-retrofit load test took place 10 weeks after completion of the retrofit, on Thursday, April 2, 2015. The AU HRC team arrived at the Letohatchee bridge around 7:30 AM to begin preparation for the load test. After examining and replacing damaged transducer mounts, instrumentation was set up and tested. The ALDOT load truck arrived at the bridge around 9:00 AM. Weather during testing was overcast, with a temperature of 72°F (22°C) all day and winds between 5 and 10 miles per hour.

Testing began at 9:42 AM with the LC-5 load truck configuration. Two tests were run according to the first sequence from the pre-retrofit load test, where the load truck momentarily stopped at each position on the bridge in ascending then descending order. Next, three load tests were conducted to replicate the second sequence from the pre-retrofit load test. In these load tests the load truck backed onto the bridge, stopping only at Position 4, and then the truck was removed from the bridge.

Two new testing sequences involving two LC-5 load trucks were introduced during the post-retrofit load test, as shown in Figure 5.30. In the third testing sequence, the first load truck was parked at Position 4 and remained there at all times when the second load truck was on the bridge. The second load truck was moved onto the bridge stopping at Position 1 for about 20 seconds before moving from Position 1. The second load truck then moved into Position 2 for about 20 seconds before moving from Position 2. This pattern of stopping the second load truck at each position for about 20 seconds continued through Position 4 while moving the truck onto the bridge and was also followed when removing the load truck from the bridge in a descending numerical sequence from Positions 3–1. When the second load truck was completely removed

from the bridge, the first load truck moved from Position 4 off of the bridge. A test with both load trucks on the bridge is shown in Figure 5.31.

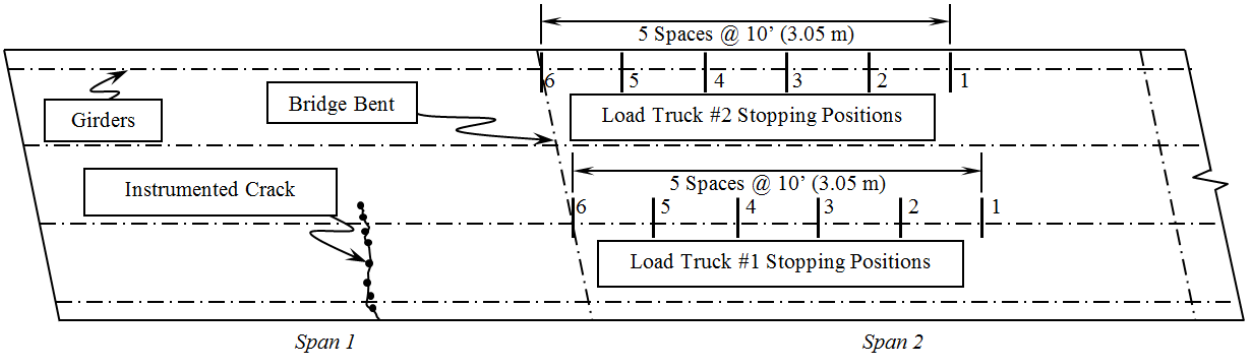

Figure 5.30 Stopping Position for Tests with Two Load Trucks

Figure 5.31 Load Test with Two Load Trucks

A fourth test sequence was then conducted where the first load truck was parked in Position 4, then the second load truck was moved directly into Position 4. After stopping for about 20 seconds, the second load truck was removed from the bridge. Once the second load truck was completely removed from the bridge the first load truck was also removed from the bridge. This sequence was repeated for a total of three data sets.

The first two testing sequences were used to compare the pre-retrofit and post-retrofit bridge behavior. The third and fourth testing sequences were used to provide a second measure of post-retrofit behavior.

5.5 Long-Term Load Test

The long-term load test took place on Thursday, December 17, 2015. The AU HRC team arrived at the Letohatchee bridge around 7:30 AM to begin preparation for the load test. After examining and replacing damaged transducer mounts, instrumentation was set up and tested. The ALDOT load truck arrived at the bridge around 9:00 AM. Weather during testing was overcast, with temperatures around 60°F (16°C) all day and winds between 5 and 10 miles per hour.

The long-term load test was conducted with only one load truck, according to the same regimen as the pre-retrofit load test sequence. The test was scheduled for two load trucks, as in the post-retrofit load test, but one of the ALDOT load trucks was unavailable during the test due to long-term mechanical problems with no definite return-to-service date.

Testing began at 11:37 AM with the LC-5 load truck configuration. Three tests were run according to the first test sequence, where the load truck momentarily stopped at each position on the bridge in ascending then descending order. Next, three load tests were conducted to replicate the second test sequence, where the load truck backed onto the bridge, stopping only at Position 4, and then the truck was removed from the bridge.

Data captured from the long-term load test were used to examine performance of the retrofit one year after installation.

CHAPTER 6:BRIDGE TEST RESULTS, ANALYSIS, AND DISCUSSION

6.1 Bridge Testing Results Overview

In this chapter, an explanation of the NSM FRP retrofit analysis technique is presented first, followed by reporting and discussion of the test results. A theoretical estimate of the pre- and post-retrofit behavior of the Letohatchee bridge was conducted using linear-elastic, cracked-section analysis. Bridge test results from each load test were then analyzed to determine the behavior of the bridge during testing. Experimental results from each test were then compared and the change in strain in the negative-moment reinforcing steel was compared to the theoretical strain reduction due to FRP strengthening.

6.2 Letohatchee Bridge Analysis

The following method based on linear-elastic analysis was used to analyze the Letohatchee bridge.

6.2.1 Letohatchee Bridge Analysis Method

Crack opening displacements were measured at the surface of the tension face of the member before and after strengthening the bridge. These values are proportional to the crack opening displacements at the level of reinforcement by a correction factor, *R*, as recommended by Broms and Gergely and Lutz. Therefore, the following equation can be developed based on these principles,

$$\boldsymbol{COD_b = R(COD_s)} \qquad \textbf{\textit{Equation 6.1}}$$

where COD_b is the crack opening displacement at the tension face; COD_s is the crack opening displacement at the level of the tension reinforcement; and *R* is the proportion of

distances from the neutral axis to the tension face of the member and tension steel, according to Equation 2.5.

Crack opening displacements measured for a specific loading before and after strengthening a structural member will result in a percent change in crack opening displacement due to strengthening, as shown by Equation 6.2,

$$\textbf{Percent change} = \frac{COD_i - COD_f}{COD_i} \times 100 \qquad \textit{Equation 6.2}$$

where COD_i is the crack opening displacement prior to strengthening; and COD_f is the crack opening displacement after strengthening.

Based on Equation 6.1 and Equation 2.2, the following relationship can be developed:

$$\textbf{Percent change} = \frac{(COD_b)_i - (COD_b)_f}{(COD_b)_i} = \frac{R(COD_b)_i - R(COD_b)_f}{R(COD_b)_i} \qquad \textit{Equation 6.3}$$

Therefore, the percent change in crack opening displacement at the tension face of the bridge gives the percent change in crack opening displacement at the level of the tension reinforcement. This method was used to identify the percent change in strain due to strengthening of the Letohatchee bridge.

6.2.2 Letohatchee Bridge Theoretical Analysis

Cracked-section analysis was performed in order to validate strain changes due to strengthening of the Letohatchee bridge. Cracked-section analysis relies on linear-elastic theory, and is based on the following methodology (Wight and MacGregor 2012).

Reinforced concrete consists of two materials, therefore the cross section must be transformed into a uniform concrete section for analysis. The modular ratio, n_s, is used to convert steel into an equivalent area of concrete of the same axial stiffness, as shown in Equation 6.4,

$$n_s = \frac{E_s}{E_c} \qquad \textit{Equation 6.4}$$

where E_s is the modulus of elasticity of reinforcing steel; and E_c is the modulus of elasticity of concrete. Therefore, the area of reinforcing steel in tension and compression is,

$$\boldsymbol{Area\ of\ tensile\ steel = n_s A_s} \qquad \textit{Equation 6.5}$$

$$\boldsymbol{Area\ of\ compression\ steel = (n_s - 1)A_s'} \qquad \textit{Equation 6.6}$$

where A_s is the area of tensile steel; and $A_s^{'}$ is the area of compression steel. When considering the FRP strengthened section, the same principles are applied. Therefore, Equation 6.5 is used to transform FRP reinforcement into an equivalent area of concrete with the same axial stiffness,

$$\boldsymbol{n_{frp} = \frac{E_{frp}}{E_c}} \qquad \textit{Equation 6.7}$$

where n_{frp} is the modular ratio of the FRP; and E_{frp} is the modulus of elasticity of the FRP. Therefore, the area of the FRP reinforcement is,

$$\boldsymbol{Area\ of\ FRP\ reinforcement = n_{frp} A_{frp}} \qquad \textit{Equation 6.8}$$

The neutral axis of the cracked, transformed section, c_{cr}, is located at the centroid of the area, which is defined according to Equation 6.9,

$$\boldsymbol{\sum A_i \bar{y}_i = 0} \qquad \textit{Equation 6.9}$$

where A_i is the area of the *i*th section; and $\bar{y}_i$ is the distance from the neutral axis to the centroid of the *i*th area. All of these variables are illustrated in Figure 6.1, which models the top of the T-beam in tension and the bottom in compression.

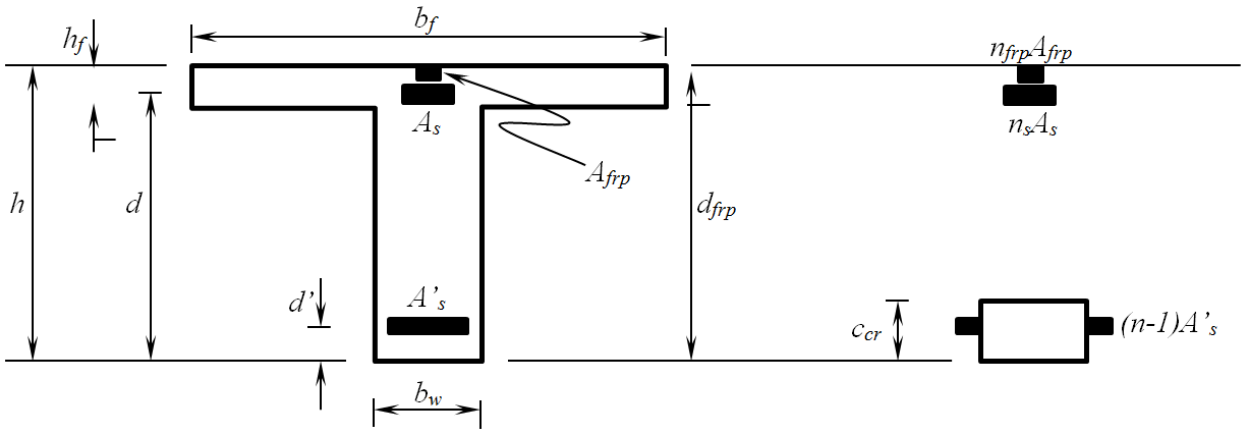

Figure 6.1 Illustration of Cracked-Section Analysis

Moment of inertia of the cracked section can be determined after locating the neutral axis, and is defined as,

$$\boldsymbol{I_{cr} = I_c + I_s + I_{frp}} \qquad \textbf{\textit{Equation 6.10}}$$

where I_c is the moment of inertia of the concrete; I_s is the moment of inertia of the reinforcing steel; and I_{frp} is the moment of inertia of the FRP. Therefore, based on the assumptions of linear-elastic theory explained in Equation 2.1 and Equation 2.2, strain can be expressed as

$$\boldsymbol{E\varepsilon_s = \frac{My_{cr}}{I_{cr}}} \qquad \textbf{\textit{Equation 6.11}}$$

or

$$\boldsymbol{\varepsilon_s = \frac{My_{cr}}{EI_{cr}}} \qquad \textbf{\textit{Equation 6.12}}$$

The change in strain can then be described by,

$$\boldsymbol{(\varepsilon_s)_i - (\varepsilon_s)_f = \left(\frac{My_{cr}}{EI_{cr}}\right)_i - \left(\frac{My_{cr}}{EI_{cr}}\right)_f} \qquad \textbf{\textit{Equation 6.13}}$$

where E and M are constants, because they are the same in the unstrengthened and strengthened structure. Therefore, the percent change in strain in the reinforcing steel is expressed as,

$$\textbf{Percent change} = \frac{(\varepsilon_s)_i - (\varepsilon_s)_f}{(\varepsilon_s)_i} = \frac{\left(\frac{My_{cr}}{EI_{cr}}\right)_i - \left(\frac{My_{cr}}{EI_{cr}}\right)_f}{\left(\frac{My_{cr}}{EI_{cr}}\right)_i} \qquad \textit{Equation 6.14}$$

and Equation 6.14 simplifies to,

$$\textbf{Percent change} = \frac{(\varepsilon_s)_i - (\varepsilon_s)_f}{(\varepsilon_s)_i} = \frac{\left(\frac{y_{cr}}{I_{cr}}\right)_i - \left(\frac{y_{cr}}{I_{cr}}\right)_f}{\left(\frac{y_{cr}}{I_{cr}}\right)_i} \qquad \textit{Equation 6.15}$$

Therefore, by considering the change in $^{y_{cr}}/_{I_{cr}}$ before and after strengthening, the expected percent change in strain in the Letohatchee bridge tension reinforcement can be determined. This method of theoretical analysis was used to verify experimental results from bridge testing.

6.3 Cracked-Section Analysis

Cracked section analysis of the Letohatchee bridge was performed to examine load test results. Analyzed cross sections were based on the instrumented cross section of the bridge. Three cross sections were considered during analysis—one modeling a single exterior girder, one modeling a single interior girder, and one modeling the complete bridge cross section. Figure 6.2 shows each cross section that was analyzed through linear-elastic, cracked-section analysis for negative bending.

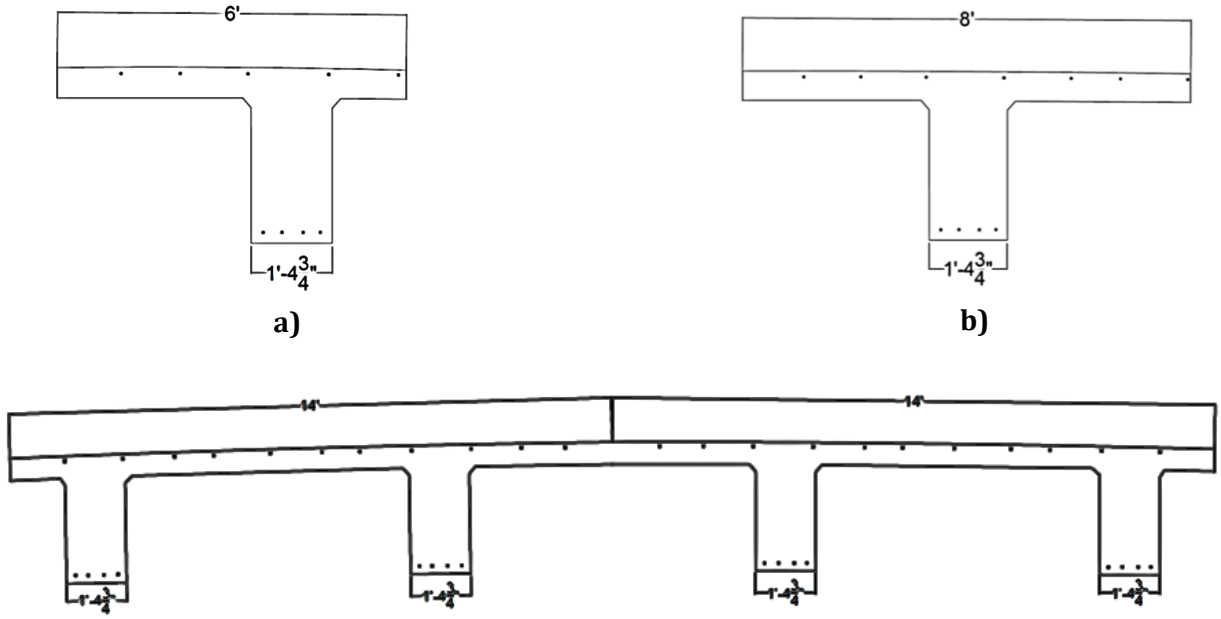

Figure 6.2 Cross Sections Analyzed with Cracked Section Analysis of a) Exterior Girder, b) Interior Girder, and c) Full Bridge

Concrete and steel material properties were based on historical data in the original construction documents and the preliminary investigation of the bridge conducted earlier in this project (Alabama Department of Transportation 2014; Alexy 2009). FRP properties were determined from the manufacturer's test report, located in Appendix A. Material properties used during analysis are presented in Table 6.1.

Table 6.1 Cracked-Section Analysis Material Properties

Concrete Properties			**Steel Properties**			**FRP Properties**		
f'_c	3000	psi	f_y	40	ksi	f_{frp}	467	ksi
γ_{conc}	145	pcf	E_s	29000	ksi	A_{strip}	0.050	in^2
E_c	3100	ksi	n_s	9.29		E_{frp}	24300	ksi
						n_{frp}	7.78	

Cross-sectional properties were also determined according to the original bridge plans. Cross-sectional properties used for each modeled cross section are tabulated in Table 6.2.

Table 6.2 Modeled Cross Section Properties

Interior Girder			Exterior Girder			Complete Bridge		
h	43.375	in.	h	43.375	in.	h	43.375	in.
b_f	96.0	in.	b_f	72.0	in.	b_f	336	in.
h_f	6.25	in.	h_f	6.25	in.	h_f	6.25	in.
b_w	16.75	in.	b_w	16.75	in.	b_w	67.0	in.

Reinforcing steel and FRP areas were determined according to reinforcement present in each analyzed cross section. Steel flexural reinforcement was also separated into compression and tension steel for analysis. Reinforcement for each cross section is presented in Table 6.3.

Table 6.3 Cross Section Reinforcement Properties

Interior Girder			Exterior Girder			Complete Bridge		
A_s	1.92	in^2	A_s	1.92	in^2	A_s	7.68	in^2
d	40.20	in.	d	40.20	in.	d	40.20	in.
A'_s	15.6	in^2	A'_s	15.6	in^2	A'_s	62.4	in^2
d'	5.80	in.	d'	5.80	in.	d'	5.80	in.
FRP	6	strips	FRP	6	strips	FRP	24	strips
A_{frp}	0.29	in^2	A_{frp}	0.29	in^2	A_{frp}	1.18	in^2
d_{frp}	42.88	in.	d_{frp}	42.88	in.	d_{frp}	42.88	in.

Each modeled cross section was analyzed for negative bending response according to the method of linear-elastic, cracked-section analysis. Analysis results for all three cross sections are tabulated in Table 6.4.

Table 6.4 Cracked Section Analysis Results

Pre-Retrofit								
Interior Girder			**Exterior Girder**			**Complete Bridge**		
c_{cr}	7.1	in.	c_{cr}	7.1	in.	c_{cr}	7.1	in.
y_{cr}	33.1	in.	y_{cr}	33.1	in.	y_{cr}	33.1	in.
I_{cr}	21750	in^4	I_{cr}	21750	in^4	I_{cr}	87003	in^4
I_{cr}/y_{cr}	658	in^3	I_{cr}/y_{cr}	658	in^3	I_{cr}/y_{cr}	2630	in^3
Post-Retrofit								
Interior Girder			**Exterior Girder**			**Complete Bridge**		
c_{cr}	7.4	in.	c_{cr}	7.4	in.	c_{cr}	7.4	in.
y_{cr}	32.8	in.	y_{cr}	32.8	in.	y_{cr}	32.8	in.
I_{cr}	24660	in^4	I_{cr}	24660	in^4	I_{cr}	98620	in^4
I_{cr}/y_{cr}	752	$1/in^3$	sI_{cr}/y_{cr}	752	$1/in^3$	I_{cr}/y_{cr}	3006	$1/in^3$
% Change in strain	-14%		*% Change in strain*	-14%		*% Change in strain*	-14%	

As shown in Table 6.4, cracked-section analysis of all three cross sections predict a 14% reduction in strain at the tension face of the cross section. This correlates directly to a reduction of strain in the reinforcing steel. Therefore, theoretical analysis indicates that the crack opening displacement and stress in the reinforcing steel at the instrumented cross section should reduce by 14% after strengthening when the cross section is subjected to the same bending moment.

6.4 Bridge Load Test Results

The Letohatchee bridge was load tested before and after strengthening to determine effectiveness of the retrofit. Data from each load test was examined to determine the maximum crack opening displacement. The method for reducing raw crack opening displacement data and results from load tests are discussed in this section.

6.4.1 Load Test Data Analysis

The following process was used to examine the data to determine the maximum crack opening displacement for each load test. Figure 6.3 displays crack opening displacement measurements from a single load test run.

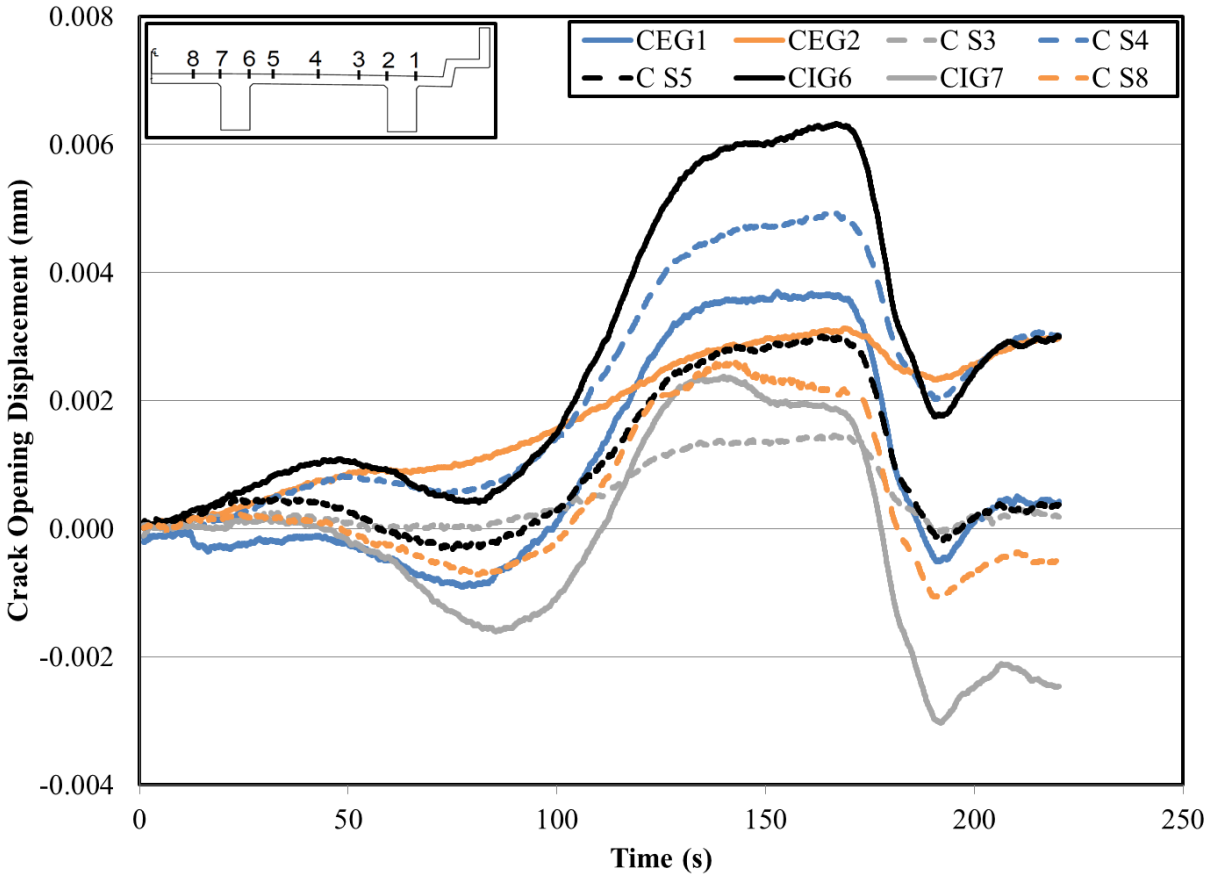

Figure 6.3 Raw Data for all Transducers for One Test Run

Figure 6.3 allows for two observations—all transducers did not experience the same crack opening displacement and there is an indication of measurement drift during the duration of the run. Therefore, to effectively examine the results, drift must be addressed and the results should be split into separate plots for each transducer. Drift was examined by capturing a period of data with no traffic or load trucks on the bridge, as shown in Figure 6.4.

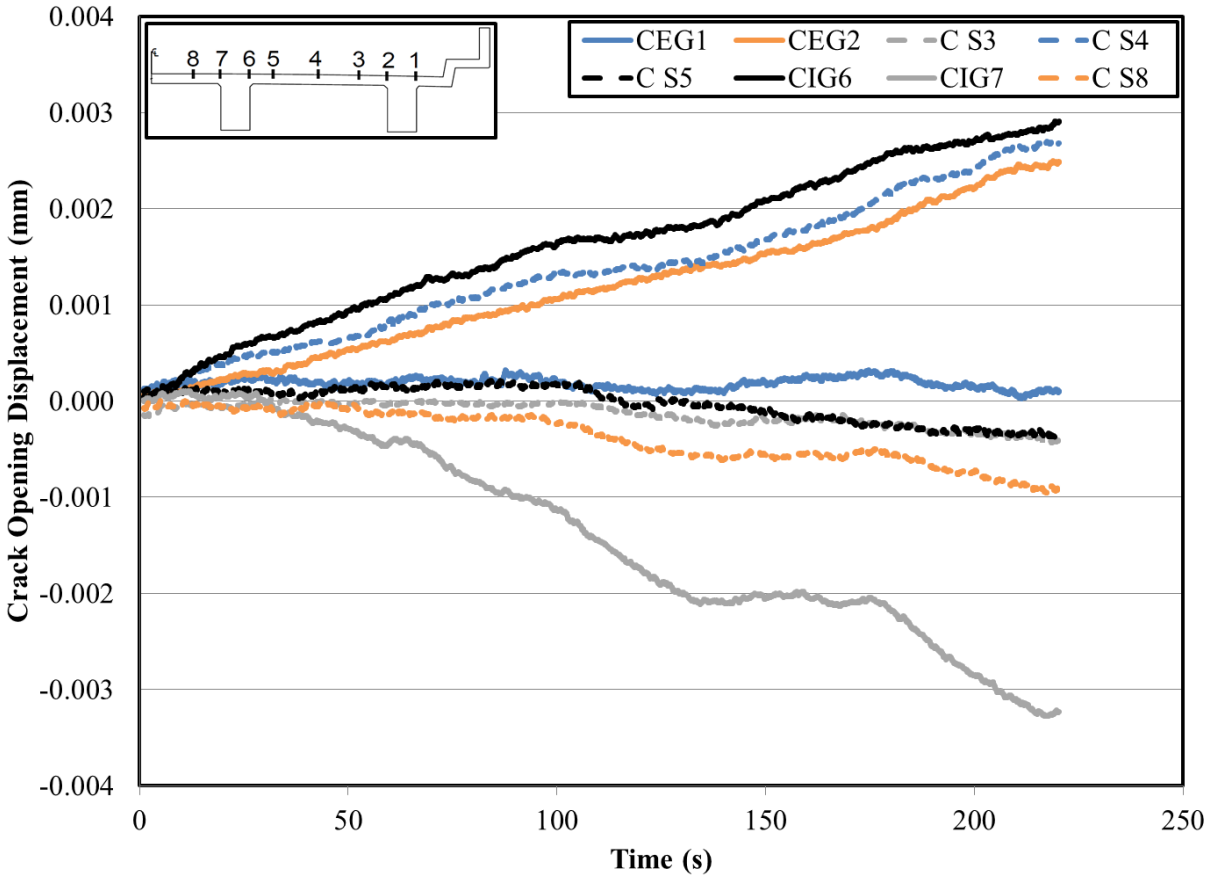

Figure 6.4 Transducer Linear Drift without Loading on Bridge

Figure 6.4 depicts a continuous drift in the transducers over time. This drift could be estimated as a linear drift. Drift in transducer measurements could be caused by many external factors during the load test. However, in these tests it was concluded that drift was primarily caused by temperature gradients in the bridge deck created by exposure to sunlight. Although transducers were shaded from direct sunlight, the bridge deck temperature and ambient

temperature around the transducers increased during testing. The assumption of drift due to temperature is also validated by comparing results from the pre-retrofit load test, which occurred on a sunny morning, and the post-retrofit load test, which occurred on an overcast morning. Figure 6.5 and Figure 6.6 show raw data from the pre-retrofit and post-retrofit load tests, respectively.

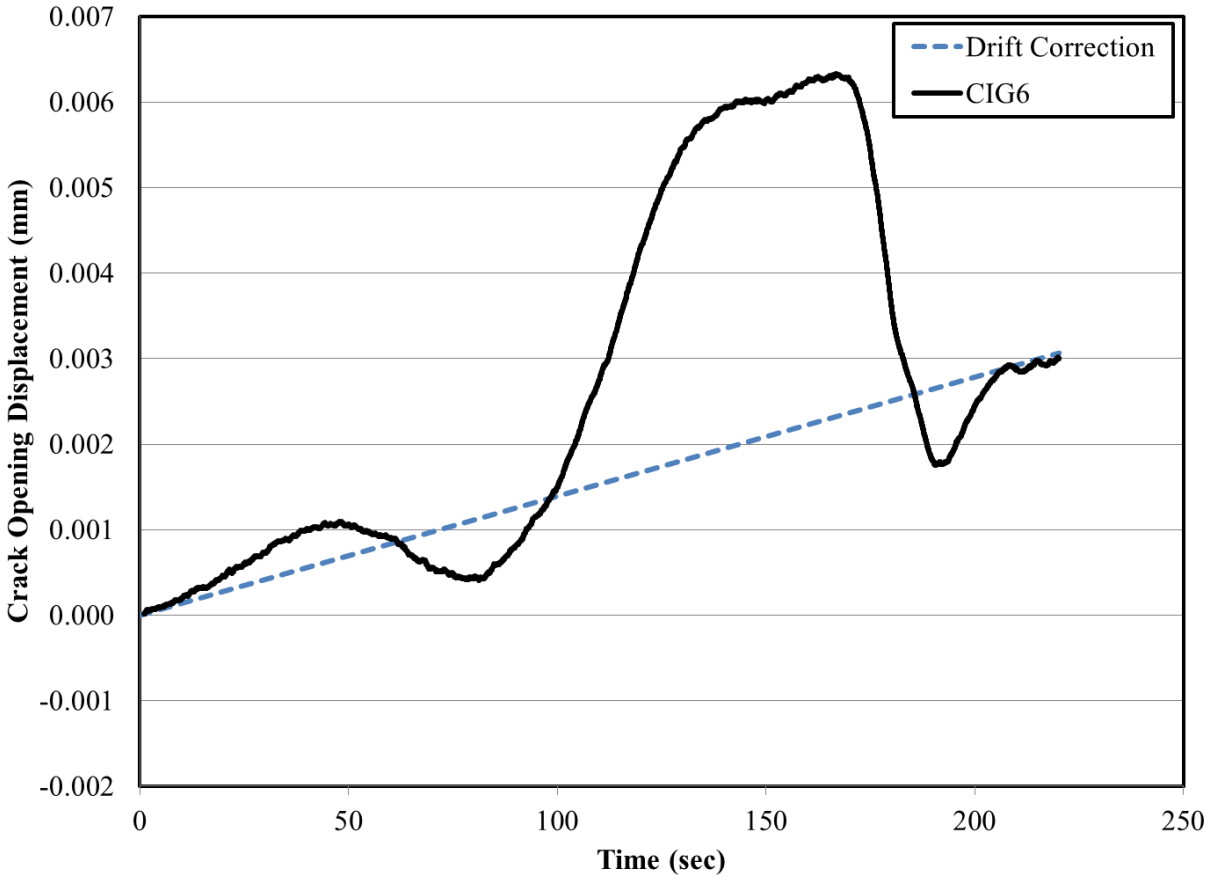

Figure 6.5 Transducer CIG6 Raw Data from Pre-Retrofit Load Test on Sunny Morning

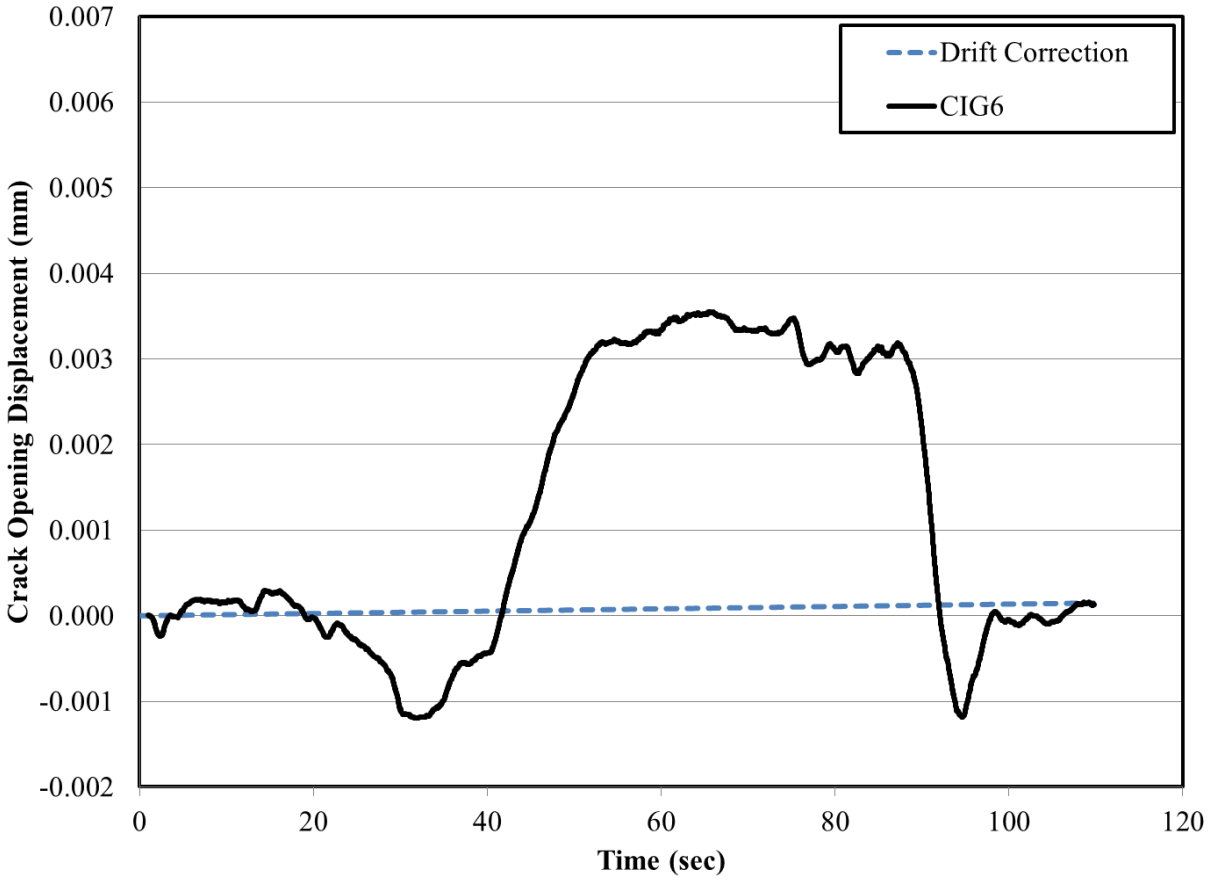

Figure 6.6 Transducer CIG6 Raw Data from Post-Retrofit Load Test on Overcast Morning

In Figure 6.5 and Figure 6.6, the drift correction shown provides an assumed linear representation of the drift from the beginning to end of the test. At both of these points there was no load truck on the bridge. These two figures clearly indicate that the transducer experienced much less drift during the post-retrofit (overcast) load test than during the pre-retrofit (sunny) load test.

A linear drift correction was applied to the raw data, based on the assumption of temperature-induced drift. The first and last data point determined endpoints for the linear drift correction. The drift correction value at each recorded data point during the test was subtracted from the raw measurement to produce a corrected value for each measurement. Figure 6.7 shows corrected data for a transducer from a single truck run.

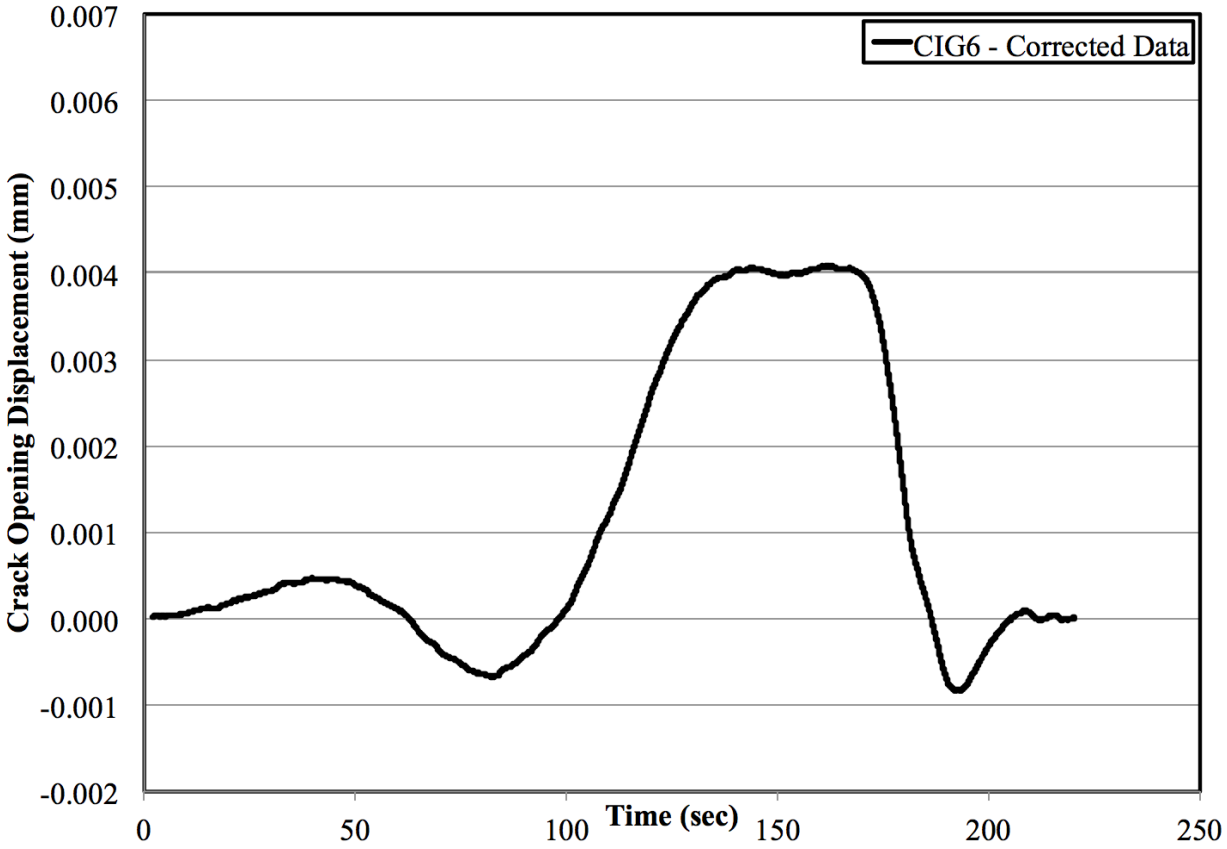

Figure 6.7 Transducer CIG6 Corrected Data from Pre-Retrofit Load Test

After applying a linear drift correction to the data, each transducer was individually examined for each run. The maximum crack opening displacement was determined by averaging the displacement recorded while the load truck was placed at the critical position. Figure 6.8 shows an example of corrected data from a single transducer for one run and the determination of the maximum crack opening displacement.

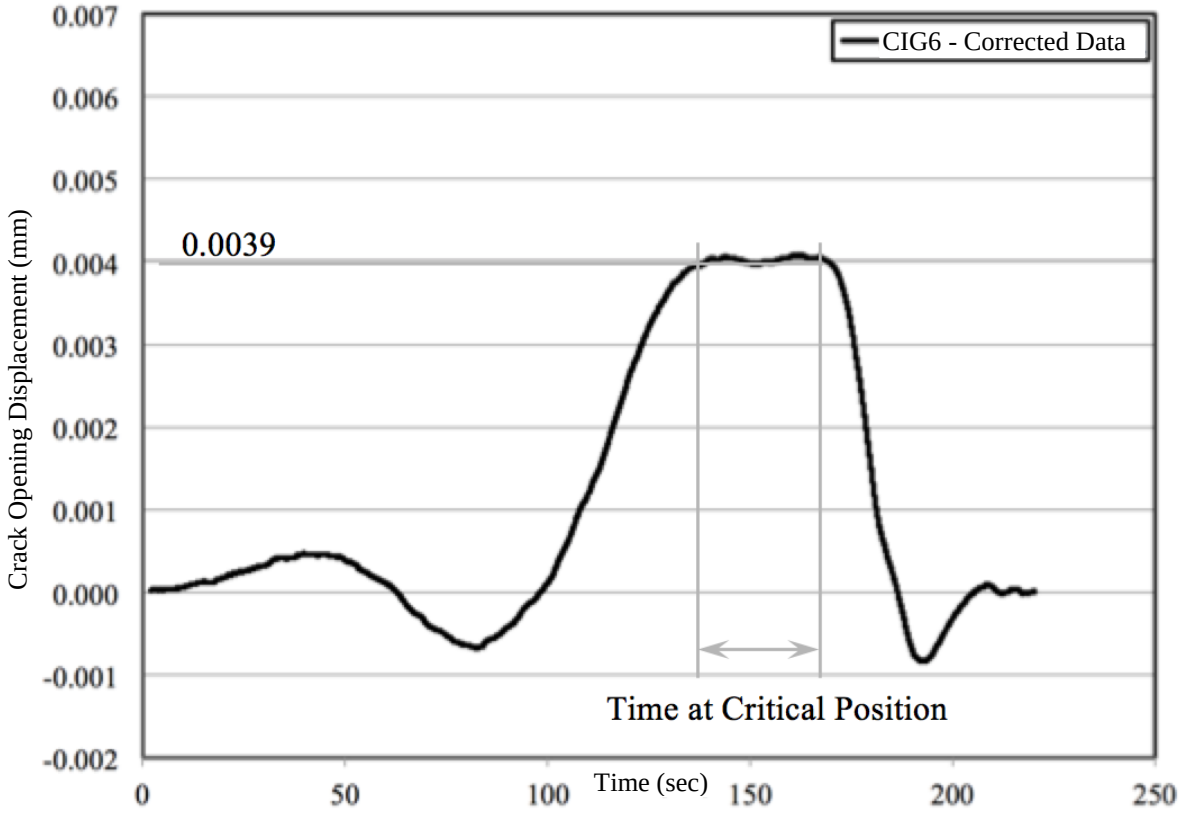

Figure 6.8 Determination of Maximum Crack Opening Displacement for Transducer CIG6 for the Pre-Retrofit Load Test

The first value from each run, or the displacement when the truck was not on the bridge, was subtracted from the maximum crack opening displacement value to determine the change in crack opening displacement during each run. Each transducer was examined according to this process for each run of all three load tests.

6.4.2 Pre-Retrofit Load Test

The pre-retrofit load test provided baseline data representing the performance of the unstrengthened bridge. Crack opening displacements for the first load test were recorded for one sequential loading with a single load truck stopping at all loading positions and four test runs with a single load truck stopping only at the critical load position. Two maximum crack opening

displacements were recorded for the sequential loading, indicating the maximum COD when the load truck passed the critical position on the bridge for the first and second time. Maximum crack opening displacements for each transducer were averaged for similar loading patterns. Maximum displacements for all runs and average maximum crack opening displacements of the pre-retrofit load test are listed in Table 6.5.

Table 6.5 Pre-Retrofit Maximum Crack Opening Displacements

Run No.	Test Run Description	No. of Load Trucks	Crack Opening Displacement (mm)							
			C S8	CIG7	CIG6	C S5	C S4	C S3	CEG2	CEG1
1A	Sequential - First Pass	1	0.0027	0.0034	0.0040	0.0027	0.0028	0.0009	0.0008	0.0032
1B	Sequential - Second Pass	1	0.0028	0.0034	0.0038	0.0024	0.0027	0.0007	0.0008	0.0030
Sequential Run Average		**1**	**0.0028**	**0.0034**	**0.0039**	**0.0026**	**0.0028**	**0.0008**	**0.0008**	**0.0031**
2	Critical Position	1	0.0026	0.0039	0.0039	0.0027	0.0027	0.0013	0.0009	0.0035
3	Critical Position	1	0.0026	0.0034	0.0037	0.0021	0.0026	0.0009	0.0007	0.0031
4	Critical Position	1	0.0026	0.0038	0.0038	0.0023	0.0028	0.0009	0.0008	0.0032
5	Critical Position	1	0.0029	0.0037	0.0039	0.0026	0.0026	0.0011	0.0007	0.0036
Critical Position Average		**1**	**0.0027**	**0.0037**	**0.0038**	**0.0024**	**0.0027**	**0.0011**	**0.0008**	**0.0034**

Results from both the sequential and critical position loadings yielded very similar results, as shown in Figure 6.9.

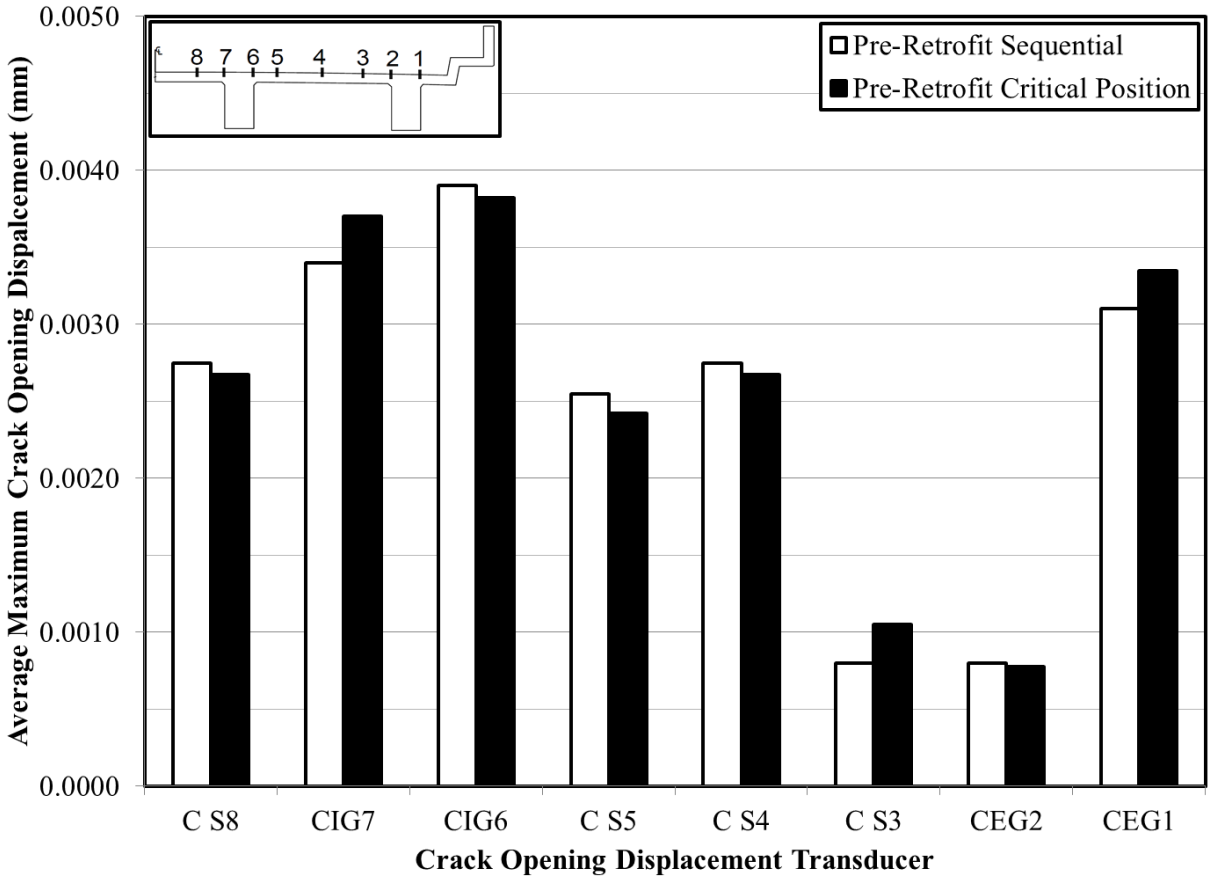

Figure 6.9 Pre-Retrofit Maximum Average CODs for Sequential and Critical Position Loadings

As shown in Figure 6.9, cracks in girders exhibited larger CODs than cracks in the slab. As stiffer elements, girders attract a larger percentage of the moment in the bridge. This behavior is consistent across both girders, except for transducer CEG2. This is primarily due to prior bridge cracking. At the area of the bridge where both C S3 and CEG2 were located, the single, large instrumented crack spreads into multiple, small, closely spaced cracks. Therefore, the COD at this location was split among several small, closely spaced cracks in this area, and only one of the small cracks was instrumented.

Ranges between maximum and minimum COD recordings for all test runs were also examined to better understand dispersion in the results. Average COD range for each transducer is tabulated in Table 6.6.

Table 6.6 Pre-Retrofit Average COD Range

COD Transducer	C S8	CIG7	CIG6	C S5	C S4	C S3	CEG2	CEG1
Minimum COD (mm)	0.0026	0.0034	0.0037	0.0021	0.0026	0.0007	0.0007	0.0030
Maximum COD (mm)	0.0029	0.0039	0.0040	0.0027	0.0028	0.0013	0.0009	0.0036
Average COD (mm)	0.0027	0.0036	0.0039	0.0025	0.0027	0.0010	0.0008	0.0033
COD Range	**0.0003**	**0.0005**	**0.0003**	**0.0006**	**0.0002**	**0.0006**	**0.0002**	**0.0006**
Average COD Range (mm)	**0.0004**							

As shown in Table 6.6, bridge test results exhibited an average range between maximum and minimum CODs of 0.0004 mm for the same truck position. This range indicates the relatively large within-test variability associated with these load tests. Considering the consistency of the means of the critical and sequential data relative to the dispersion of the data in each set, results from all pre-retrofit runs could be averaged together to estimate the behavior of the Letohatchee bridge before strengthening.

CODs fluctuated within this range due to the inherent inconsistency of field-testing an active bridge with a moving load truck. Load truck positioning was repeated as carefully as possible, but slight discrepancies in load truck positioning, as well as deviations from the assumed linear drift, for each run could affect measured COD.

6.4.3 Post-Retrofit Load Test

Post-retrofit load test data represents the performance of the strengthened bridge. Crack opening displacements for the second load test were recorded for two sequential loadings with a single load truck stopping at all loading positions and three test runs with a single load truck

stopping only at the critical load position. The single load truck test runs were directly compared to the pre-retrofit load test results.

The post-retrofit load test also included test runs with two load trucks. CODs were recorded for two sequential loadings with the second load truck stopping at all loading positions and three test runs with the second truck only stopping at the critical load position. When using two load trucks, the second load truck never traveled beyond the critical loading position. Therefore, there is only one maximum COD recorded for the two load truck sequential loadings. Maximum CODs for the post-retrofit load test are tabulated in Table 6.7.

Table 6.7 Post-Retrofit Maximum Crack Opening Displacements

Run No.	Test Run Description	No. of Load Trucks	Crack Opening Displacement (mm)							
			C S8	CIG7	CIG6	C S5	C S4	C S3	CEG2	CEG1
1A	Sequential - First Pass	1	0.0035	0.0039	0.0018	0.0027	0.0042	0.0025	0.0014	0.0035
1B	Sequential - Second Pass	1	0.0034	0.0039	0.0033	0.0027	0.0041	0.0024	0.0014	0.0034
2A	Sequential - First Pass	1	0.0032	0.0036	0.0029	0.0025	0.0041	0.0022	0.0008	0.0031
2B	Sequential - Second Pass	1	0.0032	0.0035	0.0032	0.0024	0.0040	0.0022	0.0008	0.0031
Sequential Run Average		**1**	**0.0033**	**0.0037**	**0.0028**	**0.0026**	**0.0041**	**0.0023**	**0.0011**	**0.0033**
3	Critical Position	1	0.0032	0.0034	0.0032	0.0021	0.0036	0.0016	0.0007	0.0030
4	Critical Position	1	0.0031	0.0032	0.0040	0.0024	0.0038	0.0018	0.0006	0.0030
5	Critical Position	1	0.0031	0.0034	0.0035	0.0022	0.0039	0.0017	0.0006	0.0030
Critical Position Average		**1**	**0.0031**	**0.0033**	**0.0036**	**0.0022**	**0.0038**	**0.0017**	**0.0006**	**0.0030**
6	Sequential	2	0.0067	0.0067	0.0060	0.0042	0.0067	0.0036	0.0016	0.0046
7	Sequential	2	0.0065	0.0074	0.0074	0.0041	0.0067	0.0033	0.0013	0.0048
Sequential Run Average		**2**	**0.0066**	**0.0071**	**0.0067**	**0.0042**	**0.0067**	**0.0035**	**0.0015**	**0.0047**
8	Critical Position	2	0.0068	0.0077	0.0077	0.0043	0.0068	0.0033	0.0012	0.0048
9	Critical Position	2	0.0067	0.0074	0.0077	0.0043	0.0068	0.0035	0.0016	0.0052
10	Critical Position	2	0.0071	0.0072	0.0072	0.0048	0.0073	0.0041	0.0019	0.0048
Critical Position Average		**2**	**0.0069**	**0.0074**	**0.0075**	**0.0045**	**0.0070**	**0.0036**	**0.0016**	**0.0049**

6.4.3.1 Single Load Truck Results

There was an apparent discrepancy between the sequential run and critical position run results in single load truck tests. This is most likely due to the behavior of the bridge during the post-retrofit load test. Maximum average CODs for the sequential load test during the post-

retrofit load test were almost all significantly higher than the CODs for the critical position runs. This may be due to the crack not fully returning to its pre-loaded state when the load truck was removed from the bridge. Evidence of this phenomenon can be seen through decreasing CODs during the sequential load tests, as shown in Figure 6.10.

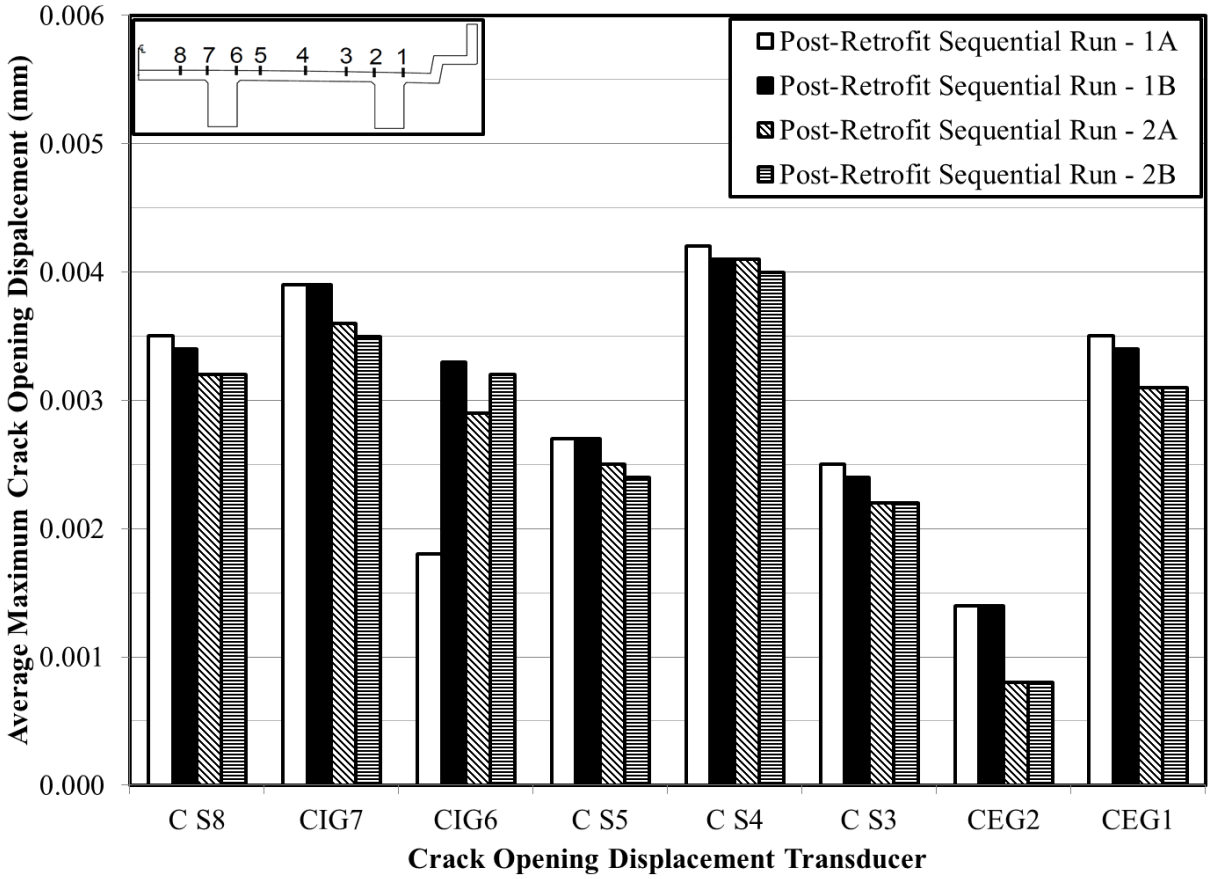

Figure 6.10 Post-Retrofit Maximum Average COD for Sequential Runs with One Load Truck

Figure 6.10 shows that except for CIG6, CODs steadily decreased during the post-retrofit sequential runs, as Run 1 occurred prior to Run 2. This may indicate that the crack was not closing back to its original state during this test. However, at the end of the critical runs, the crack appeared to be closing back to the position it began at for each run. This is evident by

examining the consistency in maximum CODs during the critical position runs, which followed the sequential runs, as shown in Figure 6.11.

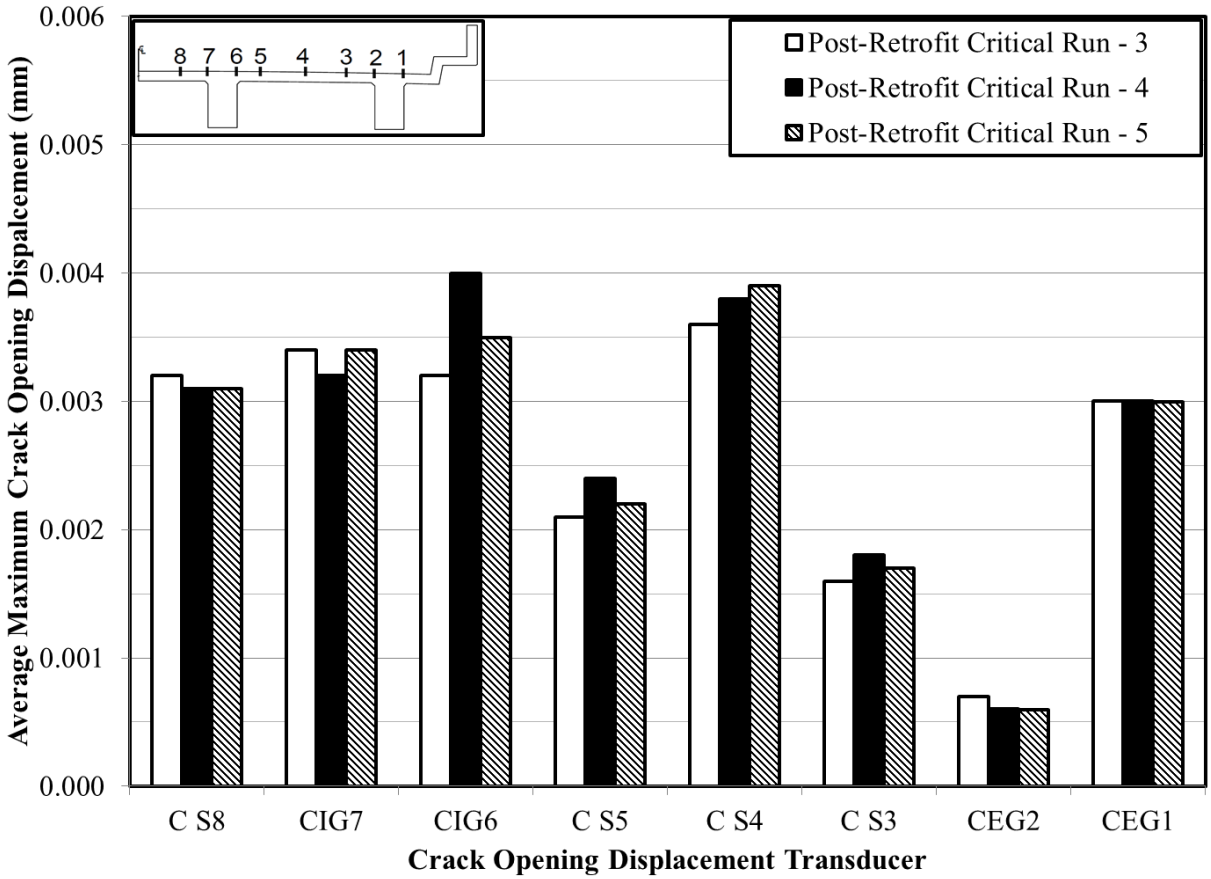

Figure 6.11 Post-Retrofit Maximum Average COD for Critical Runs with One Load Truck

Therefore, the post-retrofit sequential run results are not a good basis for examining the effectiveness of the Letohatchee bridge strengthening. Critical position runs from the post-retrofit load test provide more consistent results.

Ranges between maximum and minimum COD recordings for critical position runs were also examined to better understand post-retrofit load test results. Average COD range for critical position runs for each transducer is tabulated in Table 6.8.

Table 6.8 Post-Retrofit Critical Position Runs Average COD Range

COD Transducer	C S8	CIG7	CIG6	C S5	C S4	C S3	CEG2	CEG1
Minimum COD (mm)	0.0031	0.0032	0.0032	0.0021	0.0036	0.0016	0.0006	0.0030
Maximum COD (mm)	0.0032	0.0034	0.0040	0.0024	0.0039	0.0018	0.0007	0.0030
Average COD (mm)	0.0031	0.0033	0.0036	0.0022	0.0038	0.0017	0.0006	0.0030
COD Range (mm)	**0.0001**	**0.0002**	**0.0008**	**0.0003**	**0.0003**	**0.0002**	**0.0001**	**0.0000**
Average COD Range (mm)	**0.0002**							

According to Table 6.8, post-retrofit bridge test results exhibited an average range between maximum and minimum CODs of 0.0002 mm. This range is smaller than the pre-retrofit load test range of 0.0004 mm. Therefore, the critical position results were examined to compare the post-retrofit and pre-retrofit behavior of the bridge.

6.4.3.2 Two Load Truck Results

Results from tests with two load trucks provided fairly consistent results between both sequential and critical position runs. Figure 6.12 shows maximum average CODs for sequential and critical position loadings with two load trucks.

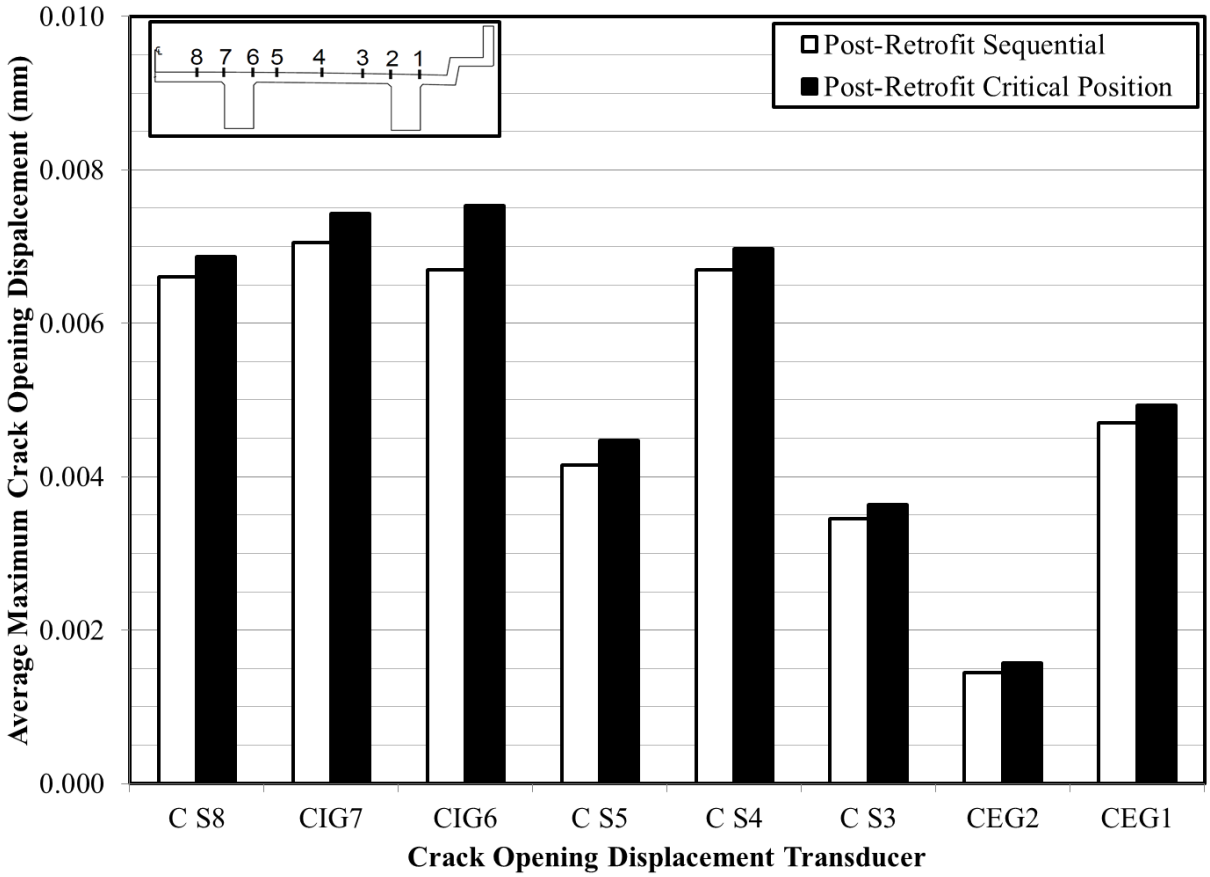

Figure 6.12 Post-Retrofit Maximum Average COD for Critical Runs with Two Load Trucks

Ranges between maximum and minimum COD recordings for all runs with two load trucks were also examined to better understand the results. Average COD range for each transducer is tabulated in Table 6.9.

Table 6.9 Post-Retrofit Critical Position Runs Average COD Range

COD Transducer	C S8	CIG7	CIG6	C S5	C S4	C S3	CEG2	CEG1
Minimum COD (mm)	0.0065	0.0067	0.0060	0.0041	0.0067	0.0033	0.0012	0.0046
Maximum COD (mm)	0.0071	0.0077	0.0077	0.0048	0.0073	0.0041	0.0019	0.0052
Average COD (mm)	0.0068	0.0073	0.0072	0.0043	0.0069	0.0036	0.0015	0.0048
COD Range (mm)	**0.0006**	**0.0010**	**0.0017**	**0.0007**	**0.0006**	**0.0008**	**0.0007**	**0.0006**
Average COD Range (mm)	**0.0008**							

According to Table 6.9, post-retrofit bridge test results exhibited an average range between maximum and minimum CODs of 0.0008 mm. All of the two truck results will be examined to compare the post-retrofit behavior of the bridge because these results were fairly consistent and there was very little data collected with two trucks.

6.4.3.3 Single Load Truck Comparisons

Comparison of single load truck CODs from the pre-retrofit and post-retrofit load test could indicate a reduction in stress in the reinforcing steel in the Letohatchee bridge. Percent reduction in CODs for each transducer for critical position runs are tabulated in Table 6.10.

Table 6.10 Pre-Retrofit and Post-Retrofit COD Comparison

Test Run Description	No. of Load Trucks	Crack Opening Displacement Transducers							
		C S8	CIG7	CIG6	C S5	C S4	C S3	CEG2	CEG1
Critical Position Runs Only Average Maximum COD (mm)									
Pre-Retrofit	1	0.0027	0.0037	0.0038	0.0024	0.0027	0.0011	0.0008	0.0034
Post-Retrofit	1	0.0031	0.0033	0.0036	0.0022	0.0038	0.0017	0.0006	0.0030
Percent Reduction	**1**	**-15%**	**10%**	**5%**	**8%**	**-41%**	**-55%**	**25%**	**12%**

A positive value of percent reduction in CODs indicates an overall reduction in reinforcing steel stress. However, there are some unexpected results, indicated by shading in Table 6.10. If the shaded results are omitted, the critical position runs indicate an average stress reduction of 12%. However, the unexpected results must be analyzed to justify exclusion.

The unexpected results could have been caused by transducers slipping in the pre-retrofit load test. If transducers slipped where attached to the bridge deck, then the transducers would not have moved as much as the crack opening displaced during testing. This would result in transducer measurements that are less than the actual CODs in the pre-retrofit load test. If transducers did not slip in the post-retrofit load test, then the post-retrofit results might indicate larger CODs than those recorded during the pre-retrofit test. However, any transducer slipping would result in poor repeatability and could be the cause of unexpected test results.

Another cause of the unexpected results could be transducer lateral distance from girders and reinforcing steel. Cross-sectional geometry of the instrumented section is shown in Figure 6.13. Horizontal location of reinforcing steel in the original plans was verified through field rebar location using a cover meter (Proceq Profometer PM-6).

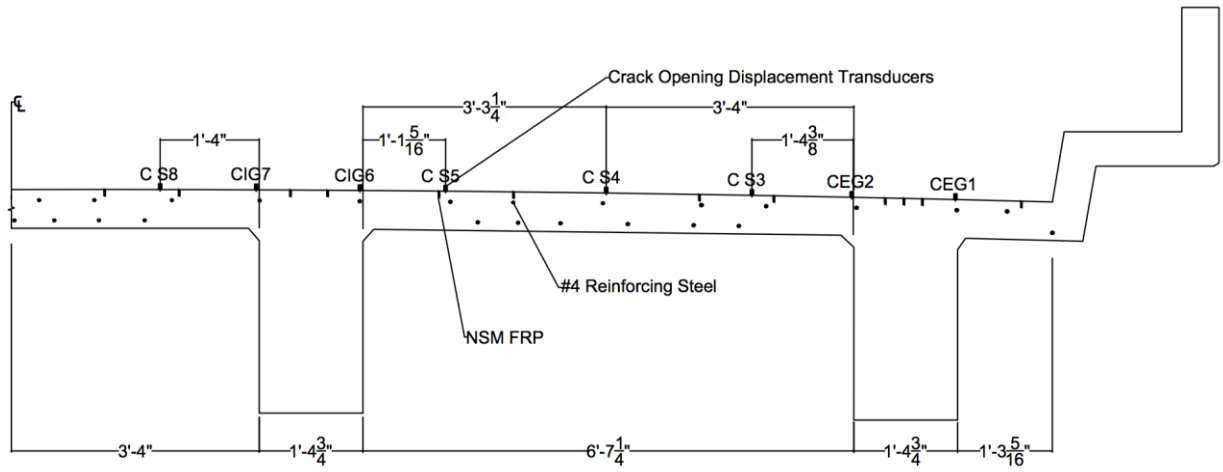

Figure 6.13 Instrumented Cross Section of the Letohatchee Bridge

COD transducers CS 8, CS 4, and CS 3 were located farther from girders than other transducers. Also, C S8 and C S3 are located noticeably farther away from reinforcing steel than the other transducers. Therefore, this could indicate that the addition of FRP strips into the slab created an increase in localized stiffness at these locations. This increase in stiffness could have

drawn more of the moment response into the slab that was previously resisted by the girder in the pre-retrofit test. This would result in an increased COD in slab transducers near FRP stiffened areas and lower COD in girders.

It is also very important to consider the dispersion of test results. Results from the pre-retrofit and post-retrofit load tests exhibited a range of 0.0004 mm and 0.0002 mm, respectively. Changes in CODs from the pre-retrofit to post-retrofit load tests range from 0.0002 mm to 0.0011 mm. Therefore, it is impossible to reliably determine if there was an actual reduction in reinforcing steel stress because results could have fluctuated by about half of the maximum recorded change within a single load test. Ideally, heavier load trucks would have created larger CODs during testing, which could have increased the measured COD. However, only a single load was used in the pre-retrofit load test to ensure safety during testing due to the age of the Letohatchee bridge and the active interstate highway traffic below the bridge.

Therefore, based on the post-retrofit load test results, it cannot be concluded that the NSM FRP system decreased demand on all the flexural reinforcing steel; however, it does appear to have reduced the demand on the flexural steel over the girders. In addition, the COD values are more evenly distributed across the entire bridge than before the retrofit. The long-term test provides additional data to further verify the behavior of the Letohatchee bridge after strengthening.

6.4.3.4 Two Load Truck Comparisons

Linear-elastic behavior of the bridge was investigated by examining the change in maximum CODs from one to two load trucks. Increases in CODs from tests with one load truck to tests with two load trucks are tabulated in Table 6.11.

Table 6.11 Increase in CODs with 2 Load Trucks versus 1 Load Truck

Description	Crack Opening Displacement Transducers								Average Increase
	Interior Girder				Exterior Girder				
	C S8	CIG7	CIG6	C S5	C S4	C S3	CEG2	CEG1	
Increase in COD	116%	118%	102%	94%	82%	109%	140%	61%	**103%**
Average Increase	**108%**				**98%**				

There was an average increase in COD of 103% during the two load truck tests, in comparison to the single load truck tests. Therefore, when the load on the bridge was doubled, CODs approximately doubled. This behavior is consistent with linear-elastic behavior. It is also notable that the interior girder exhibited a greater increase in COD, possibly because it was closer to the second load truck than the exterior girder.

6.4.4 Long-Term Load Test

The long-term load test data represent the condition of the retrofit one year after strengthening. Crack opening displacements for the long-term load test were recorded for three sequential loadings with a single load truck stopping at all loading positions and three test runs with a single load truck stopping only at the critical load position. Maximum CODs for the long-term load test are tabulated in Table 6.12.

Table 6.12 Long-Term Load Test Maximum Crack Opening Displacements (mm)

Run No.	Test Run Description	No. of Load Trucks	Crack Opening Displacement Transducers							
			C S8	CIG7	CIG6	C S5	C S4	C S3	CEG2	CEG1
1A	Sequential - First Pass	1	0.0051	0.0041	0.0033	0.0021	0.0033	0.0021	0.0007	0.0026
1B	Sequential - Second Pass	1	0.0050	0.0035	0.0031	0.0018	0.0028	0.0015	0.0003	0.0027
2A	Sequential - First Pass	1	0.0026	0.0038	0.0030	0.0019	0.0022	-0.0001	0.0006	0.0025
2B	Sequential - Second Pass	1	0.0027	0.0041	0.0031	0.0022	0.0027	0.0019	0.0008	0.0024
3A	Sequential - First Pass	1	0.0030	0.0035	0.0031	0.0011	0.0020	0.0012	0.0002	0.0026
3B	Sequential - Second Pass	1	0.0029	0.0039	0.0032	0.0018	0.0025	0.0015	0.0004	0.0027
Sequential Run Average		**1**	**0.0036**	**0.0038**	**0.0031**	**0.0018**	**0.0026**	**0.0014**	**0.0005**	**0.0026**
4	Critical Position	1	0.0033	0.0040	0.0031	0.0020	0.0029	0.0018	0.0004	0.0027
5	Critical Position	1	0.0025	0.0043	0.0031	0.0023	0.0026	0.0016	0.0009	0.0029
6	Critical Position	1	0.0028	0.0043	0.0031	0.0024	0.0027	0.0014	0.0008	0.0035
Critical Position Average		**1**	**0.0029**	**0.0042**	**0.0031**	**0.0022**	**0.0027**	**0.0016**	**0.0007**	**0.0030**

Only critical position results from the long-term load test were examined for comparison to the post-retrofit load test due to the previously discussed discrepancy in the sequential test results in the post-retrofit load test. Ranges between maximum and minimum COD recordings for critical position runs were examined to better understand dispersion of the results. Average COD range for each transducer is tabulated in Table 6.13.

Table 6.13 Long-Term Test Critical Position Runs Average COD Range

COD Transducer	C S8	CIG7	CIG6	C S5	C S4	C S3	CEG2	CEG1
Minimum COD (mm)	0.0025	0.0040	0.0031	0.0020	0.0026	0.0014	0.0004	0.0027
Maximum COD (mm)	0.0033	0.0043	0.0031	0.0024	0.0029	0.0018	0.0009	0.0035
Average COD (mm)	0.0029	0.0042	0.0031	0.0022	0.0027	0.0016	0.0007	0.0030
COD Range (mm)	**0.0008**	**0.0003**	**0.0000**	**0.0004**	**0.0003**	**0.0004**	**0.0005**	**0.0008**
Average COD Range (mm)	**0.0004**							

According to Table 6.13, the post-retrofit bridge test results exhibited an average range between maximum and minimum CODs of 0.0004 mm. This range is consistent with the pre-retrofit load test range of 0.0004 mm, and larger than the post-retrofit load test range of 0.0002 mm.

6.4.4.1 Post-Retrofit and Long-Term Load Test Comparisons

CODs for critical position runs were similar for the post-retrofit and long-term load tests. Percent reduction in maximum average CODs from the post-retrofit and long-term load tests are tabulated in Table 6.14.

Table 6.14 Post-Retrofit and Long-Term COD Percent Reductions

Test Run Description	No. of Load Trucks	Crack Opening Displacement Transducers								Average Percent Reduction
		C S8	CIG7	CIG6	C S5	C S4	C S3	CEG2	CEG1	
Critical Position Runs Only Averaged (mm)										
Post-Retrofit	1	0.0031	0.0033	0.0036	0.0022	0.0038	0.0017	0.0006	0.0030	
Long-Term	1	0.0029	0.0042	0.0031	0.0022	0.0027	0.0016	0.0007	0.0030	
Percent Reduction	**1**	**8%**	**-26%**	**14%**	**0%**	**27%**	**7%**	**-8%**	**-1%**	**3%**

An examination of the maximum average CODs for critical position loadings in the post-retrofit and long-term load tests show that the results from both post-strengthening tests provide very similar results. Most average CODs were within the range of dispersion measured during any single test, or 0.0004 mm, and there was an average percent reduction of only 3% across all

transducers. Figure 6.14 graphically shows maximum average CODs for critical position loadings for the post-retrofit and long-term load tests.

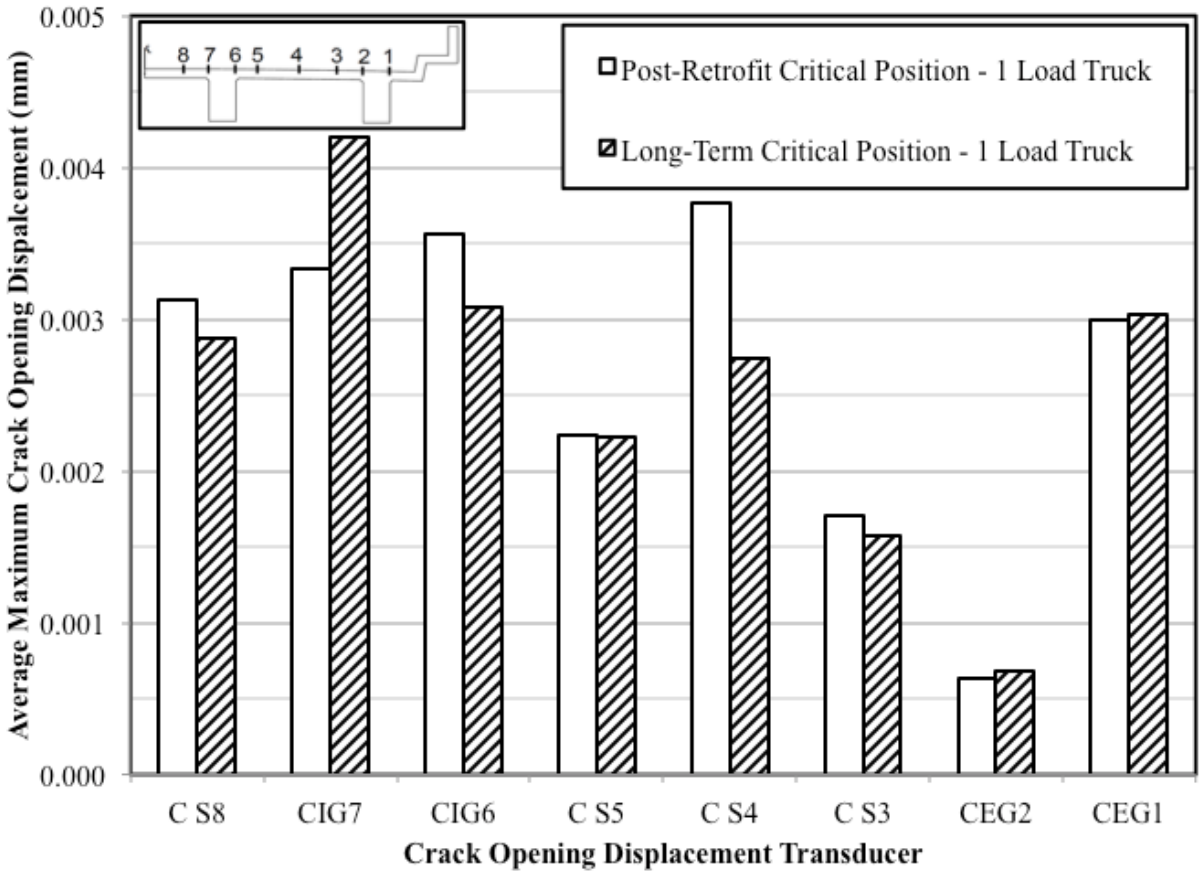

Figure 6.14 Post-Retrofit and Long-Term Load Test Average Maximum CODs for Critical Position Runs

Therefore, it can be observed that the Letohatchee bridge behaved similarly during both the post-retrofit and long-term load tests. This most likely indicates that there was no noticeable change in effectiveness of the FRP strengthening system one year after construction.

Due to the similarity of results from both load tests of the strengthened bridge, the results from the post-retrofit and long-term critical position load tests were averaged together to better estimate the behavior of the bridge after strengthening. Average maximum CODs from all

critical position runs with one load truck from the post-retrofit and long-term load test were averaged as the strengthened critical position results, and are tabulated in Table 6.15.

Table 6.15 Average Maximum CODs for Strengthened Critical Position Results

	No. of Load Trucks	Crack Opening Displacement Transducers							
		C S8	CIG7	CIG6	C S5	C S4	C S3	CEG2	CEG1
Critical Position Average (mm)	**1**	**0.0030**	**0.0038**	**0.0033**	**0.0022**	**0.0033**	**0.0016**	**0.0007**	**0.0030**

6.4.4.2 Pre-Retrofit and Strengthened Bridge Load Test Comparisons

Pre-retrofit load test results were compared to the strengthened critical position results to determine effectiveness of the retrofit. Results from the strengthened bridge presented in Table 6.15, were plotted against the pre-retrofit load test results in Figure 6.15.

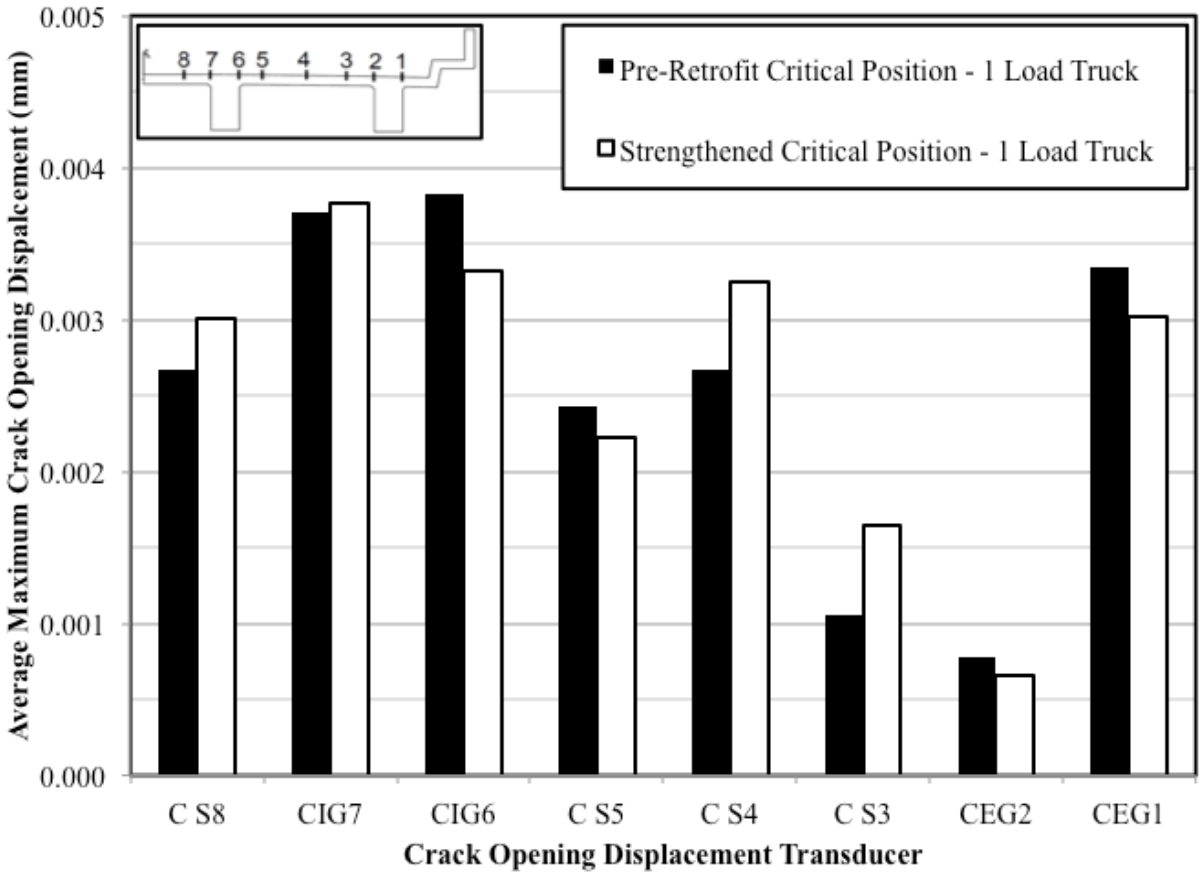

Figure 6.15 CODs of the Pre-Retrofit and Strengthened Letohatchee Bridge

Percent reduction in CODs due to strengthening are tabulated in Table 6.16.

Table 6.16 Pre-Retrofit and Strengthened Bridge COD Comparison

Test Run Description	No. of Load Trucks	Crack Opening Displacement Transducers							
		C S8	CIG7	CIG6	C S5	C S4	C S3	CEG2	CEG1
Critical Position Runs Only Average Maximum COD (mm)									
Pre-Retrofit	1	0.0027	0.0037	0.0038	0.0024	0.0027	0.0011	0.0008	0.0034
Post-Retrofit	1	0.0030	0.0038	0.0033	0.0022	0.0033	0.0016	0.0007	0.0030
Percent Reduction	**1**	**-12%**	**-2%**	**13%**	**8%**	**-22%**	**-56%**	**15%**	**10%**

According to the results presented in Table 6.16, there was a reduction in COD recorded at four of the eight crack opening displacement transducers. Transducer CIG7 indicates a very slight increase in COD after strengthening. Transducers C S8, C S4, and C S3 indicate larger

CODs after strengthening. Discrepancies at these three transducers can be attributed to cross-sectional stiffness differences due to distance from girders and reinforcing steel, as previously discussed. However, it is reasonable to consider that due to the dispersion of results over a range of 0.0004 mm, this indicates little change after strengthening.

Based on these results, girder flexural reinforcement may have experienced an average decrease in strain of approximately 10%. Likewise, slab transducers indicate that the slab reinforcement may have experienced an increase in strain of 20%. According to these results, the reduction in strain due to this retrofit was constrained to the bridge girders. Installing FRP in the slab could have increased localized stiffness in areas of the slab, drawing more moment into the slab that was previously resisted by the girder. Also, the retrofit design placed NSM FRP strips with significantly less spacing over girders than in slab regions. Therefore, in the areas where NSM FRP strips were located closer together there could have been a greater reduction in strain after strengthening due to the increase in reinforcement. Overall, the COD was slightly more uniform across the width of the bridge after the retrofit than it was prior to strengthening.

6.4.5 Visual Inspection

A visual inspection of the strengthened bridge was conducted one year after construction. There was no sign of bond degradation between the epoxy and the concrete nor between the FRP and the epoxy one year after construction. No portion of an FRP strip was visibly exposed at any location. While the majority of the NSM FRP did not show any signs of wear, there were areas of concern that were observed. Widely scattered throughout the retrofit there were small areas where epoxy appeared to be brittle and only a thin layer of epoxy protected the FRP strip. A picture of the NSM FRP one year after installation without apparent degradation is shown in

Figure 6.16, and a picture of a typical area of concern of epoxy degradation is shown in Figure 6.17.

Figure 6.16 Epoxy Showing No Degradation One Year After Installation

Figure 6.17 Typical Area of Epoxy Degradation

There were some signs of epoxy degradation near the ends of strips, such as that shown in Figure 6.18. This may be due to thin epoxy at the edge of grooves where the curve of the saw blade created a tapering groove depth. Deepening the shallow end portions of grooves to be consistent with the specified depth could remedy some degradation. This could be achieved by drilling down the tapered groove end prior to FRP installation.

Figure 6.18 Degradation of Epoxy Near Ends of Strips

Degradation of epoxy is a potential issue for the longevity of this retrofit technique and can have many causes. The areas of concern were primarily isolated to apparent low points in the epoxy and could have been associated with ponding of water in these depressions. Another possible source of epoxy degradation could be exposure to ultraviolet (UV) light. However, it seems unlikely that potential degradation due to UV exposure would be limited to small, discrete areas. Figure 6.19 shows another typical area of degradation. The orange paint was used to mark the area.

Figure 6.19 Typical Epoxy Degradation

There was no sign of bond degradation between the epoxy and the concrete nor between the FRP and the epoxy one year after construction. No portion of an FRP strip was visibly exposed at any location. The individual areas of apparent epoxy degradation occurred in average lengths of 4 in. (14 cm) at an average spacing of 30 ft in a strip. The visible areas of concern comprised only 0.64% of the total length of NSM FRP retrofit one year after construction.

The long-term durability of this strengthening technique is yet unknown. There were no noticeable changes in structural performance due to one year of exposure to the environment and traffic, but degradation could occur over an extended period of time through exposure to UV light, water, chemicals, and abrasion. Therefore, further research should be conducted to better understand the long-term durability and effectiveness of this retrofit technique.

CHAPTER 7:SUMMARY AND CONCLUSIONS

7.1 Summary

The Letohatchee bridge is an ALDOT maintained bridge along AL 97 over I-65 near Letohatchee, Alabama. The bridge is a standard ALDOT bridge (Standard Drawing No. IC 2806) that is deficient for certain truck types. The Letohatchee bridge is a continuous, reinforced concrete deck-girder bridge, with deficiencies in negative-moment capacity. It was proposed to strengthen the bridge using near-surface mounted fiber-reinforced polymer strips. The project began (Alexy 2009) with a review of models and codes to determine the optimum NSM FRP retrofit design for the Letohatchee bridge. Alexy (2009) detailed a proposed laboratory testing program, a portion of which was conducted by Bertolotti (2012). Bertolotti (2012) examined the strength and performance of NSM FRP strengthened cracked girders that approximated the condition of the Letohatchee bridge. He verified that the NSM FRP strengthening scheme proposed by Alexy (2009) performed well under conditions similar to the Letohatchee bridge.

On Tuesday, October 21, 2014, a load test of the Letohatchee bridge was conducted to determine the behavior of the bridge before strengthening. NSM FRP installation took place from Monday, December 8, 2014, to Wednesday, January 21, 2015. A post-retrofit load test was performed on April 2, 2015, in order to examine the behavior of the bridge after strengthening. Finally, a long-term load test and visual inspection was performed on December 17, 2015, which indicated the performance of the retrofit after a year of exposure to service loads and the environment. Test results and the visual inspection verified that there was no evidence of bond degradation one year after installation.

7.2 Conclusions

Several conclusions are reported based on construction methods and NSM FRP performance. Conclusions from this research are in addendum to those determined through laboratory testing (Bertolotti 2012).

7.2.1 Laboratory Testing (Bertolotti 2012)

Bertolotti (2012) documented many conclusions from laboratory testing of cracked, reinforced-concrete girders strengthened with NSM FRP. The following conclusions are reiterated due to their relevance to the field performance of the Letohatchee bridge strengthening.

1. For specimens with concrete compressive strengths of 3000 psi, failure resulted from crushing of concrete and there were no signs of bond degradation due to cyclic loading of 50,000 service-load cycles.
2. Specimen reinforcement ratio within a range of 0.2-0.6% does not affect strengthening from NSM FRP.
3. Six FRP strips per girder per deficient region is more than sufficient to strengthen the Letohatchee bridge negative-moment capacity deficiency (Bertolotti 2012).

7.2.2 Construction

The following conclusions were determined based on the documented processes and methods used during the construction process.

1. Groove cutting using a track-mounted saw required six days per lane, or two days per group of cuts over a single bent.
2. FRP installation took about one day per group of strips over a single bent.
3. FRP installation was completed twice as fast as groove cutting, but was dependent on groove cutting speed to begin FRP installation.

4. Cold temperatures increase the length of time the lane must be closed to traffic because of increases in epoxy curing time.
5. The material cost of FRP and epoxy for this Letohatchee bridge NSM FRP retrofit in 2015 was approximately $3 and $6 per linear foot of strip, respectively.

7.2.3 NSM FRP Structural Performance

The following conclusions were determined based on load test results and performance of the NSM FRP strengthening system.

1. There was an apparent 10 percent reduction in stress in girder negative-moment reinforcement.
2. Stress in slab reinforcement may have increased due to a more even distribution of moment across the bridge cross section.
3. The NSM FRP strengthening system did not show any signs of loss of load resistance or bond degradation one year after installation.

7.3 Recommendations

Preconstruction, construction, and research recommendations are reported based on the results and conclusions from this research.

7.3.1 Preconstruction

During the preconstruction process, it is suggested to observe the following recommendations.

1. Non-destructive evaluation methods, such as ground-penetrating radar (GPR), should be utilized if there are concerns regarding conflict between bridge reinforcement and groove depth or locations.

2. A preconstruction meeting should be conducted involving ALDOT design, maintenance, and construction personnel; project technical advisors, and contractors prior to construction. ALDOT should also consider a pre-bid meeting with qualified contractors to minimize uncertainties about project requirements.
3. The NSM FRP specification and project notes created for the Letohatchee bridge project should be used for future implementations and updated with project specific information as necessary. The specification and project notes are included in Appendices B and C, respectively.

7.3.2 Construction

The following recommendations are based on processes and methods used during the Letohatchee bridge NSM FRP retrofit.

1. Saw types in addition to a track-mounted saw should be considered for groove cutting, because by increasing the rate of groove cutting could reduce the time required for installation by up to 43%.
2. Squaring up the end of grooves with a drill bit should be considered to avoid areas of very thin epoxy in an attempt to create stronger bonds at strip ends.
3. Movability of grooves should be determined and utilized to avoid conflicts when necessary.
4. Installation should be scheduled during seasons when deck temperatures are typically between about 70-100°F (21-38°C) in order to ensure reasonable curing time and limit duration of lane closures.
5. The following process is recommended for installation of NSM FRP strips oriented along the surface of a concrete bridge deck.

- Determine and mark all strip locations on the bridge deck.
- Saw cut grooves in the first lane.
    - Start at the area of highest elevation. This forces the resulting slurry to drain away from this section of cuts; therefore, installation of FRP can begin in this section while groove cutting continues in other areas of the bridge.
    - Vacuum the slurry behind the cutting operation. This significantly reduces the amount of slurry on the bridge deck.
- Clean grooves by power washing immediately after cutting and by pressurized air after grooves have dried.
- Cut FRP strips to length, and place into the dry, cleaned groove. Examine and address any areas where the FRP does not seat below the surface of the bridge deck.
- After verifying proper groove depth, remove the FRP strip and place a bead of epoxy in the bottom of the groove.
- Insert the FRP strip into the epoxied groove and seat it at the proper depth.
- Fill the remaining void space in the groove with epoxy.
- Manually consolidate epoxy into groove around the FRP strip using a putty knife.
- Remove excess epoxy from the deck surface.
- Spread sand on the curing epoxy to promote traction.
- Keep strengthened lane closed to traffic until epoxy initial cure time is reached.

7.3.3 Research

The following items are recommendations for future research to increase the efficiency or effectiveness of NSM FRP strengthening systems.

1. The Letohatchee bridge should be monitored periodically, to determine if further degradation of epoxy occurs and the rate at which it occurs.
2. Required material properties should be determined for alternative adhesives and FRP than those used throughout this research. Workability, constructability, and durability of epoxy and FRP strips should be studied to determine the required material properties for NSM FRP retrofits.
3. A method for acceptance testing of adhesives and FRP should be developed, along with criteria to determine acceptability of the system.
4. The effect of groove straightness on performance should be studied to determine construction tolerances that could allow for other groove cutting methods than a track-mounted saw system.
5. Degradation of epoxy due to environmental exposure should be studied, along with possible overlays, or other methods of delaying epoxy degradation.

REFERENCES

AASHTO. 1996. *AASHTO Standard Specifications for Highway Bridges* . 16th ed. Washington , D.C.: American Association of State Highway and Transportation Officials (AASHTO).

ACI Committee 318. 2014. *Building Code Requirements for Structural Concrete (ACI 318-14).* Farmington Hills, MI: Report by ACI Committee 318, American Concrete Institute.

ACI Committee 440. 2008. *Guide for the Design of Construction of Externally Bonded FRP Systems for Strengthening Concrete Structures (ACI 440.2R).* Farmington Hills, MI: Report by ACI Committee 440, American Concrete Institute.

Aidoo, John, Kent A. Harries, and Michael F. Petrou. 2006. "Full-Scale Experimental Investigation of Repair of Reinforced Concrete Interstate Bridge Using CFRP Materials." *Journal of Bridge Engineering* 350-358.

Alabama Department of Transportation. 2014. "Fiber-Reinforced Polymer Reinforcement of Bridge Deck SR-97 Over I-65 BIN 008847 Lowndes County." *ALDOT Plans of Proposed Project No. IBRCP-00978 (502).* Montgomery, AL: Alabama Department of Transportation.

Alabama Department of Transportation. 2014. "Special Provision No. 12-0991 - Section 595 Fiber-Reinforced Polymer." *Alabama Standard Specifications, 2012.* Montgomery, AL: Alabama Department of Transportation, June 27.

Alexy, Jeffrey Kyle. 2009. "Near-Surface Mounted, Fiber-Reinforced Polymer Strips for Negative-Moment Strengthening of Concrete Bridges—Design Methodology." M.S. Thesis, Auburn University.

ASCE. 2013. *2013 Report Card for America's Infrastructure.* ASCE.

Aslan FRP. 2015. *Aslan FRP.* Accessed May 7, 2014. http://aslanfrp.com/frpstrengthening.html.

Aslan FRP. 2014. *Tensile Testing of CFRP Rebar.* Material Test Report, Seward, NE: Hughes Brothers, Inc.

Bakis, C. E., L. C. Bank, V. L. Brown, E. Cosenza, J. F. Davalos, J. J. Lesko, A. Machida, S. H. Rizkalla, and T. C. Triantafillou. 2003. "Fiber-Reinforced Polymer Composites for Construction - State-of-the-Art Review." *Perspectives in Civil Engineering: Commemorating the 150th Anniversary of the American Society of Civil Engineers* 369-383.

Bergström, Markus, Björn Täljsten, and Anders Carolin. 2009. "Failure Load Test of a CFRP Strengthened Railway Bridge in Örnsköldsvik, Sweden." *Journal of Bridge Engineering* 300-308.

Bertolotti, Eric Arthur. 2012. "Near-Surface-Mounted Fiber-Reinforced Polymer Strips for Strengthening of Reinforced Concrete Girders." M.S. Thesis, Auburn University.

Blaschko, M., and K. Zilch. 1999. "Rehabilitation of concrete structures with CFRP strips glued into slits." *Proc., 12th International Conference on Composite Materials.* International Committee on Composite Materials.

Broms, Bengt B. 1965. "Crack Width and Crack Spacing in Reinforced Concrete Members." *ACI Journal, Proceedings V. 62, No. 10* 1237-1255.

Bullock, W. O., R. W. Barnes, and A. K. Schindler. 2011. "Repair of Cracked Prestressed Concrete Girders, I-565, Huntsville, Alabama."

CALTRANS. 2012. "Special Provisions for Construction on State Highway in Santa Barbara County near Buellton and Nojoqui Creek Bridge No 15-75 R/L." CALTRANS.

Carmichael, Benjamin M., and Robert W. Barnes. 2005. "Repair of the Uphapee Creek Bridge with FRP Laminates." Thesis, Auburn University.

Casadei, P., N. Galati, R. Parretti, and A. Nanni. 2003. "Strengthening of a Bridge Using Two FRP Technologies." *ACI Special Publication* 219-238.

Clark, Arthur P. 1956. "Cracking in Reinforced Concrete Flexural Members." *ACI Journal, Proceedings V. 27, No. 8* 851-862.

El-Hacha, Raafat, and Sami H. Rizkalla. 2004. "Near-Surface-Mounted Fiber-Reinforced Polymer Reinforcements for Flexural Strengthening of Concrete Structures." *ACI Structural Journal* 717-726.

Frosch, Robert J. 1999. "Another Look at Cracking and Crack Control in Reinforced Concrete." *ACI Structural Journal* 437-442.

Gergely, Peter, and Leroy A. Lutz. 1968. "Maximum Crack Width in Reinforced Concrete Flexural Members." *SP-20, American Concrete Institute* 87-117.

Google Maps. 2015. Accessed June 22, 2015. https://www.google.com/maps.

Hibbeler, R. C. 2011. *Mechanics of Materials, Eighth Edition.* New Jersey: Pearson Education, Inc.

Hilti Inc. 2014. "2014 Hilti North American Product Technical Guide." Accessed November 1, 2014. http://www.hilti.com.

Hughes Brothers, Inc. 2011. "Carbon Fiber Reinforced Polymer (CFRP) Tape - Alsan 500 Series." *Hughes Brothers.* November 10. Accessed May 7, 2014. http://aslanfrp.com/Aslan500/aslan500-pg1.html.

ISIS Canada. 2010. *Educational Module 4: An Introduction to FRP Strengthening of Concrete Structures.* Winnipeg, Manitoba, Canada: Prepared by ISIS Canada Research Network.

Jung, W. T., Y. H. Park, J. S. Park, J. Y. Kang, and Y. J. You. 2005. "Experimental Investigation on Flexural Behavior of RC Beams Strengthened by NSM CFRP Reinforcements." *American Concrete Institute Special Publication Vol. 230* 795-806.

Parretti, Renato, and Antonio Nanni. 2004. "Strengthening of RC Members Using Near-Surface Mounted FRP Composites: Design Overview." *Advances In Structural Engineering Vol. 7 No 5`*.

Seracino , Rudolf, Nicola M. Jones, M. S. M. Ali, Mark W. Page, and Deric J. Oehlers. 2007. "Bond Strength of Near-Surface Mounted FRP Strip-to-Concrete Joints." *Journal of Composites for Construction* 11 (4): 401-409.

Sheikh, Shamim A., and S. Mukhtar Homam. 2004. "A Decade of Performance of FRP-Repaired Structures." *In Proceedings of the ISIS-SHM 2004 Workshop.* Winnipeg, Manitoba, Canada.

Standards Australia. n.d. *Design handbook for RC structures retrofitted with FRP and metal plates: beams and slabs (HB 305-2008).* Sydney: Standards Australia.

Tumialan, J. Gustavo, Milan Vatovec, and Paul L. Kelley. 2007. "Case Study: Strengthening of Parking Garage Decks with Near-Surface-Mounted CFRP Bars." *Journal of Composites for Construction* 523-530.

Vasquez Rayo, Diego L. 2008. *Plate-End Debonding of Longitudinal Near-Surface Mounted Fiber Reinforced Polymer Strips on Reinforced Concrete Flexural Members.* M.S. Thesis, North Carolina State University.

Wight, James K., and James G. MacGregor. 2012. *Reinforced Concrete Mechanics & Design.* Upper Saddle River, NJ: Pearson Eduction, Inc.

Wyoming Department of Transportation. 2009. *BRASS Program.* Accessed July 21, 2015. https://www.dot.state.wy.us/home/engineering_technical_programs/bridge/brass.html.

APPENDIX A: ASLAN FRP MATERIAL TEST REPORT

Tensile Testing of CFRP Rebar

Aslan FRP
Hughes Brothers

TEST MACHINE
Baldwin Model 120 CS S/N: 1005
Electromechanical
120,000 lbs Capacity Tension/Compression
Certification Number 148082613133713
By Instron 26-August-2013
Operating System - MTEST Windows
Grip V Style Per ASTM E4-13

Rebar Size	RBCT2
Order	730
Work Order	
Date Produced	
Lot Color Code	
Matrix	
Formulation	
Test Temp	71.3°F
Test R/H	25%
Load Rate	

Tested By	R Kruse
Test Date	11/6/2014
Carbon Type	
Tow	
# of Ends	
Sample Length	48.00"
Anchor Length	10.00"
Free Length	28.00"
Potting Material	M-183

Sample #	Load @ Failure (lbs)	Tensile Strength (psi)	Tensile Strength (MPa)	Ultimate Strain (in/in)	Modulus of Elasticity (psi)	Modulus of Elasticity (GPa)
1	22,293.2	447,654.6	3,086.6	0.0183	24,503,730	168.9
2	23,248.4	466,835.3	3,218.8	0.0195	23,960,708	165.2
3	23,213.0	466,124.5	3,213.9	0.0194	24,085,092	166.1
4	22,247.9	446,745.0	3,080.3	0.0183	24,393,054	168.2
5	23,952.0	480,963.9	3,316.2	0.0202	23,812,474	164.2
6	23441.0	470,702.8	3,245.5	0.0190	24,819,644	171.1
7	23120.6	464,269.1	3,201.1	0.0189	24,626,320	169.8
8	24392.2	489,803.2	3,377.2	0.0202	24,230,654	167.1
			Averages	0.0192	24,303,960	167.6

	PSI	MPa	Strain
Average Tensile	466,637.3	3,217.5	
Sigma	13,785.8	95.1	
3 Sigma	41,357.5	285.2	
-3 Sigma	425,279.8	2,932.3	0.0192

Extensonmeter Epsilon Model 3543

Distance from Anchors	
LBS of Load at Removal	
Percent of Load Required at Removal	50%
Span	6.00"

Lot Comments

Sample	Mode of Failure
1	Center Delam
2	Center Delam
3	Center Delam
4	Center Delam
5	Center Delam
6	Center Delam
7	Center Delam
8	Center Delam

* Samples cut using Diamond Blade Cutoff Saw
** Anchorages are cut to length and wheel abrated Schedule 40 Pipe

Rebar Size	Required Tensile Strength(psi / MPa)	Load Cell Min (lbs / N)	Actual ⌀ (in)	Actual CSA A_o (in)	Standard ⌀ (in / mm)	Standard CSA A_o (in / mm)
						0.0498"

Per ASTM D 7205-06 Rebar
Per ASTM D 3039-00 Flat or Tape
Metric Reference

As of 1 Jan 2012: Tensile Strength and Modulus of Elasticity on this sheet are NOT calculated using Actual Cross Sectional Area, but are calculated using a standard Cross Sectional Area.

Hughes Brothers, Inc. Seward, NE

APPENDIX B: ALDOT SPECIFICATION

ALABAMA DEPARTMENT OF TRANSPORTATION

DATE: March 11, 2014 Special Provision No. xx-xxxx

SUBJECT: Near-Surface-Mounted Fiber-Reinforced Polymer Strips for Structural Strengthening, Project No. IBRCP-0097(502), Lowndes County.

Alabama Standard Specifications, 20xx Edition, shall be amended by the addition of a new Section xxx as follows:

SECTION xxx
NEAR-SURFACE-MOUNTED FIBER-REINFORCED POLYMER REINFORCEMENT

xxx.01 Description.

This Section shall cover the work of strengthening or repairing concrete structures with near-surface-mounted (NSM) fiber-reinforced polymer (FRP) reinforcement. The NSM FRP reinforcement shall be installed in grooves cut into the concrete surface to increase the strength of a structure.

xxx.02 Materials.

(a) CARBON FIBER REINFORCED POLYMER (CFRP) REINFORCING STRIPS.

The NSM FRP reinforcement shall consist of carbon fiber reinforced polymer (CFRP) strips designated Aslan 500 CFRP Tape supplied by Hughes Brothers, Inc., 210 N. 13th St., Seward, NE 68434, (800) 869-0359. All manufacturer instructions for the CFRP strips shall be followed.

The guaranteed tensile strength of the CFRP strips shall be not less than 300,000 psi as tested per ASTM D3039, Standard Test Method for Tensile Properties of Polymer Matrix Composite Materials. The guaranteed modulus of elasticity shall be not less than 18,000,000 psi as tested per ASTM D3039. Material test certificates for each production lot of the CFRP strips used shall be furnished to the Engineer no later than 15 calendar days prior to installation in the structure.

(b) INJECTABLE ADHESIVE.

The injectable adhesive to bond the CFRP reinforcing strips to the concrete shall be HIT-RE 500 supplied by the Hilti, Inc., 5400 S. 112nd E. Ave., Tulsa, OK 74146 (800)879-8000. The system to dispense the injectable adhesive shall be selected by the contractor. All manufacturer instructions for the injectable adhesive shall be followed.

Material safety data sheets (MSDS) for the adhesive shall be obtained from the manufacturer, and shall be accessible at the job site at all times. All adhesive handling instructions defined by the manufacturer shall be followed.

xxx.03 Construction Requirements.

(a) COOPERATION OF THE CONTRACTOR.

The Engineer will obtain the assistance of a representative of the Auburn University Highway Research Center in inspecting and documenting the work. The Contractor shall provide assistance to this representative as directed by the Engineer.

Auburn University Highway Research Center Contact:
Robert W. Barnes
(334)663-9092
barnerw@auburn.edu
238 Harbert Engineering Center
Auburn University, AL 36849-5337

(b) PREPARATION AND PROTECTION OF CONSTRUCTION SITE.

The Contractor shall provide necessary pathways, scaffolding, and other means of access to the project site and to the installation area for personnel, equipment, and materials. The Contractor shall remove and reinstall all obstructions as directed by the Engineer without additional compensation.

The Contractor shall provide the Engineer with documentation (photographs or drawings) of all materials that the Engineer designates to be reinstalled after the installation of the NSM FRP. The materials shall not be removed until the Engineer informs the Contractor that the documentation is acceptable.

Bridge testing instrumentation (sensors, wires, etc.) shall not be removed from the bridge without the prior written approval of the Engineer.

(c) CONTRACTOR'S INSTALLATION PLAN.

The Contractor shall submit four copies of a proposed NSM FRP Installation Plan. The plan shall include the following:

- manufacturer literature detailing physical and chemical properties;
- equipment and procedures for locating, cutting, and preparing grooves for installation;
- FRP reinforcement and adhesive installation procedure including sequence and timing of operations;
- materials and procedures for the protection of the NSM FRP during installation and curing;
- weather restrictions (temperature, humidity, etc.);
- installation tolerances;
- quality control plan;
- procedures for documentation of the installation.

The submittal will not be approved by the Engineer but will be reviewed for completeness. The installation of the FRP shall not begin until the Engineer informs the Contractor in writing that the submittal is complete.

Incomplete submittals will be returned to the Contractor for completion and the resubmittal of four copies.

(d) STORAGE AND HANDLING OF NSM FRP COMPONENTS.

1. STORAGE REQUIREMENTS.

All components of the NSM FRP system shall be delivered and stored in the original factory sealed, unopened packaging or in containers with proper labels identifying the manufacturer, brand name, system identification number, date of manufacture, shelf life, and expiration date. Components shall be stored according to manufacturer instructions. All components shall be protected from dust, moisture, chemicals, direct sunlight, physical damage, fire, and temperatures outside the range specified in the system data sheets. Any component that has been stored in a condition different from the required storage conditions shall be disposed.

2. SHELF LIFE.

Any component of the NSM FRP system that has been stored longer than the shelf life shown on the system data sheet shall be disposed.

3. HANDLING.

All components of the NSM FRP system shall be handled with care according to the manufacturer's recommendations. The careful handling shall be done to protect the components from damage.

4. CLEANING CONSTRUCTION SITE.

The Contractor is responsible for the clean-up of the equipment and the project site using appropriate solvents, as shown in the NSM FRP Installation Plan.

5. DISPOSAL OF MATERIALS.

Any component of the NSM FRP system that has exceeded its shelf life or pot life, or has not been properly stored or has been contaminated, and any unused or excess material that is deemed waste shall be disposed of in a manner specified by the manufacturer and in accordance with state and federal environmental control regulations.

(e) CONCRETE PREPARATION.

1. GROOVE CUTTING.

Groove locations shall be reviewed by the Engineer prior to cutting. If a groove location is designated as moveable on the plans, the entire groove may be shifted laterally as much as 6 inches to avoid an obstruction without prior approval of the Engineer. However, adjacent grooves shall be spaced no less than 2 inches (center to center). Grooves shall be cut using a diamond-blade concrete wet saw. The groove depth shall not exceed the specified depth, nor shall it be less than the specified depth minus 3/32 inch. The groove width shall not be less than the specified width, nor shall it exceed the specified width plus 1/8 inch. The groove shall not deviate more than 1/4 inch from the specified straight line. Misaligned ends of discontinuous cuts that form a single groove shall be ground smooth to create a smooth transition. The Contractor shall notify the Engineer when steel reinforcement is cut while cutting the grooves.

2. GROOVE CLEANING.

The inside faces of the groove shall be cleaned with compressed air to allow the adhesive to securely bond to the concrete. At the time of NSM FRP installation, each groove shall be free of dust, oil, moisture, laitance, and other compounds that may interfere with bond. The surfaces of the groove shall be dry when the adhesive is placed.

3. MASKING.

Temporary masking of the concrete surface adjacent to each groove is allowed to facilitate removal of excess adhesive after installation. Masking material must be fully removed before exposure to vehicular traffic.

(f) INSTALLATION OF NSM FRP.

1. TEMPORARY PROTECTION.

Temporary protection may be required during installation and until the adhesive has cured. FRP reinforcement and uncured adhesive shall be protected from direct contact by rain, dust, dirt, and vandalism. Adhesive temperature must remain above 41°F during mixing and curing. Concrete temperature shall not exceed 120°F during adhesive curing. Strengthened structural components shall not be subjected to direct traffic loading during the initial curing time specified by the adhesive manufacturer.

2. INITIAL ADHESIVE INJECTION AND CONSOLIDATION.

Adhesive shall be mixed and injected into the grooves in accordance with the manufacturer's recommended procedures. All adhesive and reinforcement placement operations for a single element of FRP reinforcement shall be completed within the adhesive manufacturer's recommended working time for the ambient conditions encountered during installation. Prior to and at hourly intervals during adhesive injection, 3 fl oz of mixed epoxy shall be sampled from the injection gun. Should a sample show any visual evidence of improper proportioning or mixing, work shall be suspended until the equipment or procedures are corrected. Prior to insertion of FRP reinforcement, at least half of the groove depth shall be filled with adhesive, and the adhesive shall be consolidated to remove entrapped air voids. Manual consolidation may be performed using a putty knife.

3. FRP PLACEMENT.

Each element of FRP reinforcement shall consist of a continuous strip or bar. Splicing of reinforcement is only permitted when indicated on the project drawings. FRP reinforcement shall be inserted into the groove until approximately flush with the concrete surface. The reinforcement shall then be approximately centered in the groove, and then seated to the specified depth. A concrete grooving trowel may be used to seat the reinforcement. The seated FRP reinforcement shall be at least ¼ inch below the concrete surface, and adhesive shall be present between the FRP reinforcement and both vertical groove surfaces.

4. FINAL ADHESIVE INJECTION.

After the FRP reinforcement is properly seated and while the initially injected adhesive remains workable, any remaining space in the groove shall be filled with a finishing bead of adhesive. Excess adhesive shall be struck-off flush with the surface of the concrete.

5. FINAL SURFACE CLEANING.

The hardened adhesive shall extend no more than 1/8 inch laterally beyond the edge of each groove. The hardened adhesive shall extend no more than 1/16 inch above the concrete surface. Sandblasting shall be permitted for surface cleaning of adhesive.

(g) REPAIR OF DEFECTS.

The Contractor shall propose a repair procedure for all defects in the installed NSM FRP system or damage to the surrounding structure that is designated by the Engineer to be repaired.

xxx.04 Method of Measurement.

The Near-Surface-Mounted Fiber-Reinforced Polymer Reinforcement will be measured in units of linear feet of length of NSM FRP placed, regardless of the required width or depth of the required placement.

xxx.05 Basis of Payment.

(a) UNIT PRICE COVERAGE.

The near-surface-mounted (NSM) fiber-reinforced polymer (FRP) reinforcement will be paid for at the contract unit price which shall be full compensation for furnishing all materials, equipment, tools, labor, submittals, and incidentals necessary to complete this item of work.

(b) PAYMENT WILL BE MADE UNDER ITEM NO.:

xxx-A Near-Surface-Mounted Fiber-Reinforced Polymer Reinforcement - per linear foot

APPENDIX C: ALDOT PROJECT NOTES

PROJECT NOTES

REFERENCE PROJECT NO.	FISCAL YEAR	SHEET NO.
IBRCP-0097 (502)	2014	2

200 GROOVING OF THE BRIDGE DECK SHALL BE ACCOMPLISHED WITH TRACK MOUNTED, 1/4" THICK DIAMOND BLADE CONCRETE WET CUT SAWS TO A DEPTH OF 1 INCH.

201 THE SAW CUT GROOVES SHALL ONLY BE BE EXPOSED TO TRAFFIC (3) DAYS PRIOR TO BEGINNING PLACEMENT OF THE FIBER STRIPS

202 THE SAW CUT GROOVE SHALL NOT DEVIATE MORE THAN 1/4" INCH FROM THE PRESCRIBED STRAIGHT LINE.

203 CLEARANCE TO EXISTING DECK REINFORCEMENT SHALL BE VERIFIED USING NON-DESTRUCTIVE MEANS SUCH AS GROUND-PENETRATING RADAR.

204 THE USE OF COMPRESSED AIR SHALL BE USED TO CLEAN GROOVES OF SLURRY AT THE TIME OF GROOVE CUTTING AND JUST PRIOR TO TO APPLYING EPOXY.

205 DURING THE INITIAL INJECTION OF EPOXY, THE EPOXY SHALL BE CONSOLIDATED WITH A TOOL (SUCH AS A PUTTY KNIFE) TO ELIMINATE AIR VOIDS.

206 ALL WORK SHALL BE COMPLETED IN ONE ROADWAY LANE BEFORE WORK CAN BEGIN ON THE ADJACENT LANE

207 A CONCRETE GROOVING TROWEL SHALL BE USED TO SEAT THE STRIP TO THE CORRECT DEPTH. (SEE SHEET 4)

208 TO CREATE A FINSIHED SURFACE WITHOUT EXCESS EPOXY, IT IS RECOMMENDED TO APPLY TAPE TO THE EDGES OF THE GROOVE. IF TAPE IS APPLIED, TAPE SHALL BE REMOVED TOWARD THE END OF THE WORKABLE PERIOD AS DEFINED BY AMBIENT TEMPERATURE OR WHEN THE EPOXY SEEMS TO HAVE SUFFICIENTLY SET TO PREVENT HARDENING OF THE EXCESS EPOXY TO THE POINT OF MAKING TAPE REMOVAL IMPRACTICAL.

209 DURING THE CURING PERIOD THE CONTRACTOR SHALL HAND BROADCAST MORTAR SAND ON THE BRIDGE DECK AS A TEMPORARY SAFETY MEASURE UNTIL THE DECK IS SAND BLASTED

210 THE FOLLOWING INFORMATION IS PROVIDED FROM THE HILTI PRODUCT TECHNICAL GUIDE FOR INITIAL CURING TIMES:

°F	$t_{initial\ cure}$
41	18 hr
50	12 hr
59	8 hr
68	6 hr
86	4 hr
104	2 hr

211 NO TRAFFIC SHALL BE ALLOWED ON THE NEWLY PLACED EXPOXY UNTIL THE INITIAL CURING PERIOD HAS EXPIRED OR AS DIRECTED BY THE ENGINEER

212 ANCHOR HOLES REQUIRED BY TRACK SAW SHALL BE FILLED WITH EPOXY AS DIRECTED BY THE ENGINEER

213 THE CONTRACTOR SHALL MONITOR INCLEMENT WEATHER AND DURING THE THREAT OF A HURRICANE LANE CLOSURES SHALL BE REMOVED AND ALL WORK SHALL CEASE AS DIRECTED BY THE ENGINEER

800 IT SHALL BE THE CONTRACTOR'S RESPONSIBILITY TO DETERMINE THE EXACT LOCATION OF ALL UNDERGROUND UTILITIES BEFORE COMMENCING WORK. THE CONTRACTOR AGREES TO BE FULLY RESPONSIBLE FOR ANY AND ALL DAMAGES WHICH MIGHT BE OCCASIONED BY HIS FAILURE TO EXACTLY LOCATE AND PRESERVE ANY AND ALL UNDERGROUND UTILITIES.

900 NPDES PERMIT COVERAGE IS NOT REQUIRED FOR THIS PROJECT.

901 THERE SHALL BE NO FUEL TANKS STORED ON THE RIGHT OF WAY. IN ADDITION, NO FUEL TRUCKS OR VEHICLES TRANSPORTING CHEMICAL, FERTILIZER, ETC. SHALL BE LEFT UNATTENDED ON THE RIGHT OF WAY.